Chapter 6

In Situ Chemical Reduction of Chlorinated Organic Compounds

Romain Rodrigues[1,2,3], Stéphanie Betelu[1], Stéfan Colombano[1], Theodore Tzedakis[2], Guillaume Masselot[3], Ioannis Ignatiadis[1]

1: BRGM (French Geological Survey), 3 avenue Claude Guillemin, 45060 Orléans Cedex 2, France

2: LGC (Chemical Engineering Laboratory), 118 route de Narbonne 31062 Toulouse Cedex 9, France

3: ADEME (French Environment and Energy Management Agency), 20 Avenue du Grésillé, 49000 Angers Cedex 1, France

Email adresses: r.rodrigues@brgm.fr, s.betelu@brgm.fr, s.colombano@brgm.fr, tzedakis@chimie.ups-tlse.fr, guillaume.masselot@ademe.fr, i.ignatiadis@brgm.fr

Abstract

Chlorinated organic compounds (COCs) are common anthropogenic contaminants of soil and groundwater. COCs were industrially produced for different applications, such as dry cleaning, degreasing, or as pesticides. The presence of COCs in the environment is a major concern because of their toxicity and persistence.

The most widely used method for their remediation is the conventional pump-and-treat system. However, this technology can hardly achieve a complete remediation because of geological characteristics and the presence of pore space pollution/adsorbed pollution, leading to a residual saturation. Hence, in addition to the improvement of pump-and-treat systems, *in situ* chemical processes have been largely developed. These chemical processes involve the injection of chemical reagents for the removal of residual source pollution and/or the treatment of plume contamination.

Chemical degradation of COCs can be achieved by oxidative or reductive processes. If chemical oxidation has been first developed for *in situ* application, chemical reduction is one of the most important emerging remediation techniques for COCs treatment. Due to the electronegative character of chlorine substituents, COCs can effectively be transformed via reductive pathways. Moreover, reductive dechlorination has shown higher efficiency on highly chlorinated compounds.

This chapter focuses on the presentation of the chemical reduction of the most common COCs pollutants, followed by kinetic and mechanistic approaches related to the use of iron-based particles. Developments on *in situ* chemical reduction technologies in order to enhance remediation rates are also exposed. Influence of environmental conditions for *in situ* applications is then developed. Finally, a case study is presented.

Keywords

Chlorinated organic compounds; chemical reduction; zero-valent iron; kinetics; degradation pathways; solution geochemistry

Table of contents

1. Introduction

Chlorinated organic compounds (COCs) are common contaminants of soils and groundwater. Some COCs like chloromethane, dichloromethane and chloroform are naturally produced by living organisms, especially in marine environment – algae, sponges, fungi, and bacteria (Ballschmiter 2003; Gribble 2003) – but the main production is anthropogenic. For example, chloromethanes production was about 2.79 million tons in 2014 (Sherry 2015). Most chlorinated solvent families, like chlorinated methanes, chlorinated ethanes, chlorinated ethylenes and chlorinated benzenes, were industrially produced by chlorination – addition, electrophilic or radical reactions – of saturated or unsaturated hydrocarbons. COCs such as perchloroethylene (PCE) and trichloroethylene (TCE) are used as dry-cleaning solvents and metal degreasing agents as they are nonflammable, or as chemical intermediate for various applications – for example, trichloromethane is used as an intermediate in the production of organic fine chemicals – or extracting agents, or as functional fluids (e.g. hydraulic fluids in industrial equipment) (European Chlorinated Solvent Association). Some of them, such as hexachlorobenzene (HCB), have been used as pesticides (Hawley 1981; Verschueren 1983; Budavari 1996). Because of their toxicity, the use of COCs have been regulated since the 1970s, and production tends to be well reduced. For example, PCE production in United States dropped from 318 million tons in 1970 to 45 million tons in 1994 (Doherty 2000a, b).

However, an important part have been introduced in the environment, in which they are transported into the subsurface by vapor-phase migration, by infiltration in water, and as a moving dense non-aqueous phase liquid (DNAPL) (Johnson and Pankow 1992). The life cycle of a COCs source zone can be resumed as: (i) DNAPL release, (ii) DNAPL redistribution, (iii) dissolution and aging, (iv) depletion and (v) back diffusion and desorption (Kueper et al. 2014). The relatively low viscosities of COCs (same order of magnitude as water) allow the rapid downward movement in the subsurface

(Johnson and Pankow 1992). The low interfacial tension between liquid chlorinated solvent phase and water allows chlorinated solvent DNAPL to enter small fractures and pore spaces, facilitating deep penetration into the subsurface (Johnson and Pankow 1992). Alternatively, the unstable nature of DNAPL flow mechanisms can cause the solvent to continue migrating as a continuous body, or in thin "fingers" which can lead to the collection of large amounts of solvent in "pools" on the top of low permeable layers (Johnson and Pankow 1992). The low solubility of COCs mean that when a significant quantity of solvent is introduced to the environment, liquid solvent will dissolve slowly and persist for decades or centuries (Johnson and Pankow 1992). Moreover, most COCs exhibit low biotic and abiotic degradation rates and can persist in the subsurface for extended periods of time.

Different remediation technologies are effective to remove COCs pollution, especially physical and thermal treatments. Pump-and-treat systems are well developed and industrially applied in order to remove most pollutant, as the technology was available and relatively fast and easy to operate (Colombano et al. 2010). However, 'rebound' effect generally occurs after the end of the treatment, and pump-and-treat technologies can't achieve a complete remediation after many years because of pollutant persistence (Travis and Doty 1990; Pankow and Cherry 1996). Thermal treatment and surfactant/foam flushing were thus proposed as support techniques to reduce as possible residual saturations or to confine a source zone (Kingston et al. 2014; Pennell et al. 2014; Portois et al. 2018; Maire et al. 2018), before implementing more costly remediation methods such as *in situ* remediation.

Development of *in situ* chemical processes, which involves the injection of a chemical reagent directly in front of the pollution, has shown promising results for the remediation of COCs pollution, for both source remediation and plume control (McCarty 2010; Kueper et al. 2014). If *in situ* chemical oxidation (ISCO) has been first applied for the remediation of chlorinated solvents, *in situ* chemical reduction (ISCR) is more effective on highly chlorinated compounds, due to the electron deficiency on carbon atoms (Brown 2010). It is often presented as a more environmentally friendly alternative than oxidation as it is less destructive with respect to soil organic matter (Colombano et al. 2010).

This chapter describes the preliminary step concerning the implementation of *in situ* chemical reduction technologies, with the presentation of the prerequisites related to chlorinated solvent properties and transport/fate in soils and groundwater. Discussions are essentially focused on the development and improvement of zero-valent iron-based particles for the chemical reduction of COCs, with kinetic and degradation pathway approaches in order to highlight chemical reduction mechanisms. Effects of environmental conditions on degradation rate are then developed. Finally, injection technologies and a case study are presented.

2. Chlorinated solvents

Chlorinated solvents ($C_xH_yCl_z$) are organic compounds containing at least one carbon-chlorine bond in their structure. The presence of chlorine instead of hydrogen atoms plays a significant role on the physical and chemical properties of COCs, their toxicity and all transport and fate processes in groundwater.

2.1. Physical and chemical properties

Table **6.1** lists the names, formulas, abbreviations and main physical and chemical properties at atmospheric pressure of the most common COCs encountered in polluted soil and groundwater. The presence of chlorine atoms affects physical and chemical properties of organic compounds, such as density, aqueous solubility and volatility. Most chlorinated solvents are part of the volatile organic compounds (VOCs) group, as they have low boiling points. Molecules are susceptible to evaporate

from liquid (or sublimate from solid), resulting in the formation of a gaseous plume, especially in the vadose zone, which causes pollution to the surface.

Nevertheless, COCs are denser than water and form a non-aqueous phase, so they are part of dense non-aqueous phase liquid (DNAPL) group. Their low solubilities *s* are frequently represented by the octanol/water partition coefficient K_{ow} (also noted *P*) characterizing their hydrophobic nature (log K_{ow} > 0), showing an affinity with organic phases. Knowledge of solubility is important as it permits to predict and model DNAPL transport and fate in groundwater. In a DNAPL mixture, a co-solvent effect must be considered to represent the mole fraction of each constituent of the mixed DNAPL. In addition to solubility, others physical properties, e.g. diffusion coefficients and Henry's law constant, are important to understand their fate.

Ionization potential (IP) represents the energy required to remove the valence electron of an atom or a molecule. Generally, from a same chemical structure, the presence of double bonds decreases IP values, while the presence of chlorine atoms increases them (Brown 2010). COCs are preferentially oxidized when carbon atoms have a high electron density, and preferentially reduced when carbon atoms have a low electron density. IP parameter is therefore, in a first approach, a good indicator to select the appropriate remediation technology.

In addition, their electrochemical properties are also affected by the nature of the COCs. Table **6.2** lists reductive half-reactions of COCs redox couple and their associated standard potential $E°$ (Boethling and Mackay 2000; Dolfing et al. 2006). First, the standard aqueous-phase free energy of formation is estimated from the standard gas-phase free energy of formation and the values of Henry's law constant *H* (Vogel et al. 1987; Dean 2004).

$$\Delta_f G°\,(\mathrm{aq}) = \Delta_f G°\,(\mathrm{g}) + RT\ln(H) \qquad \text{(Eq. 6.1)}$$

where $\Delta_f G°$ (aq) is the standard aqueous-phase free energy of formation (J·mol^{-1}), $\Delta_f G°$ (g) is the standard gas-phase free energy of formation (J mol^{-1}), *R* is the universal gas constant (8.314 J mol^{-1} K^{-1}) and *T* is the absolute temperature (K).

For a given half-reaction, the standard free energy changes $\Delta_r G°$ (aq) is calculated using Eq. **6.2**.

$$\Delta_r G°\,(\mathrm{aq}) = \sum \Delta_f G°\,(\mathrm{aq})\ \text{for products} - \sum \Delta_f G°\,(\mathrm{aq})\ \text{for reactants} \qquad \text{(Eq. 6.2)}$$

The value can then be adjusted to the desired reference state to calculate the standard potential value $E°$ (V) with Eq. **6.3** (Vogel et al. 1987).

$$E° = -\frac{\Delta_r G°\,(\mathrm{aq})}{nF} \qquad \text{(Eq. 6.3)}$$

where *n* is the number of electrons transferred in the reaction and *F* is the Faraday constant (96485 C mol^{-1}).

Table 6.1. Name, formula, physical and chemical properties of selected COCs at atmospheric pressure (data from Mackay et al. 2006; Montgomery 2007; Schwartz and Zhang 2003).

Compounds	Formula	Abbrev.	M (g mol^{-1})	d (20 °C)	Melting point (°C)	Boiling point (°C)	s (20 °C) (mg L^{-1})	log(K_{ow})	H (20 °C) (Pa m^3 mol^{-1})	D_{air} (m^2 s^{-1})	D_{water} (m^2 s^{-1})	IP (eV)
Carbon tetrachloride	CCl_4	CT	153.8	1.58	-23.0	76.5	793.4	2.83	2352	7.80 10^{-6}	8.80 10^{-10}	11.47
Chloroform	$CHCl_3$	CF	119.4	1.48	-63.5	61.7	7920	1.97	307	1.04 10^{-5}	1.00 10^{-9}	11.42
Dichloromethane	CH_2Cl_2	DCM	84.9	1.33	-95.1	39.8	13030	1.25	220	1.01 10^{-5}	1.17 10^{-9}	11.35
Chloromethane	CH_3Cl	CM	50.5	0.92	-97.6	-23.9	5325	0.91	743	-	-	11.30
Hexachloroethane	C_2Cl_6	HCA	236.7	2.09	183-187 (sublim.)		50	4.14	285	2.50 10^{-7}	6.80 10^{-10}	11.22-12.11
Pentachloroethane	C_2HCl_5	PCA	202.3	1.68	-29	162	499.5	3.05	-	-	-	11.00-11.28
1,1,1,2-Tetrachloroethane	$C_2H_2Cl_4$	1,1,1,2-TeCA	167.8	1.54	-36	146.2	1,100	3.03	-	-	-	-
1,1,2,2-Tetrachloroethane	$C_2H_2Cl_4$	1,1,2,2-TeCA	167.8	1.60	-70.2	130.2	2962	2.93	34.12	7.10 10^{-6}	7.90 10^{-10}	11.10
1,1,1-Trichloroethane	$C_2H_3Cl_3$	1,1,1-TCA	133.4	1.34	-30.6	74.1	1485	2.49	1370	7.80 10^{-6}	8.80 10^{-10}	10.82
1,1,2-Trichloroethane	$C_2H_3Cl_3$	1,1,2-TCA	133.4	1.44	-36.5	113.8	4394	1.89	66.78	-	-	11.00
1,1-Dichloroethane	$C_2H_4Cl_2$	1,1-DCA	99.0	1.18	-97.4	57.3	4767	1.79	500	7.42 10^{-6}	1.05 10^{-9}	11.06
1,2-Dichloroethane	$C_2H_4Cl_2$	1,2-DCA	99.0	1.25	-35.3	83.5	8608	1.48	102	7.42 10^{-6}	9.90 10^{-10}	11.12
Chloroethane	C_2H_5Cl	CA	64.5	0.90	-136.4	12.3	5678	1.43	1019	-	-	10.97-11.01
Tetrachloroethylene	C_2Cl_4	PCE	165.8	1.62	-19	121.2	206	3.4	1299	7.20 10^{-6}	8.20 10^{-10}	9.71
Trichloroethylene	C_2HCl_3	TCE	131.4	1.46	-86.4	87.2	1280	2.42	765	7.90 10^{-6}	9.10 10^{-10}	9.94
1,1-Dichloroethylene	$C_2H_2Cl_2$	1,1-DCE	96.9	1.22	-122.1	31.56	2420	2.13	2376	9.00 10^{-6}	1.04 10^{-9}	9.81
cis-1,2-Dichloroethylene	$C_2H_2Cl_2$	cis-1,2-DCE	96.9	1.28	-80	60.1	6410	1.86	341	7.36 10^{-6}	1.13 10^{-9}	-
trans-1,2-Dichloroethylene	$C_2H_2Cl_2$	trans-1,2-DCE	96.9	1.26	-50	47.5	4520	2.09	875	7.07 10^{-6}	1.19 10^{-9}	9.64
Vinyl chloride	C_2H_3Cl	VC	62.5	0.91	-153.8	-13.4	2763	0.60	2172	1.06 10^{-5}	1.23 10^{-10}	9.99
Hexachlorobenzene	C_6Cl_6	HCB	284.8	2.05	230	323-326	0.005	5.44	35.1	5.42 10^{-6}	5.91 10^{-10}	9.00
Pentachlorobenzene	C_6HCl_5	PeCB	250.3	1.83	86	277	0.419	5.17	52.6	-	-	9.11
1,2,3,4-Tetrachlorobenzene	$C_6H_2Cl_4$	1,2,3,4-TeCB	215.9	-	47.5	254	3.44	4.63	58.5	-	-	9.11
1,2,3,5-Tetrachlorobenzene	$C_6H_2Cl_4$	1,2,3,5-TeCB	215.9	-	54.5	246	3.44	4.63	-	-	-	9.16
1,2,4,5-Tetrachlorobenzene	$C_6H_2Cl_4$	1,2,4,5-TeCB	215.9	1.86	140	243-246	0.528	4.63	-	-	-	9.00
1,2,3-Trichlorobenzene	$C_6H_3Cl_3$	1,2,3-TCB	181.4	1.69	53-54	218-219	19.31	4.05	-	-	-	9.18
1,2,4-Trichlorobenzene	$C_6H_3Cl_3$	1,2,4-TCB	181.4	1.45	17	213.5	36.5	4.02	172	3.00 10^{-6}	8.23 10^{-10}	9.04
1,2,5-Trichlorobenzene	$C_6H_3Cl_3$	1,2,5-TCB	181.4	1.39	63-64	208	8.46	4.15	-	-	-	9.30
1,2-Dichlorobenzene	$C_6H_4Cl_2$	1,2-DCB	147.0	1.30	-45.6	180.5	147	3.38	133	3.00 10^{-6}	7.90 10^{-10}	9.06
1,3-Dichlorobenzene	$C_6H_4Cl_2$	1,3-DCB	147.0	1.29	-24.7	173	106	3.52	288	-	-	9.12
1,4-Dichlorobenzene	$C_6H_4Cl_2$	1,4-DCB	147.0	1.25	53.1	174.4	82.9	3.45	275	6.90 10^{-6}	7.90 10^{-10}	9.07
Chlorobenzene	C_6H_5Cl	CB	112.6	1.11	-45.6	132	495	2.84	297	7.30 10^{-6}	8.70 10^{-10}	9.07

Table 6.2. Reductive half-reactions of COCs and their standard potential E° at pH 7 and 25 °C (Tratnyek and Macalady 2000; Dolfing et al. 2006).

Redox couple	Reductive half-reaction	Standard potential E° (V/SHE) (pH = 7, T = 25 °C)
HCA/PCE	$C_2Cl_6 + 2\,e^- \rightarrow C_2Cl_4 + 2\,Cl^-$	1.140
1,1,2-TCA/VC	$C_2H_3Cl_3 + 2\,e^- \rightarrow C_2H_3Cl + 2\,Cl^-$	0.827
1,2-DCA/Ethylene	$C_2H_4Cl_2 + 2\,e^- \rightarrow C_2H_4 + 2\,Cl^-$	0.738
CCl_4/$CHCl_3$	$CCl_4 + H^+ + 2\,e^- \rightarrow CHCl_3 + Cl^-$	0.673
PCE/TCE	$C_2Cl_4 + H^+ + 2\,e^- \rightarrow C_2HCl_3 + Cl^-$	0.574
1,1,1-TCA/1,1-DCA	$C_2H_3Cl_3 + H^+ + 2\,e^- \rightarrow C_2H_4Cl_2 + Cl^-$	0.561
$CHCl_3$/CH_2Cl_2	$CHCl_3 + H^+ + 2\,e^- \rightarrow CH_2Cl_2 + Cl^-$	0.560
TCE/DCE	$C_2HCl_3 + H^+ + 2\,e^- \rightarrow C_2H_2Cl_2 + Cl^-$	0.527-0.550
1,1,2-TCA/DCA	$C_2H_3Cl_3 + H^+ + 2\,e^- \rightarrow C_2H_4Cl_2 + Cl^-$	0.513-0.538
CH_2Cl_2/CH_3Cl	$CH_2Cl_2 + H^+ + 2\,e^- \rightarrow CH_3Cl + Cl^-$	0.493
HCB/PeCB	$C_6Cl_6 + H^+ + 2\,e^- \rightarrow C_6HCl_5 + Cl^-$	0.470
CH_3Cl/Methane	$CH_3Cl + H^+ + 2\,e^- \rightarrow CH_4 + Cl^-$	0.464
CA/Ethane	$C_2H_5Cl + H^+ + 2\,e^- \rightarrow C_2H_6 + Cl^-$	0.462
VC/Ethylene	$C_2H_3Cl + H^+ + 2\,e^- \rightarrow C_2H_4 + Cl^-$	0.450
DCE/VC	$C_2H_2Cl_2 + H^+ + 2\,e^- \rightarrow C_2H_3Cl + Cl^-$	0.397-0.420
1,1-DCA/CA	$C_2H_4Cl_2 + H^+ + 2\,e^- \rightarrow C_2H_5Cl + Cl^-$	0.397
1,2-DCA/CA	$C_2H_4Cl_2 + H^+ + 2\,e^- \rightarrow C_2H_5Cl + Cl^-$	0.375

Standard potential values of half-reactions of COCs are all positive and generally close or higher than 0.4 V/SHE (standard hydrogen electrode) at pH = 7 and at 25 °C. In agreement with standard potential values provided in Table **6.2**, reduction reactions appear favorable under reductive conditions. Electrochemical properties are in good agreement with the literature which reports favorable experimental results for COCs reduction, more particularly for the removal of highly chlorinated compounds (McCarty and Semprini 1994; Brown 2010).

2.2. Toxicity

Chlorinated solvents are harmful to both human and environment health (McDaniel et al. 2004; Chiu et al. 2012). In the body, the main penetration pathway is the respiratory tract and, to a lesser extent, the dermal or digestive tract by accident. By inhalation, COCs cause irritation of the airways, chest pain, or disturbance of the heart rhythm, which can lead to dizziness sensations or even coma for heavy exposure. Common symptoms of dermal exposure are irritation and chemical burns, conjunctivitis or ocular projection. Chronic exposure to COCs lead to long-lasting and often irreversible effects, such as sleep disorders, vertigo, memory loss, concentrating trouble or depressive tendencies (Ruder 2006). Chlorinated methanes, especially carbon tetrachloride, are known to give rise to ozone depletion when important amounts are released into the environment (Doherty 2000a; Wang et al. 2009b).

Toxicity on humans of many COCs is not proven in the current state of knowledge by lack of studied cases. Indeed, each COC has its own toxicological characteristics as shown in Table **6.3** which lists some COCs – and possible reductive dechlorination products – according to their classification by the International Agency for Research on Cancer (IARC):

- Group 1: carcinogenic to humans;
- Group 2A: probably carcinogenic to humans;
- Group 2B: possibly carcinogenic to humans;

- Group 3: not classifiable as to carcinogenicity in humans.

Table 6.3. IARC classification of COCs and their reductive dechlorination products.

Group 1	Group 2A	Group 2B	Group 3
Benzene	PCE	Carbon tetrachloride	Chloroethane
Butadiene	Trichloropropane	Chlordecone	Chloromethane
TCE		Chloroform	Dichloroacetylene
VC		Dichloroethane	Dichlorobenzene
		Dichloromethane	Hexachlorobutadiene
		Hexachlorobenzene	Pentachloroethane
		Hexachloroethane	Trichloroethane
		Tetrachloroethane	
		Trichloromethane	

In addition, the Stockholm Convention on Persistent Organic Pollutants has classified initially 12 COCs (aldrin $C_{12}H_8Cl_6$, chlordane $C_{10}H_6Cl_8$, dieldrin $C_{12}H_8Cl_6O$, endrin $C_{12}H_8Cl_6O$, heptachlor $C_{10}H_5Cl_7$, hexachlorobenzene C_6Cl_6, mirex $C_{10}Cl_{12}$, toxaphene $C_{10}H_8Cl_8$, polychlorinated biphenyls $C_{12}H_{10-x}Cl_x$, dichlorodiphenyltrichloroethane $C_{14}H_9Cl_5$, polychlorinated dibenzo-*p*-dioxins and polychlorinated dibenzofurans) in order to eliminate or restrict their production and use. New compounds are frequently proposed and added to the different annexes of the convention, such as hexachlorocyclohexane isomers ($C_6H_6Cl_6$), chlordecone ($C_{10}Cl_{10}O$) and pentachlorobenzene (C_6HCl_5) in 2009 or hexachlorobutadiene (C_4Cl_6) in 2015.

The risks and impact of DNAPL pollution are especially significant as different chlorinated compounds are involved (Kueper et al. 2003). Moreover, reductive dechlorination of COCs can lead to the formation of more harmful compounds, especially VC and TCE, which are both PCE by-products. Knowledge of dechlorination mechanisms is therefore necessary to prevent a possible accumulation of more toxic byproducts.

As the presence of COCs in the environment represents a major concern because of their toxicity, understanding the fate and transport of these compounds in groundwater is crucial.

2.3. Transport and fate processes in groundwater

Transport phenomena are one of the steps of the overall chemical remediation mechanism, as the contact between the pollutant and the chemical reagent can be the limited step. Different transport and fate phenomena characterize the movement of a contaminant in groundwater: advection, diffusion, dissolution, volatilization, and adsorption. Dilution may also occur by natural infiltration or injection of uncontaminated water in groundwater, but it is generally not a significant factor (Alvarez and Illman 2005a).

In addition to physical and chemical properties, and geological characteristics such as wettability and permeability, transport processes have a high influence on COCs migration pathways. Dissolution and volatilization are responsible for the respective formation of dissolved and vapor phase plumes, leading to a long-term pollution and aging/weathering of the pollution. Thus, source zones are progressively enriched in the less volatile and soluble compounds, which will form plumes by diffusion phenomena. Back diffusion can finally occur with COCs desorption (Kueper et al. 2014).

All these transport processes, in addition with chemical and biological processes, are part of the natural attenuation of contaminated soils and groundwater. However, natural attenuation is known to be relatively slow, especially with recalcitrant compounds, but its understanding is of great interest in order to perform and control chemical degradation.

2.3.1. Advection

Advection is the mass transport related to groundwater velocity (Morrison 2000). It is often considered as the main pollution transport phenomena in groundwater (Alvarez and Illman 2005b). Experimental Darcy's law is written for the one-dimensional case as:

$$Q = K * A * \frac{\Delta h}{\Delta x} \qquad \text{(Eq. 6.4)}$$

where Q is the flow rate ($m^3\ s^{-1}$), K is the hydraulic conductivity ($m\ s^{-1}$) which represents the ease or difficulty of water to flow through the medium, A is the cross-sectional area of the flow system (m^2) and $\frac{\Delta h}{\Delta x}$ is the hydraulic gradient (dimensionless).

The medium effective porosity Φ_e may also be taken into account according to Eq. **6.5**:

$$Q = \frac{K * A}{\Phi_e} * \frac{\Delta h}{\Delta x} \qquad \text{(Eq. 6.5)}$$

Knowledge of the water table flow rate is necessary in order to calculate the required reactant flow rate to introduce to obtain the desired concentration.

2.3.2. Diffusion

Diffusion is the "transport of mass in its ionic or molecular state due to differences in concentration of a given species in space" (Ogata 1970). Diffusion causes natural equilibration of a solution and is related to the random motion of the dissolved solute, which is itself related to thermal agitation. Transport by diffusion is frequently neglect when transport by advection predominates (flow of rapid groundwater), but it should be considered in cases where hydraulic conductivity or hydraulic gradient are low (Alvarez and Illman 2005b).

According to the Fick's first law, the diffusion flux J ($mol\ s^{-1}$) is proportional to the concentration gradient (here, in one dimension).

$$J = -D * A * \frac{\partial C}{\partial x} \qquad \text{(Eq. 6.6)}$$

where D is the diffusion coefficient ($m^2\ s^{-1}$), A is the area (m^2) et $\frac{\partial C}{\partial x}$ is the concentration gradient ($mol\ m^{-3}\ m^{-1}$).

In porous media, molecular diffusion flux J_{total} is the result of solid, liquid and gaseous phase diffusion fluxes:

$$J_{\text{total}} = J_{\text{solid}} + J_{\text{liquid}} + J_{\text{gas}} \qquad \text{(Eq. 6.7)}$$

Generally, solid phase diffusion is negligible in soils due to the larger time scales compared to transport in gas or liquid phases (Calvet et al. 2005). For porous or fractured media, the diffusion coefficient may

be much lower, due to obstacles on the way. An impedance factor f_L is used to connect the diffusion coefficient in homogeneous media D_w with the diffusion coefficient in porous media D_p.

$$D_p = f_L * D_w \quad \text{(Eq. 6.8)}$$

An impedance factor accounts for the porosity ϵ_T and the tortuosity τ (ratio between the length of real pathway and the length of normalized pathway) of the medium, and can be expressed as (Kutílek and Nielsen 1994):

$$f_L = \epsilon_T * \tau^{-n} \quad \text{(Eq. 6.9)}$$

For unsaturated water porous media, the impedance factor takes also into account the volumetric water content – or water-filled porosity – θ (Millington and Quirk 1961).

$$\theta = \frac{V_{water}}{V_T} \quad \text{(Eq. 6.10)}$$

where V_{water} is the volume of water (m^3) and V_T is the total volume of wet material (m^3).

When a temporal evolution of the solute concentration in addition to the spatial variation, Fick's second law can be applied (here, in one dimension):

$$\frac{\partial C}{\partial t} = D\frac{\partial^2 C}{\partial x^2} \quad \text{(Eq. 6.11)}$$

2.3.3. Dissolution

Dissolution is a process in which solid, liquid or gas become solutes into a liquid to form a homogeneous solution. It defines the concentration of a pollutant in the dissolved form and persistence of the DNAPL phase. Besides water solubility, many parameters have an influence on the dissolution, such as groundwater velocity, surface contact between water and DNAPL or the diffusion coefficient of species in water (Pankow and Cherry 1996).

Dissolution of a mixture of chlorinated compounds is influenced by the respective solubility of each compound. Raoult's Law – valid for ideal (or diluted) solution – can be applied to approximate the aqueous phase concentration of each compound *i* (Pankow and Cherry 1996).

$$C_i = x_i * C_{sat} * \gamma_i \quad \text{(Eq. 6.12)}$$

where C_i is the molar solubility of *i* in the aqueous phase (mol L^{-1}), x_i is the molar fraction of *i* in the NAPL phase (dimensionless), C_{sat} is the molar solubility of *i* in the NAPL phase (mol L^{-1}) and γ_i is the activity coefficient of *i* in the NAPL phase ($\gamma_i = 1$ for an ideal dissolution). This relationship can be used for mixtures of chlorinated compounds because they have a similar chemical structure.

Mass transfer rate *N* (kg·s^{-1}) can be expressed by the equation:

$$N = K_C * \Delta C * A_S \quad \text{(Eq. 6.13)}$$

where K_c is the mass transfer coefficient (m s^{-1}), ΔC is the difference in concentration between pure phase and aqueous phase (dissolved pollutant) (kg m^{-3}) and A_S is the contact surface between the two phases (m^2).

2.3.4. Volatilization

Volatilization is the phenomenon of vaporization of a dissolved solute. Even if Raoult's law can be used, the mathematical relationship characterizing the equilibrium between the aqueous phase and the gas phase is the Henry's law:

$$p_i = H * C_i \quad \text{(Eq. 6.14)}$$

where p_i is the partial pressure of i (Pa), C_i is the concentration of i in the liquid phase (mol L^{-1}) and H is the Henry's constant of i (Pa L mol^{-1}). The unit of the Henry's law constant can vary according to the writing of the law and the quantities used (molar fraction, concentration or molality).

Volatilization is an important parameter to model the fate and distribution in groundwater of very volatile compounds, e.g. PCE or VC (Schwarzenbach et al. 2003; Alvarez and Illman 2005b).

2.3.5. Sorption

Sorption is related to the partitioning of a substance from one phase onto or into another phase. For COCs, it represents mainly their partitioning from the aqueous solution onto (e.g. adsorption) or into (e.g. absorption) a solid phase (Stumm et al. 1992). Both absorption and adsorption processes have to be considered (Allen-King et al. 2002). The relative concentration of COCs in the water and solid phases is generally described using Eq. **6.15**:

$$C_s = K_d C_w \quad \text{(Eq. 6.15)}$$

where C_s (mg kg^{-1}) and C_w (mg L^{-1}) are the concentration in the solid phase and in the aqueous phase, respectively, and K_d is the linear distribution coefficient ($L \cdot kg^{-1}$). Sorption of COCs are generally non-linear and can be described by the Freundlich isotherm (Chiou and Kile 1998); however, this linear relation can be used at low COCs concentrations to obtain a good approximation.

The fraction of organic carbon f_{oc} in the solid phase can be used to estimate the organic carbon/water partitioning coefficient K_{oc}.

$$K_{oc} = \frac{K_d}{f_{oc}} \quad \text{(Eq. 6.16)}$$

As K_d values are not often available, K_{oc} can be estimated from K_{ow} values by different linear free energy relationships (LFERs), with the most widely relation is:

$$\log K_{oc} = a \log K_{ow} + b \quad \text{(Eq. 6.17)}$$

where a = 0.72 and b = 0.49 according to Schwarzenbach and Westall (1981). Hence, aqueous solubility and K_{ow} are good indicators to characterize the tendency of COCs to partition out of water.

Sorption is responsible for the accumulation of contaminants on solids, and thus their subsequent release compared to the normal flow rate of groundwater. A retardation factor R_f can be calculated using Eq. **6.18** (Bouwer 1991):

$$R_f = 1 + \frac{K_d \rho_s}{\theta} \quad \text{(Eq. 6.18)}$$

where ρ_s is the dry bulk density of the solid phase (kg L^{-1}) and θ is the volumetric water content. As shown in a natural gradient experiment on solute transport in a sand aquifer, PCE and CT plumes were retarded compared to non-reactive tracers, and the effect was more important for PCE which is more hydrophobic than CT (Mackay et al. 1986; Roberts et al. 1986).

Other equations involved in adsorption processes, such as Freundlich or Langmuir isotherms, are detailed later in this chapter (§3.5.1).

2.4. Degradation mechanisms

Abiotic degradation reactions of COCs include number of probable reactions, such as substitution, dehydrochlorination, oxidation and reduction (Sweeny 1980; Vogel et al. 1987). The first two are chemical reactions, and the last two are redox reactions, which require external electron acceptors or donors.

COCs can undergo substitution reactions with water (hydrolysis, Eq. **6.19**) or with an anionic nucleophile N^- (nucleophilic substitution, Eq. **6.20**). Generally, the reaction with water (or hydroxide ions HO^- at high pH), resulting in the formation of an alcohol, is considered as the main contributor to substitution reactions because of the environmental abundance of water, despite its low nucleophilic strength (Schwarzenbach et al. 2003).

Hydrolysis $$RCl + H_2O \rightarrow ROH + HCl \quad \text{(Eq. 6.19)}$$

Nucleophilic reactions $$RCl + N^- \rightarrow RN + Cl^- \quad \text{(Eq. 6.20)}$$

Dehydrochlorination, or non-reductive elimination reaction, is the elimination of HCl in two vicinal carbon atoms by a moderate (e.g. H_2O) or strong (e.g. HO^-) base, resulting in the formation of a new carbon-carbon bond (Cwiertny and Scherer 2010). Thus, chlorinated alkanes are transformed to chlorinated alkenes (Eq. **6.21**), and chlorinated alkenes to chlorinated alkynes (Eq. **6.22**).

Dehydrochlorination $$R_2CCl - HCR'_2 \xrightarrow{\text{base}} R_2C = CR'_2 + HCl \quad \text{(Eq. 6.21)}$$

$$RCCl = HCR' \xrightarrow{\text{base}} RC \equiv CR' + HCl \quad \text{(Eq. 6.22)}$$

COCs can be chemically oxidized or reduced, with an oxidative or a reducing agent respectively. Oxidation is a loss of electron, while reduction is a gain of electron. Oxidation and reduction occur simultaneously as they involve an electron transfer between species from two redox couples. The redox reaction is spontaneous if the oxidizing agent has a higher standard electrode potential than the reducing agent (e.g. the standard cell potential of the reaction is positive). Each COC presents a different reactivity and predominance for oxidation or reduction according to its chemical structure and environmental conditions. Reduction is more susceptible to occur on compounds with a high number of chlorine atoms, as atoms of carbon are more electron deficient (Brown 2010).

COCs can undergo four oxidative degradation pathways – α-hydroxylation, halosyl oxidation, epoxidation, and biohalogenation – or three reductive degradation pathways – hydrogenolysis, dichloroelimination, and coupling reactions between two identical COCs –, depending on the nature of

the reactant and the structure of the pollutant (Vogel et al. 1987). In agreement with the objective of this chapter, only reductive pathways will be discussed here.

Hydrogenolysis is the substitution of a chlorine atom by a hydrogen atom, with a two sequential electron-transfer (ET) and the formation of chloride ion.

Hydrogenolysis $$RCl + H^+ + 2\,e^- \rightarrow RH + Cl^-$$ (Eq. 6.23)

Dichloroelimination – or reductive elimination – is the elimination of two chlorine atoms and the formation of an unsaturated hydrocarbon; alkanes are transformed to alkenes (Eq. **6.24**), and alkenes to alkynes (Eq. **6.25**). As hydrogenolysis, this reaction involves a two sequential electron-transfer.

Dichloroelimination $$R_2CCl - ClCR_2 + 2\,e^- \rightarrow R_2C = CR_2 + 2\,Cl^-$$ (Eq. 6.24)

$$CCl = ClCR + 2\,e^- \rightarrow RC \equiv CR + 2\,Cl^-$$ (Eq. 6.25)

Dichloroelimination is called α-elimination when the two chlorine atoms are located on the same carbon atom and β-elimination when the two chlorine atoms are located on two vicinal carbon atoms.

For both reactions, the first ET leads to the formation of a chlorinated radical and a chloride ion; the second ET leads to a reaction of this radical with a proton for hydrogenolysis and the formation of a new C-C bond with the loss of a second chloride ion for dichloroelimination (Bylaska et al. 2008).

Coupling reactions between two chlorinated hydrocarbon fragments or two COCs can also occur.

Coupling $$2\,RCl + 2\,e^- \rightarrow R - R + 2\,Cl^-$$ (Eq. 6.26)

3. Chemical reduction of chlorinated organic compounds

Chemical reduction is the use of reductants – electron donors – for the remediation of COCs – electron acceptors. For soil and groundwater remediation, the technology is referred as *In Situ* Chemical Reduction (ISCR). ISCR was primarily designed for plume management and remediation, especially with permeable reactive barriers applications (Henderson and Demond 2007; Brown 2010; Gillham et al. 2010). Since then, injections in front of COCs source zone have been developed (Kueper et al. 2014; Tratnyek et al. 2014).

This section will firstly present different efficient chemical reductants for COCs remediation, but is thereafter focused on the use of zero-valent iron (ZVI) due to its large number of effective *in situ* applications (Kueper et al. 2014). The latter will then be particularly focused on iron properties and reactivity enhancement – by using nanoscale or microscale particles, polymetallic particles, or a combination of reactants –, kinetic laws and mechanism pathways observed for common COCs.

3.1. Reductants used

The chemical reduction of COCs is generally performed with reduced sulfur species, reduced metal species or hydrogen. Figure **6.1A** illustrates different redox couples that can be involved in ISCR and the potential range of reductive half-reactions of COCs.

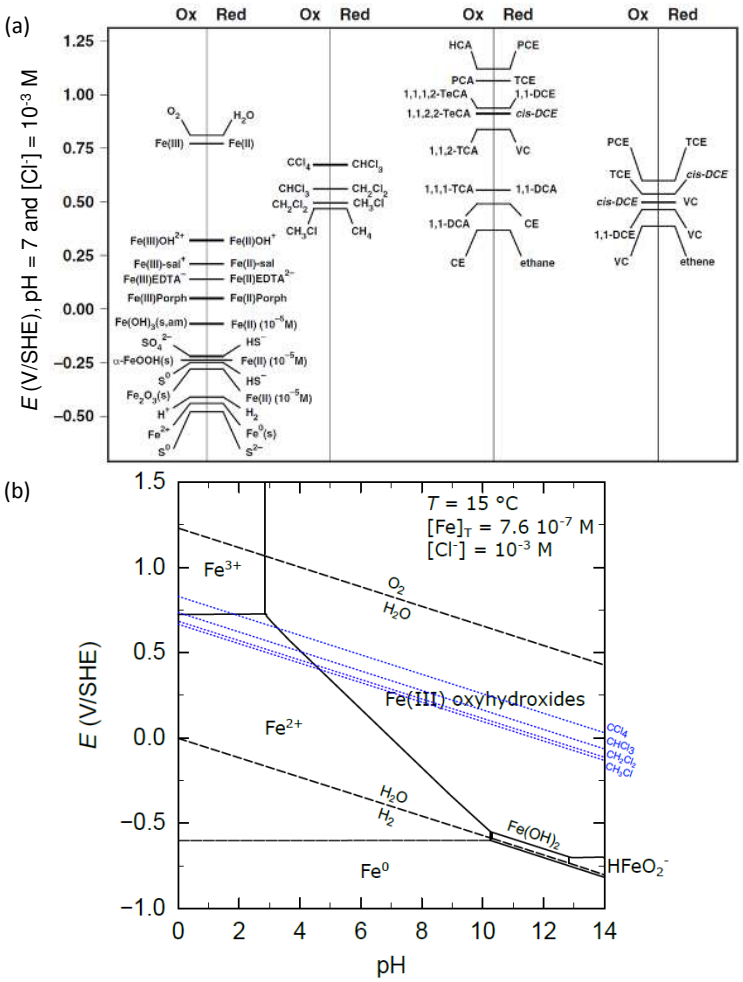

Figure 6.1. (a) Oxidation-reduction potential (ORP) of iron and sulfur species and chlorinated methanes, ethanes and ethylenes at pH = 7 and $[Cl^-] = 10^{-3}$ M (from Cwiertny and Scherer (2010), adapted from Schwarzenbach et al. (2003)). (b) Simplified Pourbaix diagram for Fe/H_2O system under reference conditions (adapted from Matheson and Tratnyek 1994; T = 15 °C, $[Cl^-] = 10^{-3}$ M, $Fe_T = 7.6\ 10^{-7}$ M).

Electrochemical half-reactions of some chemical reductants and their standard potential are shown in Table **6.4**.

Table 6.4. Half-reaction of chemical reductant and their associated standard potential.

Reactant	Half-reaction	Standard potential $E°$ (V/SHE) (T = 25 °C)
Hydrogen	$H_2 \rightarrow 2\,H^+ + 2\,e^-$	0
Iron	$Fe \rightarrow Fe^{2+} + 2\,e^-$	-0.44
Sulfide	$S^{2-} \rightarrow S + 2\,e^-$	-0.48
Dithionite	'$S_2O_4^{2-} - HSO_3^- - SO_2^-$' system	-0.66
Zinc	$Zn \rightarrow Zn^{2+} + 2\,e^-$	-0.76
Aluminum	$Al \rightarrow Al^{3+} + 3\,e^-$	-1.66

Complete half-reactions of chlorinated compounds (i.e. leading to the formation of non-chlorinated compounds) can be generally expressed using Eq. **6.27**.

$$C_xH_yCl_z + z\,H^+ + 2z\,e^- \rightarrow C_xH_{y+z} + z\,Cl^- \qquad \text{(Eq. 6.27)}$$

Table **6.5** lists complete half-reactions of selected COCs. Complete reduction leads to the formation of non-chlorinated hydrocarbons and chloride ions. Depending on the type of reagent, it is possible to observe the formation of saturated compounds from unsaturated compounds (e.g. the transformation of alkenes in alkanes).

Table 6.5. List of complete half-reactions of selected COCs.

Compounds	Complete reductive half-reaction
Carbon tetrachloride	$CCl_4 + 4\,H^+ + 8\,e^- \rightarrow CH_4 + 4\,Cl^-$
Chloroform	$CHCl_3 + 3\,H^+ + 6\,e^- \rightarrow CH_4 + 3\,Cl^-$
Dichloromethane	$CH_2Cl_2 + 4\,H^+ + 4\,e^- \rightarrow CH_4 + 2\,Cl^-$
Chloromethane	$CH_3Cl + H^+ + 2\,e^- \rightarrow CH_4 + Cl^-$
Hexachloroethane	$C_2Cl_6 + 6\,H^+ + 12\,e^- \rightarrow C_2H_6 + 6\,Cl^-$
Pentachloroethane	$C_2HCl_5 + 5\,H^+ + 10\,e^- \rightarrow C_2H_6 + 5\,Cl^-$
Tetrachloroethane	$C_2H_2Cl_4 + 4\,H^+ + 8\,e^- \rightarrow C_2H_6 + 4\,Cl^-$
Trichloroethane	$C_2H_3Cl_3 + 3\,H^+ + 6\,e^- \rightarrow C_2H_6 + 3\,Cl^-$
Dichloroethane	$C_2H_4Cl_2 + 2\,H^+ + 4\,e^- \rightarrow C_2H_6 + 2\,Cl^-$
Chloroethane	$C_2H_5Cl + H^+ + 2\,e^- \rightarrow C_2H_6 + Cl^-$
PCE	$C_2Cl_4 + 4\,H^+ + 8\,e^- \rightarrow C_2H_4 + 4\,Cl^-$ $C_2Cl_4 + 6\,H^+ + 10\,e^- \rightarrow C_2H_6 + 4\,Cl^-$
TCE	$C_2HCl_3 + 3\,H^+ + 6\,e^- \rightarrow C_2H_4 + 3\,Cl^-$ $C_2HCl_3 + 5\,H^+ + 8\,e^- \rightarrow C_2H_6 + 3\,Cl^-$
DCE	$C_2H_2Cl_2 + 2\,H^+ + 4\,e^- \rightarrow C_2H_4 + 2\,Cl^-$ $C_2H_2Cl_2 + 4\,H^+ + 6\,e^- \rightarrow C_2H_6 + 2\,Cl^-$
Vinyl chloride	$C_2H_3Cl + H^+ + 2\,e^- \rightarrow C_2H_4 + Cl^-$ $C_2H_3Cl + 3\,H^+ + 4\,e^- \rightarrow C_2H_6 + Cl^-$
Hexachlorobenzene	$C_6Cl_6 + 6\,H^+ + 12\,e^- \rightarrow C_6H_6 + 6\,Cl^-$
Pentachlorobenzene	$C_6HCl_5 + 5\,H^+ + 10\,e^- \rightarrow C_6H_6 + 5\,Cl^-$
Tetrachlorobenzene	$C_6H_2Cl_4 + 4\,H^+ + 8\,e^- \rightarrow C_6H_6 + 4\,Cl^-$
Trichlorobenzene	$C_6H_3Cl_3 + 3\,H^+ + 6\,e^- \rightarrow C_6H_6 + 3\,Cl^-$
Dichlorobenzene	$C_6H_4Cl_2 + 2\,H^+ + 4\,e^- \rightarrow C_6H_6 + 2\,Cl^-$
Chlorobenzene	$C_6H_5Cl + H^+ + 2\,e^- \rightarrow C_6H_6 + Cl^-$

Hydrogen sparging – or gas bubbling – of aquifers contaminated with chlorinated solvents has been shown as a promising method to enhance *in situ* microbial dechlorination. A concern, however, is the ability to distribute hydrogen effectively throughout the contaminated interval such that complete dechlorination can occur. Novel technologies are in development in order to incorporate hydrogen into foams such as to promote and enhance lateral gas distribution and then to enhance the desired level of dechlorination. Currently, hydrogen can be an effective reductant of COCs in the presence of supported metallic catalysts, such as palladium (Marques et al. 1993; Schreier and Reinhard 1995; Lowry and Reinhard 1999; Zhang et al. 2013).

Concerning reduced sulfur species, they generally include S(-II) and S(III) species, such as polysulfide ions S_n^{2-}, hydrogen sulfide species HS^- and H_2S (Barbash and Reinhard 1989; Roberts et al. 1992), and sodium dithionite $Na_2S_2O_4$. Some studies suggest that the reductive species is not dithionite $S_2O_4^{2-}$ but rather a dissociation product (Mayhew and Massey 1973; Mayhew 1978). The long and weak S-S bond leads to the reversible formation of very reactive $SO_2^{\bullet-}$ radicals (Amonette et al. 1994; Amonette 2002). As a water-soluble salt, sodium dithionite can easily be injected into groundwater with traditional injection methods (see §4, Injection of reductants). It has for example been successfully used for *in situ* remediation of chlorinated ethylenes (Ignatiadis et al. 2016), as developed in the case study (§5).

Nevertheless, *in situ* chemical reduction of COCs is generally performed by using zero-valent metals. The first case study has been investigated in the late 1970s to dechlorinate halogenated organic compounds – dichlorodiphenyltrichloroethane, chlorobenzene, endrin, heptachlor, chloroform and hexachlorocyclopentadiene – from a wastewater stream using copper-doped iron and aluminum (Sweeny 1980). Aluminum and magnesium are widely used for the dechlorination of organic chemicals in organic synthesis on laboratory and for wastewater treatment (Nidheesh et al. 2018), but only a few groundwater cleanup technologies has been fully implemented with these metals (Brown 2010).

Dechlorination of COCs using zero-valent iron (ZVI) has been considered in the early 1990s, with the demonstration of the efficiency of iron particles for the degradation of 14 chloromethanes, chloroethanes and chloroethenes (Gillham and O'Hannesin 1994). In addition to ZVI, zero-valent zinc (ZVZ) has also been studied for the degradation of COCs in the 1990s. Reduction of chlorinated methanes has been observed by Warren et al. (1995), as well as reduction of chlorinated ethanes (Fennelly and Roberts 1998; Arnold et al. 1999), ethylenes (Arnold and Roberts 1998) and propanes (Sarathy et al. 2010; Cushman 2014). Zinc is a good alternative to iron for *in situ* application (Cheng and Wu 2000) as its storage is easier and its tolerable concentration in drinking water is high (for example, the maximum admissible value in drinking water for iron is 200 $\mu g\ L^{-1}$ according to the Council Directive 98/83/EC of 3 November 1998 and 3 $mg\ L^{-1}$ for zinc according to the Guidelines for Drinking-Water Quality). Even if ZVZ particles have shown better degradation efficiency on the reduction of chlorinated alkanes – carbon tetrachloride or 1,2,3-trichloropropane for example –, their reactivity is more strongly impacted by environmental conditions than their size and morphology (Tratnyek et al. 2010). Also, in presence of a microbial community, dechlorination occurred faster with ZVI than ZVZ (Ma and Wu 2008). Moreover, iron is one of the ten most abundant elements in our planet (Taylor 1964). Iron plays a key role in many biogeochemical processes implying electron transfers (i.e. redox reactions) because of its abundance, ubiquity and particular physicochemical properties. Moreover, iron can be naturally found in a great variety of chemical species, such as elemental form (ZVI), aqueous ions (Fe^{3+} and Fe^{2+}), oxides, oxy-hydroxides, sulfates and sulfide minerals, silicates, carbonates, etc. (Figure **6.1**.A and B). These species form various redox couples. Iron physicochemical properties (solubility, redox potential) can dramatically change from one species to another. In all pH conditions, there are soluble iron species, and many iron couples have redox potential falling within the stability region of water, thus explaining the importance of iron in many redox mechanisms where it can act either as reductant or as oxidant.

The reduction of some alkyl halides by hydrated or complexed ferrous iron is thermodynamically possible but quite slow (Klečka and Gonsior 1984; Doong and Wu 1992). However, surface-bounded Fe^{2+} and Fe(II) precipitates are stronger reductants (Johnson et al. 1998; Amonette et al. 2000; Jeong et al. 2013; Bae and Hanna 2015) and can degrade carbon tetrachloride and hexachloroethane (Elsner et al. 2004; Shao and Butler 2007). It has been reported that green rusts – layered mixed Fe(II)/Fe(III) hydroxide minerals (Usman et al. 2018) – can also reduce chlorinated methanes (Erbs et al. 1998), ethanes and ethylenes, with a more rapid reduction for highly chlorinated compounds like HCA and PCA for chlorinated ethanes (O'Loughlin and Burris 2004) or PCE and TCE for chlorinated ethylenes (Lee and Batchelor 2002a). However, Huang et al. (2018) report that only small molecules (chlorinated methanes) can transport through the interlayer of the layered double hydroxide structure, and Mangayayam et al. (2018) have shown that the degradation of chlorinated ethylenes was not significant with four different green rusts freshly prepared, without any post-treatment. Recently, it has been shown that the use of bone char as electron mediator can eliminate the kinetic hindrance of dehalogenation of chlorinated ethylenes by green rusts (Ai et al. 2019). Other minerals, e.g. iron sulfide FeS, pyrrhotite $Fe_{1-x}S$, mackinawite

$Fe_{1+x}S$, pyrite FeS_2, and magnetite Fe_3O_4, which are present in anaerobic environments, have been shown to contribute to the reductive dechlorination of chlorinated ethylenes under specific conditions (Butler and Hayes 1998, 2000; Weerasooriya and Dharmasena 2001; Lee and Batchelor 2002b; Jeong et al. 2007; Hyun and Hayes 2015; Gong et al. 2016; Yang et al. 2017; Culpepper et al. 2018).

Among all the reactants containing iron, ZVI is the prime example of an electrochemical redox system that have been implemented to intercept and remediate (i) COCs by funnel-and-gate system and (ii) overlapping plumes of COCs by iron barrier (Zhang 2003; Wilkin et al. 2003). After four years of operations, ZVI appears as a long-term sink for carbon, sulfur, calcium, silicon, nitrogen, and magnesium (Wilkin et al. 2003). Moreover, and in agreement with the bibliography, consistent patterns of spatially variable mineral precipitation and microbial activity have been observed during the treatment. Although pore space has been lost, because of the accumulation of endogenic components, no pervasive pore clogging was evidenced (Wilkin et al. 2003).

For these reasons, we focus on the development and the improvement of ZVI particles for the chemical reduction of COCs.

3.2. Zero-valent iron

3.2.1. History, reactivity and characterization

Zero-valent iron (ZVI) particles have been considered in the late 1970s for the remediation of COCs (Sweeny 1980) and was first applied for *in situ* remediation in the 1990s as granular iron in permeable reactive barriers (PRBs) (Gillham and O'Hannesin 1994; O'Hannesin and Gillham 1998; Obiri-Nyarko et al. 2014). One of the first studies concerning *in situ* remediation of polyhalogenated hydrocarbons with zero-valent metals has been reported by Tratnyek et al. (2003). Since then, several sites have been cleaned up using ZVI, and remediation rate were around 90% in few weeks (Brown 2010).

Three reactions were proposed to explain degradation mechanisms: the direct reduction on ZVI surface (Eq. **6.28**), the reduction by ferrous iron Fe^{2+} species (Eq. **6.30**) and by hydrogen H_2 (hydrogenation reactions, Eq. **6.31**), both produced during iron anaerobic corrosion (Eq. **6.29**) (Matheson and Tratnyek 1994). However, reduction by dissolved Fe^{2+} is quite slow and reduction by H_2 requires an effective catalyst.

Direct reduction at iron surface	$Fe^0 + RCl + H^+ \rightarrow Fe^{2+} + RH + Cl^-$	(Eq. 6.28)
Iron corrosion	$Fe^0 + 2\,H_2O \rightarrow Fe^{2+} + H_{2\,(g)} + 2\,HO^-$	(Eq. 6.29)
Reduction by ferrous iron	$2\,Fe^{2+} + RCl + H^+ \rightarrow 2\,Fe^{3+} + RH + Cl^-$	(Eq. 6.30)
Reduction by hydrogen	$RCl + H_{2\,(g)} \xrightarrow{\text{catalyst}} RH + Cl^- + H^+$	(Eq. 6.31)

Due to their rapid oxidation in free atmospheric conditions, ZVI particles exhibits a core-shell structure, with an iron core surrounded by a thin mixed-valent iron oxide shell (Li et al. 2006a; Martin et al. 2008; Yan et al. 2010a; Ling et al. 2017). This shell is the seat where all remediation processes, such as adsorption, co-precipitation and chemical reduction, occur (Noubactep 2012). Its interfacial mineral composition is quite complex and include mainly – from the inner sphere to the outer sphere – FeO (wüstite, metastable), Fe_3O_4 (magnetite), Fe_2O_3 (hematite α-Fe_2O_3 and maghemite γ-Fe_2O_3) and FeOOH

(goethite α-FeOOH, lepidocrocite γ-FeOOH and feroxyhyte δ-FeOOH) (Uegami et al. 2002; Wang et al. 2009a; Yan et al. 2013; Kumar et al. 2014a; Mu et al. 2017; Ling et al. 2017). Generally, iron oxides valence increases from the core to the surface, resulting in an increase in the specific surface area (SSA) and a decrease in the density, with an increase in the expansion volume (Noubactep 2010b; Mu et al. 2017) and the possible clogging of pore in groundwater. The pollutant can then be trapped in the shell during its growth and transformation (Noubactep 2010b; Noubactep and Caré 2010). Table **6.6** presents the main iron oxides with their properties in their pure form.

Table 6.6. Band gap E_{BG} and density d of various pure iron oxides (Cornell and Schwertmann 2003).

Iron oxide	Formula	Color	Structure	E_{BG} (eV)	d (g·cm^{-3})
Wüstite	$Fe_{1-x}O$	Black	Cubic	2.3	5.9-5.99
Magnetite	Fe_3O_4	Black	Cubic	0.1	5.18
Hematite	α-Fe_2O_3	Red	Rhombohedral Hexagonal	2.2	5.26
Maghemite	γ-Fe_2O_3	Reddish-brown	Cubic Tetragonal	2.03	4.87
Goethite	α-FeOOH	Yellow-brown	Orthorhombic	2.10	4.26
Akaganéite	β-FeOOH	Yellow-brown	Monoclinic	2.12	3.52
Lepidocrocite	γ-FeOOH	Orange	Orthorhombic	2.06	4.09
Feroxyhyte	δ-FeOOH	Red-brown	Hexagonal	1.94	4.20

Different models are described in the bibliography for the electron transfer from iron core to the surface: (i) a direct transfer in the absence of oxide layer, (ii) a transfer from metal through defects (pits) in the oxide layer, (iii) a transfer from the oxide layer as a semi-conductor and (iv) a transfer from metal-to-ligand (Scherer et al. 1999). It is important to note that iron particles are not selective, and iron reacts mainly with dissolved oxygen, if present, and water, in agreement with the very low electron efficiency towards pollutant reported in the literature (Schöftner et al. 2015; Tang et al. 2017a). The direct reduction of the pollutant at Fe^0 core surface requires its diffusion through the oxide shell, which is possible because of the porous structure of the initial shell (Crane and Scott 2012; Mu et al. 2017). However, this phenomenon will be impeded by the diffusion of Fe^{2+} resulting from iron corrosion in the opposite direction of the pollutant. As it was reported that shell-bounded Fe^{2+} on different iron oxides is a strong reductant with specific redox properties (Johnson et al. 1998; Amonette et al. 2000; Elsner et al. 2004; Silvester et al. 2005; Shao and Butler 2007; Bae and Hanna 2015; Gorski et al. 2016; Stewart et al. 2018), reduction can occur before the pollutant comes into contact with the surface. The spontaneous electron transfer between Fe^{2+} and Fe(III) oxides on the shell, which is influenced by the stoichiometry between Fe^{2+} and Fe^{3+} and the presence of surface defect (Gorski and Scherer 2009; Gorski et al. 2010; Notini et al. 2018; Usman et al. 2018), results in an acceleration in the interfacial electron transfer between iron species and the pollutant (Huang and Zhang 2005; Han et al. 2016b). In addition, the presence of defects in the shell was assumed to act as a catalyst for hydrodechlorination (dechlorination by hydrogen) (Liu et al. 2005a), due to the local separation of anodic and cathodic sites on the particles (Odziemkowski et al. 1998; Odziemkowski and Simpraga 2004). However, the accumulation of H_2 bubbles near the surface of the particles can interfere the mass transport of H^+ and the pollutant (Matheson and Tratnyek 1994; Jiang et al. 2017). In the case of a non-conductive shell, which inhibits the electrons transfer from iron core, the chemical reduction occurs only via indirect reduction by Fe^{2+} and H_2 adsorbed/bounded on the shell (Noubactep 2016; Makota et al. 2017).

Knowing the importance of iron corrosion products and the presence of defects in the shell, it is possible to perform a pre-treatment of the particles to improve their reactivity. The most common pre-treatment strategies are acid washing (HCl), H_2 pre-treatment, ultrasound pre-treatment and premagnetization (Sun et al. 2016). More recently, a pre-corrosion process which consists of an aging of the particles in water before using the particles for remediation has been proposed (Ribas et al. 2017; Touomo-Wouafo et al. 2018). In addition, it is possible to obtain a highly disordered oxide shell with many defects by increasing the thickness of the shell with a thermal treatment after their synthesis (Kašlík et al. 2018). When introduced in an aqueous environment, studies have shown that a short-term depassivation is first observed, resulting in an enhanced reactivity, followed by a progressive repassivation of the particles (Sarathy et al. 2008; Kim et al. 2010a). The aging of ZVI particles in anoxic environment follows the Fe^0 – $Fe(OH)_2$ – Fe_3O_4 – γ-Fe_2O_3 route (Liu et al. 2007; Reinsch et al. 2010; Kumar et al. 2014a; Dong et al. 2016b; Pullin et al. 2017b; Velimirovic et al. 2018).

The presence of dissolved oxygen (DO) will result in the formation of reactive oxygen species (ROS, Eqs. **6.32-34**) and ferryl iron $Fe(IV)O^{2+}$ (Keenan and Sedlak 2008; Lee 2015), in order to promote oxidative processes. However, the reactive oxidant yield is generally low and does not allow to benefit from Fenton reaction for practical applications, without any modification or use of ligand (Mu et al. 2017).

$$Fe^0 + O_2 + 2\,H^+ \rightarrow Fe^{2+} + H_2O_2 \qquad \text{(Eq. 6.32)}$$

$$Fe^{2+} + O_2 \rightarrow Fe^{3+} + {}^{\bullet}O_2^- \qquad \text{(Eq. 6.33)}$$

$$Fe^{2+} + H_2O_2 \rightarrow Fe^{3+} + {}^{\bullet}HO + HO^- \qquad \text{(Eq. 6.34)}$$

The presence of DO will also result in the rapid oxidation of Fe^{2+} species (Greenlee et al. 2012; Guan et al. 2015), leading to the formation of Fe(III) oxyhydroxide passivation layer on iron surface (Matheson and Tratnyek 1994; Farrell et al. 2000; Noubactep 2008; Greenlee et al. 2012; Kumar et al. 2014a) and decrease significantly the reduction efficiency (Szecsody et al. 2000). This can be explained by a decrease of the porosity of the shell, impeding the diffusion of the pollutant and iron corrosion products (Crane and Scott 2012). In addition, the more rapid formation of a less conductive iron oxide due to the oxidation of Fe_3O_4 in Fe_2O_3 or FeOOH, notably lepidocrocite γ-FeOOH (Haneda and Morrish 1977; Greenwood and Earnshaw 1997; Huang and Zhang 2005; Reinsch et al. 2010; Rebodos and Vikesland 2010; Greenlee et al. 2012; Liu et al. 2014a), will inhibit the electron transfer from iron core to the surface of the shell. A good knowledge of the chemical properties and the structural evolution of this oxide shell, i.e. the passivation mechanism, is therefore of crucial importance as they govern iron oxidation kinetics and degradation processes (Kumar et al. 2014a; Bae et al. 2018).

Several methods can be employed to characterize the fate and effects of iron particles in groundwater (Shi et al. 2015; Chekli et al. 2016a; Li et al. 2016c). First, direct methods consist in the analysis of solids to detect unequivocally the presence of iron-based particles. Direct characterization are mainly performed by microscopic – scanning electron microscopy (SEM) generally coupled with X-ray fluorescence analysis (XRF) or energy-dispersive spectroscopy (EDS), transmission electron microscopy (TEM), aberration-corrected scanning transmission electron microscopy (STEM), and scanning probe microscopy (SPM) – and spectroscopic techniques – X-ray photoelectron spectroscopy (XPS), dynamic light scattering (DLS), Mössbauer spectroscopy, electron energy-loss spectroscopy (EELS) and inductively coupled plasma mass spectrometry (ICP-MS) – X-ray diffraction (XRD), X-ray adsorption spectroscopy (XAS), 3D

tomography or by using radiolabeled particles (Nurmi et al. 2005; Sun et al. 2006; Sarathy et al. 2008; Baer et al. 2008; Ling and Zhang 2014a, b, 2017; Filip et al. 2014; Chekli et al. 2016b). Indirect methods consist in the characterization on changes of the water chemistry solution, in order to determine the impacted zone resulting from the introduction of the particles (Shi et al. 2015). Corrosion potential, total iron, dissolved oxygen and iron concentration, the rate of hydrogen production or the use of probes to monitor pH, oxidation-reduction potential (ORP), conductivity and dissolved oxygen (DO) are good indicators of composition, structure, reactivity and mobility of ZVI (Elliott and Zhang 2001; Liu and Lowry 2006; Wei et al. 2010; Shi et al. 2011, 2015; Adeleye et al. 2013; Kocur et al. 2014; Velimirovic et al. 2014; Yu et al. 2014; Li et al. 2017d; Rodrigues et al. 2017a, 2019; Qin et al. 2018a). These methods can be used to investigate their aging in water in short and long-term time scales. For more practical field applications, development of other indirect characterization methods is necessary, such as the use of chemical redox probes, e.g. quinone (AQS) or indigo-5,5′-disulfonate (I2S), or geophysical methods (Noel et al. 2013; Orsetti et al. 2013; Shi et al. 2015; Flores Orozco et al. 2015; Fan et al. 2015, 2016a). In addition, a conservative tracer, such as bromide ions, can be used to give supporting information on the mobility of the particles (He et al. 2010; Bennett et al. 2010).

In order to improve iron reactivity, development and use of nanoscale (and microscale) zero-valent iron particles were investigated in agreement with the great progress in nanoscale technologies. In parallel and for similar reason, the development and use of polymetallic particles was also studied.

3.2.2. Nanoscale and microscale particles

Studies were rapidly focused on the development of nanoscale particles (nZVI particles, $10 < d < 100$ nm) mainly for source zone targeted injection. Intrinsic characteristics, reactivity and aging of nZVI particles are strongly impacted by their synthesis conditions (Liu et al. 2005b; Hwang et al. 2011; Kim et al. 2012; Han et al. 2015). Various physical and chemical methods of synthesis are reported (Stefaniuk et al. 2016). nZVI particles are generally prepared from a bottom-up approach (formation of nanomaterials from atoms/molecules) by the reduction of dissolved iron species – Fe(II) or Fe(III) salts – using sodium borohydride $NaBH_4$ (Wang and Zhang 1997) or sodium dithionite (Kozma et al. 2016). It is also possible to use $NaBH_4$ in presence of nZVI particles to disintegrate them into much smaller particles (Bae et al. 2016). It is important to note that the degree of purity of iron source may impact the reactivity of nZVI particles, which can exhibit hydrodechlorination activities when traces element such as nickel are present (Balda and Kopinke 2020). The top-down approach (breaking down of bulk materials such as ball milling) can also be used to create nanomaterials by physical or chemical methods, such as milling or etching (Li et al. 2009; Mu et al. 2017). The third route for nZVI production is the thermal reduction, which consists in the reduction of iron oxide precursor in hydrogen at high temperature. Direct electrochemical synthesis of nZVI with ultrasonication appears as a promising process for an economic and large-scale production (Chen et al. 2004; Iranzo et al. 2015). Finally, green synthesis by using food industry wastes of leaf extracts have been recently reported (Kharissova et al. 2013; Machado et al. 2015; Kozma et al. 2016; Saif et al. 2016). The use of vacuum annealing at 500 °C after the synthesis led to the formation of a thin, uniform and conductive oxide shell, which may be responsible for the improvement of the reactive lifetime of nZVI particles. Compared to granular ZVI, nZVI particles is much expensive, with an estimated cost of commercial particles ranging from $80 to $238 per kg in 2012 (Zhao et al. 2016). nZVI particles are generally commercialized in water-slurry form or as air-stable particles, as the pyrophoricity of “bare” nZVI particles requires precautions for their transport and storage.

The increase in the reactivity of nZVI particles was mainly attributed to the increase in the specific surface area, which provide a greater number of active sites on which reactions occur (Xie and Cwiertny 2010; Amir and Lee 2011). Specific surface areas of nZVI particles are generally reported in the range 20-55 $m^2 \cdot g^{-1}$ (Wang and Zhang 1997; Zhang 2003; Zhang and Elliott 2006; Shih et al. 2011b). However, the specific surface area can be dramatically decreased by the vacuum annealing, if performed (Scott et al. 2010). As illustrated in Figure **6.2**, the lower the particle size, the higher the specific surface area. Also, particles mobility increases as their size decreases (Tratnyek and Johnson 2006). Depending on particles size, sticking coefficient (defined as the ratio of the rate of adsorption to the rate at which the adsorptive strikes the total surface), and environmental conditions, transport distances range from millimeters to centimeters (Tratnyek and Johnson 2006).

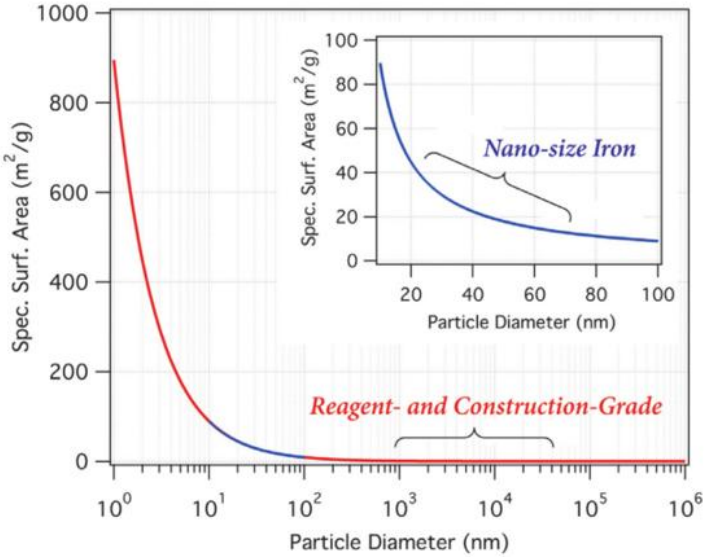

Figure 6.2. Evolution of specific surface area of iron particles depending on the diameter, calculated from diameter assuming spherical geometry and density of 6.7 $g \cdot cm^{-3}$ (average of densities for pure Fe^0 and Fe_3O_4) (from Tratnyek and Johnson 2006).

More recently, microscale zero-valent iron (mZVI) particles (diameter < 100 µm) have been used because of the high cost of nZVI particles and their very fast corrosion rate with water (Liu et al. 2005b; Liu and Lowry 2006; Li et al. 2006b; Noubactep et al. 2012), resulting in a rapid depletion of Fe^0 and a limited degradation efficiency in field application (Noubactep and Caré 2010; Comba et al. 2011b). Specific surface areas of microparticles are generally lower than 2 $m^2\ g^{-1}$ (Wang and Zhang 1997; Lien and Zhang 2001). However, the reactivity is not only linked to the specific surface area but also the chemical composition and presence of impurities on the surface, such as carbon, oxygen, sulfur or boron content (Lin and Lo 2005; Velimirovic et al. 2013a, 2017). Standardized experiments have shown that the specific reaction rate constant (k_{SA}) for COCs degradation with mZVI particles are in the same order of magnitude than those obtained with nZVI particles, while iron corrosion occurs slowly (Velimirovic et al. 2013b, 2014). Indeed, it is noted that galvanic corrosion exists between Fe^0 (anode) and iron corrosion products (cathode), as they exhibit more noble potentials (Wilhelm 1988; Zhang 2011). Consequently, the ratio between cathodic and anodic sites is less important for microscale than for nanoscale particles, resulting in lower local current densities and the increase in their reactive lifetime. In addition, higher oxidant yields can be obtained with mZVI particles (Lee et al. 2014; Ma et al. 2016). Compared to nZVI particles, the cost of commercial mZVI particles ranges from $2 to $11 per kg (Zhao et al. 2016).

A limitation to the use of nZVI and mZVI particles is respectively the aggregation and the sedimentation phenomena, resulting in a rapid decrease in specific surface area, reactivity and mobility (Phenrat et al. 2007; Hotze et al. 2010). To mitigate aggregation/sedimentation, surface modification was investigated such as to provide electrostatic and/or steric forces that counter interparticle magnetic attractive forces and thereby increase the stability (Wiesner and Bottero 2007; Phenrat et al. 2008). Surface modification includes the use of a stabilizer during the synthesis of the particles or after the synthesis by simply dispersing the particles (Zhao et al. 2016). Various polymers/polyelectrolytes or mixture of polymers can be used, such as starch (He and Zhao 2005), carboxymethyl cellulose (He and Zhao 2007; Dong et al. 2011), guar gum and xanthan gum (Tiraferri et al. 2008; Comba et al. 2011a; Xue and Sethi 2012), butyl methacrylate or polymethacrylic acid (Sirk et al. 2009), poly(4-styrenesulfonate) (Hydutsky et al. 2007), polymethylmethacrylate or polyacrylic acid (Laumann et al. 2013; Wang et al. 2013; Colombo et al. 2015), polyethylene glycol (San Román et al. 2016), agar agar (Velimirovic et al. 2016), polyphosphate (Kim et al. 2017a), polyethylenimine (Lin et al. 2018) or copolymers (Wang et al. 2017). The use of emulsified nZVI with a hydrophobic membrane is also reported and applied in field experiments (Quinn et al. 2005; Borden 2007; Berge and Ramsburg 2009). In addition, particles can be supported on a solid (Fang et al. 2018b), such as bentonite (Su et al. 2011), activated carbon such as Carbo-Iron (Mackenzie et al. 2012), zeolite, carbon nanotubes (Xu et al. 2013), membranes/resins (Xu and Bhattacharyya 2006; Ni and Yang 2014; Zhou et al. 2016), mesoporous silica (Sun et al. 2017), cellulose nanocrystal (Bossa et al. 2017) or clay (Ezzatahmadi et al. 2017; Su et al. 2017). The use of activated carbon as support can promote the sorption of hydrophobic pollutants to reduce the aqueous concentration of the pollutant, and the interspecies electron transfer for the remediation process (Liu et al. 2012).

In addition to rheological characterization (Han et al. 2016a), zeta potential measurements are good indicators of the stability of the particles. Stabilizers and supports are also known to enhance the mobility of nZVI and mZVI particles to a few meters in porous sand media and in heterogeneous aquifer sediment in column (Hydutsky et al. 2007; Li et al. 2016b; Kumar et al. 2017) and field experiments (Johnson et al. 2013; Kocur et al. 2014; Busch et al. 2015), as confirmed by rheological characterization (Gastone et al. 2014). It has been possible to observe high mobility of particles at low particles concentration (< 30 mg L^{-1}) (Schrick et al. 2004; He et al. 2007; Saleh et al. 2008). However, surface modification is reported to highly affect iron reactivity by site blocking, mass transfer inhibition and interfacial concentration decrease (Saleh et al. 2007; Phenrat et al. 2009a; Velimirovic et al. 2012, 2016). It is therefore important to investigate the best compromise between concentration of surface modifier and iron available surface for reduction, such as experimentations performed by Wang et al. (2015) for 2,4-dichlorophenol dechlorination.

3.2.3. Polymetallic particles

To improve ZVI reactivity, especially for the dechlorination of low molecular weight chlorinated hydrocarbons, the use of polymetallic particles (nano and microscale) has been studied. Iron particles are generally coated with a second metal by its reduction on iron surface in an ethanol solution (Wang and Zhang 1997). Other techniques include radiolysis, mechanical alloying method, electrochemical synthesis and green synthesis (Smuleac et al. 2011; Liu et al. 2014b; Luo et al. 2016; Weng et al. 2017). Generally, the second metal is scattered as small clusters on the surface of the particles (Yan et al. 2013; Ling and Zhang 2014c).

The use of a second metal more noble than iron ($E_M > E_{Fe}$) presents several advantages. It can (i) enhance the release of electrons at a faster rate by the formation of a galvanic cells in which the second metal acts

as the main cathode (Xu and Zhang 2000), (ii) prevent the formation of oxide film (Wang and Zhang 1997) and (iii) catalyze reactions with hydrogen (hydrodechlorination and hydrogenation reactions) (Schrick et al. 2002; Chaplin et al. 2012). Metals like palladium (Pd) and nickel (Ni) dissociate hydrogen produced by anaerobic iron corrosion to form highly reactive atomic hydrogen H^* at the surface of the particles (Kim and Carraway 2003; Li et al. 2017d). Cwiertny et al. (2006) suggest that bimetallic particles enhanced the dechlorination rates primarily by reactions with atomic hydrogen (hydrodechlorination), as the pseudo rate constants are correlated with the solubility of atomic hydrogen with each additive.

Muftikian et al. (1995) have first shown the efficiency of palladized iron for the dechlorination of C_1 and C_2 chlorinated compounds. Lien and Zhang (2007) have shown the catalytic effect of Pd deposited on iron particles for TCE reduction, with a rate constant 60 to 70 times higher than the rate obtained with traditional iron particles when the particles contain 1 to 5% by mass of Pd. Beyond, reaction rates decreased due to a diminution of iron active surface for TCE reduction, until showing an absence of reactions when Pd represents 50% or more of the particle. A similar effect has been observed for Ni/Fe, Ag/Fe or Cu/Fe particles for TCE or HCB dechlorination (Xu and Zhang 2000; Tee et al. 2005; Nie et al. 2013; Fang et al. 2018a).

Kim and Carraway (2003) have tested different bimetallic combinations for TCE dechlorination, and the particles can be classified in the following order, according to the specific surface area-normalized rate constant k_{SA}: Pd/Fe > Ni/Fe > Cu/Fe > Fe. Four noble metals – Pd, ruthenium (Ru), platinum (Pt) and gold (Au) – have also been studied by Lin et al. (2004), and the catalytic activity on the dechlorination of TCE is ranked in the order Pd ≫ Ru > Pt > Au. These results show the best overall catalytic effect on iron-based particles compared to zinc-based ones, and the highest constant rate is obtained with Pd for both metals. For the dechlorination of 1,1,1-trichloroethane, Cwiertny et al. (2006) have observed the following ranking: Ni/Fe ≈ Pd/Fe > Cu/Fe > Co/Fe > Au/Fe ≈ Fe > Pt/Fe. The authors suggest that these differences in ranking can be attributed to a different mechanism of reaction between unsaturated (e.g. chlorinated alkenes) and saturated (e.g. chlorinated alkanes) compounds.

Among all catalysts, Pd is more favorable due to its high efficiency in H^* generation, and its adsorption on Pd surface and its absorption into Pd crystal lattice, resulting in the formation of Pd hydride (Chaplin et al. 2012). Among the different hydrogen species, i.e. H^*_{abs}, H^*_{ads} and H_2 bubbles, H^*_{ads} is the only active hydrogen species in the catalytic hydrodechlorination process (Jiang et al. 2017; He et al. 2018b), and the presence of defects on Pd surface facilitates the efficient hydrodechlorination by H^*_{ads} (Liu et al. 2018). Another beneficial effect of this metal is the production of a smaller number of reaction intermediates, especially low chlorinated compounds such as DCE isomers and vinyl chloride (Zhang et al. 1998; Lowry and Reinhard 1999). This effect can be explained by the cleavage of C-Cl bonds at Pd surface (Park et al. 1997; Sriwatanapongse et al. 2006; He and Zhao 2008; Omar et al. 2011) and the formation of carbene intermediates. Heck et al. (2008) have observed with surface-enhanced Raman spectroscopy (SERS) the formation of C-Pd and Cl-Pd bonds, indicating that hydrodechlorination pathways (dechlorination by hydrogen) follow a sequence of dechlorination and hydrogenation. In addition, in presence of dissolved oxygen, the use of Pd or Ni can enhance the production of ROS, especially H_2O_2, to promote oxidation reactions (Lee and Sedlak 2008; Shih et al. 2016).

As for monometallic particles, the use of a stabilizer is highly recommended to prevent aggregation and enhance mobility of bimetallic particles (He et al. 2007; Basnet et al. 2013, 2015). The use of a support such as activated carbon can result in simultaneous adsorption and dechlorination process (Choi et al.

2008). The use of ultrasonic irradiation (20 kHz) during the synthesis of Pd/Fe or Ni/Fe nanoparticles can avoid agglomeration and improve nanoparticle disparity (Zhao et al. 2013, 2014). Trimetallic particles can also be synthesized, and appears to be more reactive than bimetallic particles due to synergistic effects between the different metals (Ghauch et al. 2011; Abazari et al. 2013; Sharma et al. 2016).

In 2009, about 30% of reductive remediation by ZVI were performed by bimetallic particles in the USA (Karn et al. 2009), while only regular nZVI particles were applied in Europe (Mueller et al. 2012). The main reasons are not technical but concern (i) the cost of the particles and the handling of the suspension and (ii) the toxicity of the catalyst, especially Ni which is considered as a priority substance in Europe. In addition, the significant improvement in degradation rates in field experiments has not been proven yet (Comba et al. 2011b; Xie and Cwiertny 2013), even if most studies were focused on the plume treatment (presence of dissolved compounds) and not on the source zone treatment (DNAPL).

3.2.4. Sulfidated particles

Sulfide species (e.g. Na_2S), dithionite $S_2O_4^{2-}$, thiosulfate $S_2O_3^{2-}$ or elemental sulfur can be used for the sulfidation of ZVI particles (Kim et al. 2011; Fan et al. 2013; Su et al. 2015; Gu et al. 2017; Bhattacharjee and Ghoshal 2018a), which is defined as their chemical modification by reducing sulfur compounds on iron surface. It is also possible to use directly sodium dithionite in combination with ZVI particles to extend the reactive lifetime of iron particles in alkaline conditions by dissolving and reducing Fe_2O_3 and $Fe(OH)_3$ layer to regenerate Fe(II) species (Xie and Cwiertny 2010). The addition of sodium dithionite or other soluble reductant to iron particles enhance reduction rates of dechlorination of chloromethanes, chloroethanes, chloroethenes and chlorobenzenes (Vermeul et al. 2000; Lee 2004; Brown 2010; Nunez Garcia et al. 2016).

Sulfidation is supposed to mimic the naturally-occurring microbial sulfate reduction in the subsurface (Shao et al. 2018). It results in the formation of a FeS_x layer which can mediate the aggregation of the particles, improve the hydrophobicity of the surface and enhance the electron transfer from Fe^0, thus resulting in the improvement of the reactivity for dechlorination. The S/Fe ratio, the sulfidation duration and the solution chemistry are three main operational variables that affect the structure and morphology of the particles (Han and Yan 2016; Fan et al. 2017; Li et al. 2017b; Kumar et al. 2018; Xu et al. 2019a), and thus their reactivity (Bhattacharjee and Ghoshal 2018a). Sulfidation is mainly used to improve the selectivity – or electron efficiency – towards the pollutant and the longevity of ZVI particles by decreasing the reactivity with water, i.e. the hydrogen evolution reaction (Rajajayavel and Ghoshal 2015; Fan et al. 2016c, b; He et al. 2018b; Li et al. 2018; Qin et al. 2018a; Xu et al. 2019b; He et al. 2020; Xu et al. 2020). Compared to bare nZVI or bimetallic particles, the main degradation mechanism is the direct electron transfer between the particles and the pollutant (Park et al. 2006; Rajajayavel and Ghoshal 2015; Li et al. 2016a; Han and Yan 2016; Cao et al. 2017; He et al. 2018b).

It has been shown in laboratory experiments that the use of sulfidated particles is a promising alternative to Pd/Fe bimetallic particles in terms of dechlorination efficiency, notably in the case of Fe^0-limited conditions (He et al. 2018b; Bhattacharjee and Ghoshal 2018a), which are expected at source zones in presence of DNAPL. Also, the cost of degradation is expected to be well reduced using sulfidated particles instead of Pd/Fe particles (Bhattacharjee and Ghoshal 2018a). But more field experiments are still required to confirm the results obtained in laboratory experiments (Nunez Garcia et al. 2020a, b). In addition, sulfidated particles are more efficient for the formation of ROS in aerobic conditions than unamended iron particles (Song et al. 2017; Rayaroth et al. 2017; Su et al. 2018), allowing the development of the technology in advanced oxidation processes and for wastewater treatment.

3.2.5. Toxicity

Potential risks of nZVI particles for *in situ* application in soils and groundwater remediation are still not clearly established (Nowack and Bucheli 2007; Grieger et al. 2010; Rajan 2011; Jang et al. 2014). Studies on other nanoscale materials, such as carbon nanotubes or fullerenes, have shown specific evidence for human and ecological risk, but iron nanoparticles are not as small, reactive, persistent or mobile (Reijnders 2006; Tratnyek and Johnson 2006). Despite this low mobility, the influence of ZVI can be expanded by the release and travelling of Fe^{2+}, thus affecting a more important zone.

The introduction of ZVI particles in the environment is responsible for a local change in biogeochemical conditions, thus affecting their fate, transport and reactivity, but also the microbial community activity and growth (Lowry et al. 2012; Jang et al. 2014; Wagner et al. 2014; Yirsaw et al. 2016). As for pollutants, the growth and transformation of the oxide shell can trap microbes, resulting in their quantitative removal from aqueous phase (Noubactep 2011). It is also suggested that the antimicrobial activity is dependent on the size and the dose of the particles, but also on the species (Fajardo et al. 2012; Velimirovic et al. 2015; Semerád and Cajthaml 2016; Gil-Díaz and Lobo 2018). As an example, a bactericidal effect on *Escherichia coli* was observed only for nanoscale particles (Lee et al. 2008), but a similar toxicity was observed for iron nanoparticles and iron filings to a TCE-degrading microbial community (Zabetakis et al. 2015). The adverse effects on microorganisms and plants can include physical damage, such as the disruption of the cell membrane architecture, or biochemical destruction, such as interference in energy transduction or oxidative stress due to the formation of ROS (Wiesner et al. 2006; Auffan et al. 2008; Keenan et al. 2009; Kim et al. 2010b; Chen et al. 2011; Fajardo et al. 2013; Fu et al. 2014b; Xie et al. 2017b; Ghosh et al. 2017). As previously mentioned, the formation of ROS, such as hydrogen peroxide (H_2O_2), superoxide radical ($^{\bullet}O_2^-$), hydroxyl radical ($^{\bullet}OH$) and Fe(IV) species, is the consequence of the oxidation of active Fe species (Fe^0 and Fe^{2+}) (He et al. 2016).

The aging of ZVI particles in water, i.e. their aggregation and the growth/transformation of iron oxides/hydroxides with time, and the use of stabilized ZVI by surface modification are likely to mitigate the cytotoxicity of nZVI particles (Phenrat et al. 2009b; Li et al. 2010; Dong et al. 2016a; Lefevre et al. 2016). The aging of bimetallic particles results generally in the deactivation of the catalyst by common groundwater solutes, e.g. sulfate and phosphate ions (Muftikian et al. 1996; Munakata and Reinhard 2007; Han and Yan 2014; Han et al. 2016c, 2018), and the gradual encapsulation of the second metal due to the growth of iron oxides/hydroxides shell (Zhu and Lim 2007; Yan et al. 2010b; Dong et al. 2018a), resulting in a progressive loss in removal efficiency and toxicity. However, the release in solution of the second metal by oxidative dissolution can also occur (Dong et al. 2018b). Sulfidated particles exhibit lower toxicity compared to bare ZVI particles, and their aging also decrease the toxicity (Cheng et al. 2019; Dong et al. 2019).

Some studies have highlighted the positive impact of the polymeric coating on iron particles due to a high bioavailability and synergetic effect with environment (He et al. 2010; Yan et al. 2013; Tosco et al. 2014b). The selection of the polymer, which can serve as a biostimulant, is therefore important in order to combine both abiotic and biotic degradation. Indeed, hydrogen is generally considered as the direct electron donor in anaerobic reductive dechlorination, and is typically produced from the anaerobic oxidation of carbon substrates (fermentation), such as organic acids or alcohols (Levin et al. 2004). In presence of iron-reducing bacteria (IRB), the reduction of Fe(III) in Fe(II) species can depassivate iron particles (Roden and Zachara 1996; Gerlach et al. 2000; Williams et al. 2005), which can result in the

reactivation of the particles for reductive dechlorination but also in the methylation or in the possible remobilization of entrapped pollutants such as metals and metalloids (Xie et al. 2017b).

More studies are still required to investigate the transformations in real environmental conditions with appropriate iron doses (Lowry and Casman 2009; Zhao et al. 2016; Lefevre et al. 2016; Lei et al. 2018), in combination with life cycle analysis (Lemming et al. 2012; Suchomel et al. 2014).

3.3. Combination of iron-based particles with other techniques

In field application, abiotic remediation processes cannot be considered separately from biotic processes (Brown et al. 2009; Koenig et al. 2016; Němeček et al. 2016; Wang et al. 2016; Cecchinc et al. 2017; You et al. 2017; Xu et al. 2017; Vogel et al. 2018). Indeed, iron particles have several effects on the microbial activity and growth. These effects are generally dose- and species-dependent and are influenced by the environmental conditions, and both synergetic and inhibitory effects are reported in the literature (Xie et al. 2017b). The production of H_2 resulting from iron corrosion can stimulate dehalorespiring bacteria (Bruton et al. 2015). In addition, the polymer coating used for the stabilization of the particles may act as a fermentable substrate (Kirschling et al. 2010, 2011; Kocur et al. 2015, 2016). However, some inhibitory effects of nZVI particles on sulfate reducing bacteria are also reported (Kumar et al. 2014b).

In addition, a lot of techniques can be used in combination to enhance ZVI technology (Jiang et al. 2018), such as physical enhanced technologies (e.g. ultrasonic assisted technology, UV-visible light, microwave, weak magnetic field) (Guan et al. 2015), the combination of nZVI particles with foam and electromagnetic induction as an alternative to ratio frequency heating (RFH) (Srirattana et al. 2017), advanced oxidation processes, e.g. modified Fenton process or ZVI-activated persulfate (Al-Shamsi and Thomson 2013; Fu et al. 2014a; Rybnikova et al. 2016), electrokinetic remediation (Fan et al. 2016d; Lima et al. 2017; Xiong et al. 2018) or the combination of ZVI with sulfite (Xie et al. 2017a) or with phytoremediation (Gong et al. 2018).

3.4. Stoichiometric requirement

Stoichiometric reductant demand (SRD) is defined as the mass (or mole) of a reductant theoretically required to obtain a complete dechlorination of a mass (or mole) of COCs, i.e. the formation of non-chlorinated hydrocarbons and free chloride ions. This notion is adapted from the stoichiometric oxidant demand (SOD), widely reported in the bibliography (Brown 2010; Lemaire et al. 2013b, a; Ranc et al. 2016). Its determination implies the knowledge of half-reactions of both oxidant (here COCs, see Table **6.5**) and reductant species. First, an equivalent weight for each oxidative and reducing reagent is calculated by dividing the molar mass by the number of electrons transferred in half-reactions (Table **6.7**).

$$\text{Equivalent weight} = \frac{\text{Molar mass}}{\text{Number of electrons transferred}} \qquad \text{(Eq. 6.35)}$$

The stoichiometric ratio can then be determined by dividing the equivalent weight of the reductant by the equivalent weight of the chlorinated organic compound (Eq. **6.36**). SRD is then calculated from the total mass of pollutant (dissolved, adsorbed and DNAPL).

$$\text{Stoichiometric ratio} = \frac{\text{Equivalent weight of reductant}}{\text{Equivalent weight of COC}} \qquad \text{(Eq. 6.36)}$$

Table 6.7. Example of equivalent weights for selected COCs and reductants.

Compounds	Formula	Products	Number of electrons transferred	Equivalent weight ($g \cdot g^{-1}$)
Carbon tetrachloride	CCl_4	CH_4	8	19.2
Chloroform	$CHCl_3$		6	19.9
Dichloromethane	CH_2Cl_2		4	21.2
Methyl chloride	CH_3Cl		2	25.2
Hexachloroethane	C_2Cl_6	C_2H_6	12	19.7
Pentachloroethane	C_2HCl_5		10	20.2
Tetrachloroethane	$C_2H_2Cl_4$		8	21.0
Trichloroethane	$C_2H_3Cl_3$		6	22.2
Dichloroethane	$C_2H_4Cl_2$		4	24.7
Chloroethane	C_2H_5Cl		2	32.3
Tetrachloroethylene	C_2Cl_4	C_2H_4	8	20.7
Trichloroethylene	C_2HCl_3		6	21.9
Dichloroethylene	$C_2H_2Cl_2$		4	24.2
Vinyl chloride	C_2H_3Cl		2	31.3
Hexachlorobenzene	C_6Cl_6	C_6H_6	12	23.7
Pentachlorobenzene	C_6HCl_5		10	25.0
Tetrachlorobenzene	$C_6H_2Cl_4$		8	27.0
Trichlorobenzene	$C_6H_3Cl_3$		6	30.2
Dichlorobenzene	$C_6H_4Cl_2$		4	36.8
Chlorobenzene	C_6H_5Cl		2	56.3
Sulfur species	S^{2-}	S^0	2	16.0
Iron	Fe^0	Fe^{2+}	2	27.9
Zinc	Zn^0	Zn^{2+}	2	32.7
Sodium dithionite	$Na_2S_2O_4$	-	2	87.1

For *in situ* application, the stoichiometric requirement is highly impacted by non-beneficial reactions (natural reductant demand, NRD), because of the presence of natural occurring oxidants such as water, dissolved oxygen or natural organic matter (Shi et al. 2015). Hence, higher dosage is generally necessary to reach a complete dechlorination, especially to compensate iron passivation and the adsorption/reduction of metal ions on iron surface. NRD is quite different from natural oxidant demand (NOD) because water is in large abundance in environmental conditions compared to indigenous oxidizable materials (Fan et al. 2016c). Hydrogen evolution rate (HER) can be measured by H_2 evolution or by using a colorimetric redox indicator (Fan et al. 2015).

Also, it is important to identify the corresponding oxidation equation depending on environmental conditions (equilibrium speciation, kinetically controlled metastable phases and spatial heterogeneity) (Tratnyek et al. 2014).

3.5. Reaction kinetics and chemical dechlorination pathways

3.5.1. Rate equations

In subsurface environment, COCs degradation kinetics are influenced by the rate of all abiotic degradation reactions previously reported (§2.4), e.g. the rate of hydrolysis, dehydrochlorination, reduction and oxidation reactions. The overall equation is:

$$r = r_{\text{hydrolysis}} + r_{\text{dehydrochlorination}} + r_{\text{reduction}} + r_{\text{oxidation}} \quad \text{(Eq. 6.37)}$$

where all rates r – assumed to occur independently and in parallel – are in mol L^{-1} s^{-1}. Table **6.8** lists combined hydrolysis and dehydrochlorination rate constants k at neutral and basic pH values for chlorinated methanes, ethanes and ethylenes at 25 °C (Jeffers et al. 1989). Hydrolysis and dehydrochlorination are very slow under most environmental conditions.

Table 6.8. Combined hydrolysis and dehydrochlorination rate constants k at neutral and alkaline pH values of chlorinated methanes, ethanes and ethylenes at 25 °C (from Jeffers et al. 1989). *Ea* represents the activation energy of the reaction.

Compounds	Neutral hydrolysis + dehydrochlorination		Alkaline hydrolysis + dehydrochlorination	
	k (min^{-1})	*Ea* (kJ mol^{-1})	k (min^{-1})	*Ea* (kJ mol^{-1})
CT	$3.26\ 10^{-8}$	114.5 ± 5.0	0.00	-
CF	$1.91\ 10^{-10}$	122.9 ± 13	$5.22\ 10^{-10}$	104.6 ± 8.0
HCA	0.00	-	$7.18\ 10^{-16}$	109.8 ± 20
PCA	$4.93\ 10^{-8}$	94.9 ± 2.9	$1.31\ 10^{-4}$	80.8 ± 10
1,1,1,2-TeCA	$2.60\ 10^{-8}$	94.9 ± 15	$2.15\ 10^{-9}$	100.3 ± 1.7
1,1,2,2-TeCA	$9.70\ 10^{-9}$	92.4 ± 3.2	$3.02\ 10^{-6}$	78.1 ± 1.0
1,1,1-TCA	$1.24\ 10^{-6}$	116.1 ± 2.0	0.00	-
1,1,2-TCA	$5.19\ 10^{-11}$	121.2 ± 5.9	$9.42\ 10^{-9}$	88.2 ± 7.5
1,1-DCA	$2.15\ 10^{-8}$	109.5 ± 3.3	$7.20\ 10^{-14}$	114.8 ± 2.0
1,2-DCA	$1.83\ 10^{-8}$	103.7 ± 10	$1.04\ 10^{-11}$	121.6 ± 6.1
PCE	0.00	-	$1.37\ 10^{-15}$	123.1 ± 9.4
TCE	0.00	-	$1.07\ 10^{-12}$	126.6 ± 4.7
1,1-DCE	0.00	-	$6.32\ 10^{-17}$	130.2 ± 20
1,2-DCE	0.00	-	$1.09\ 10^{-14}$	130.3 ± 3.9

COCs reduction by iron particles is a heterogeneous reaction. However, as to evaluate kinetic degradation, homogeneous equations are frequently used as a first approximation.

Homogeneous approach

Pseudo-orders with respect to the pollutant can be determined by using a great excess of iron particles, in order to consider a constant concentration in reactant. The concentration can thus be included in the rate constant:

$$k_{\text{obs}} = k * C_{ZVI}^{\beta} \quad \text{(Eq. 6.38)}$$

where k_{obs} is the observed rate constant, k is the rate constant, C_{ZVI} is the concentration in reactant (mol L^{-1}) and β is the order of reaction with respect to the reactant. The units of k_{obs} and k depend on the global reaction order: mol L^{-} s^{-1} for order zero, s^{-1} for order one and L mol^{-1} s^{-1} for order two.

In batch experiments, the rate equation can be written as:

$$r = -\frac{\mathrm{d}C}{\mathrm{d}t} = k_{\mathrm{obs}} * C^{\alpha} \qquad \text{(Eq. 6.39)}$$

where r is the rate of reaction (mol L^{-1} s^{-1}), C is the concentration in COC (mol L^{-1}), t is the time (s) and α is the order of reaction with respect to the COC.

Reduction of COCs by zero-valent iron can generally be described by pseudo-first order equations with respect to pollutant (Matheson and Tratnyek 1994; Burris et al. 1995; Arnold and Roberts 1998; Song and Carraway 2005):

$$\ln C = -k_{\mathrm{obs}} * t + \ln C_0 \qquad \text{(Eq. 6.40)}$$

where C_0 (mol L^{-1}) is the initial concentration in COCs. Other models derived from the pseudo first-order model, e.g. a two-compartment model, are also reported (Wang et al. 2013; Rodrigues et al. 2017a).

As reduction occurs on a surface, the observed rate constant depends on the concentration of active site on the surface, which is a function of the particle size. Therefore, a specific reaction rate constant k_{SA} can be calculated from k_{obs}, the specific surface area of particle a_{S} (m^2 g^{-1}) and the mass concentration of particles ρ_{M} (g L^{-1}).

$$k_{\mathrm{SA}} = \frac{k_{\mathrm{obs}}}{a_{\mathrm{S}} * \rho_{\mathrm{M}}} \qquad \text{(Eq. 6.41)}$$

Table **6.9** lists surface area normalized rate constants for the reductive dechlorination of COCs with iron-based particles. From the same chemical structure, dechlorination rates generally decreased as the number of chlorine atoms decreased, especially for bare ZVI. However, the use of k_{SA}-model cannot be generalized to compare the results from different studies as it is not depending only on the intrinsic reactivity of iron but also on the experimental conditions, for example mixing conditions in batch experiments or flow rate in columns (Noubactep 2009).

Table 6.9. Surface area normalized rate constants k_{SA} for COCs reductive remediation by zero-valent iron.

Reactant	Pollutant	k_{SA} (L m^{-2} h^{-1})	Reference
ZVI powder (0.057 m^2 g^{-1})	CT	$1.2\pm1.5\ 10^{-1}$	(Johnson et al. 1996)
	CF	$9.2\pm7.3\ 10^{-4}$	
	HCA	$3.1\pm3.3\ 10^{-2}$	
	1,1,1,2-TeCA	$1.4\ 10^{-2}$	
	1,1,2,2-TeCA	$1.3\ 10^{-2}$	
	1,1,1-TCA	$1.1\ 10^{-2}$	
	PCE	$2.1\pm2.7\ 10^{-3}$	
	TCE	$3.9\pm3.6\ 10^{-4}$	
	t-1,2-DCE	$1.2\pm0.4\ 10^{-4}$	
	c-1,2-DCE	$4.1\pm1.7\ 10^{-5}$	
	1,1-DCE	$6.4\pm5.5\ 10^{-5}$	
	VC	$5.0\pm1.5\ 10^{-5}$	
Aldrich ZVI (0.192 m^2 g^{-1})	CT	$1.0\ 10^{-4}$	(Lien and Zhang 1999)
ZVI nanoparticles (35 m^2 g^{-1})	CT	$5.31\ 10^{-4}$	
	CF	$8.41\ 10^{-5}$	
Pd/Fe nanoparticles	CT	$9.0\ 10^{-3}$	

(35 m² g^{-1})	CF	6.50 10^{-3}	
Pd/Fe nanoparticles (≈ 35 m² g^{-1})	PCE	12.2 10^{-3}	(Lien and Zhang 2001)
	TCE	18.2 10^{-3}	
	t-1,2-DCE	15.1 10^{-3}	
	c-1,2-DCE	17.6 10^{-3}	
	1,1-DCE	11.5 10^{-3}	
Pd/Fe nanoparticles (33.5 m² g^{-1})	HCA	2.0 10^{-2}	(Lien and Zhang 2005)
	PCA	2.6 10^{-2}	
	1,1,1,2-TeCA	2.1 10^{-2}	
	1,1,2,2-TeCA	8.8 10^{-3}	
	1,1,1-TCA	5.4 10^{-3}	
ZVI nanoparticles (27.9 m² g^{-1})	HCA	7.70 10^{-1}	(Song and Carraway 2005)
	PCA	7.96 10^{-1}	
	1,1,1,2-TeCA	5.38 10^{-1}	
	1,1,2,2-TeCA	3.03 10^{-2}	
	1,1,1-TCA	1.51 10^{-1}	
	1,1,2-TCA	2.31 10^{-3}	
	1,1-DCA	1.99 10^{-5}	
	1,2-DCA	< 4 10^{-6}	
ZVI microparticles (0.312 m² g^{-1})	CT	2.76±0.87 10^{-2}	(Onanong et al. 2007)
	CF	9.62±2.59 10^{-4}	
	DCM	1.82±0.53 10^{-5}	
	1,1,1,2-TeCA	2.98±0.71 10^{-2}	
	1,1,1-TCA	1.24±0.16 10^{-2}	
	1,1,2-TCA	9.30±0.84 10^{-4}	
	1,1,2-TCMP	1.36±0.16 10^{-3}	
	1,2,3-TCP	3.53±0.64 10^{-5}	
	1,2,3-TCMP	8.49±1.27 10^{-4}	
	1,2-DCMP	2.42±0.40 10^{-4}	
	2,2-DCP	7.16±0.83 10^{-4}	
	1,2-DCP	2.24±0.86 10^{-5}	
Pd/Fe nanoparticles (51.4 m^2 g^{-1})	CT	3.59 10^{-3}	(Wang et al. 2009c)
	CF	2.67 10^{-3}	
	DCM	3.54 10^{-5}	
Cu/Fe microparticles (2.21 m^2 g^{-1})	HCB	1.01±0.02 10^{-3}	(Yuan et al. 2010a)
	PeCB	0.15±0.01 10^{-3}	
	1,2,3,4-TeCB	0.14±0.11 10^{-3}	
	1,2,3,5-TeCB	0.11±0.04 10^{-3}	
	1,2,4,5-TeCB	0.08±0.03 10^{-3}	
	1,2,3-TCB	0.03±0.00 10^{-3}	
	1,2,4-TCB	0.03±0.00 10^{-3}	

Burris et al. (1995) have studied PCE and TCE dechlorination by iron particles in a multi-component experiment. If no competition between the two compounds seems to happen for the surface-reaction, competitive sorption has been observed, and pseudo first-order reduction reactions can be applied accounting for the high sorption to nonreactive sites. Arnold and Roberts (2000) have shown that the degradation rate of trans-1,2-DCE was inhibited by cis-1,2-DCE and acetylene. Dries et al. (2002) have noted that the presence of PCE or DCE did not influence TCE reduction by ZVI.

Although the use of the pseudo first-order is widely reported in the literature, Janda et al. (2004) reproach the possible risk of incorrect deductions about kinetics, as the reaction is heterogeneous and more complex than a simple surface reaction. Furthermore, first-order kinetics are observed at low initial concentrations of COCs, but a transition to zero-order kinetics can be observed at higher concentrations (Johnson et al. 1996), due to the saturation of reactive surface sites (Zepp and Wolfe 1987). In a batch system, the transition to constant kinetics can be described with the model (Johnson et al. 1996):

$$-\frac{\mathrm{d}[C]}{\mathrm{d}t} = \frac{r_{\mathrm{m}}[C]}{K_{1/2} + [C]} \qquad \text{(Eq. 6.42)}$$

where r_{m} is the maximum reaction rate for specific iron metal characteristics, and $K_{1/2}$ is the concentration of C at $\frac{r_m}{2}$.

Heterogeneous approach

Heterogeneous reactions imply the following steps:

1. Mass transfer of reactants to the surface of the metal particles;
2. Adsorption of the reactant onto the surface;
3. Reaction on the surface;
4. Desorption of the product;
5. Mass transfer of products to the fluid.

The overall reaction rate is determined by the slowest step, as the rate-determining step. Generally, diffusion processes require less energy than chemical reactions. Frequent values of activation energy for mass-transfer are in the range 15-30 kJ mol^{-1} (Lasaga 1981; Pilling and Seakins 1995).

Adsorption is a process where atoms or molecules of a liquid or gas phase are deposited on the surface of a solid. The process is governed by interactions of attraction between the solid (also called adsorbent) and molecules (also called adsorbate). Two types of adsorption are possible:

- Physical adsorption involving weak electrostatic forces such as Van der Waals forces or hydrogen bond. This is usually a reversible phenomenon;
- Chemical adsorption involving strong bonds such as covalent bonds (Montgomery 1985), resulting in an electron transfer and a significant change in the structure of the adsorbed molecule. Thus, contrary to the physical adsorption, chemisorption is a less reversible phenomenon.

Different models are used to characterize adsorption of COCs on iron particles or soils, like the linear model, the Freundlich isotherm and the Langmuir isotherm (Burris et al. 1995, 1998; Dries et al. 2004, 2005). It is however important to note that these adsorption isotherms are only representative for a given oxide shell, and do not reflect the dynamic evolution of the oxide shell until Fe^0 is depleted (Noubactep 2010a).

Linear model

The linear model assumes a linear relationship between the concentration of dissolved solute C (g L^{-1}) and the solute concentration adsorbed on the solid C^* (g kg^{-1}):

$$C^* = K * C \quad \text{(Eq. 6.43)}$$

where K is the partition coefficient (L kg^{-1}).

Freundlich isotherm

Freundlich isotherm is a non-linear empirical relationship between the amount of solute on the surface of the adsorbent and the amount of solute in the solution in contact with the adsorbent (Eq. **6.44**).

$$\frac{x}{m} = k * C^{\frac{1}{n}} \quad \text{(Eq. 6.44)}$$

where $\frac{x}{m}$ represents the ratio between the mass of adsorbate and the mass of adsorbent (mg g^{-1}), C is the concentration of the solute in solution at equilibrium (mg L^{-1}), and k and n are empirical constants.

Langmuir isotherm

The Langmuir isotherm is based on different assumptions, which are:

- the adsorbent surface is contacted with a solution containing an adsorbate A;
- there is a specific number of adsorption sites on the surface;
- adsorption is monolayer and there is no interaction between adsorbed molecules.

It was developed initially to describe the adsorption of a gas on a solid but is used by analogy for the adsorption of a liquid to a solid.

According to the relation:

$$\mathrm{A} + \mathrm{S} \leftrightarrow \mathrm{AS} \quad \text{(Eq. 6.45)}$$

where A is the adsorbate, S the adsorbent and AS represents a molecule adsorbed on a site of S.

The adsorption equilibrium constant $K_{\mathrm{ads,A}}$ is expressed as:

$$K_{\mathrm{ads,A}} = \frac{C_{\mathrm{AS}}}{C_{\mathrm{A}} * C_{\mathrm{S}}} \quad \text{(Eq. 6.46)}$$

This relation can be expressed with θ_{A}, the fractional occupancy of the adsorption sites by the adsorbed species A:

$$\frac{C_{\mathrm{AS}}}{C_{\mathrm{A}}} = \frac{\theta_{\mathrm{A}}}{1 - \theta_{\mathrm{A}}} \quad \text{(Eq. 6.47)}$$

Thus,

$$K_{\mathrm{ads,A}} = \frac{\theta_{\mathrm{A}}}{C_{\mathrm{A}} * (1 - \theta_{\mathrm{A}})} \quad \text{(Eq. 6.48)}$$

Finally, the Langmuir isotherm equation is:

$$\theta_{\mathrm{A}} = \frac{K_{\mathrm{ads,A}} * C_{\mathrm{A}}}{1 + K_{\mathrm{ads,A}} * C_{\mathrm{A}}} \quad \text{(Eq. 6.49)}$$

When different molecules are adsorbed, the fractional coverage of component i is given by:

$$\theta_{\mathrm{i}} = \frac{K_{\mathrm{ads,i}} * C_{\mathrm{i}}}{1 + \sum_{\mathrm{j=1}}^{\mathrm{n}} (K_{\mathrm{ads,j}} * C_{\mathrm{j}})} \qquad \text{(Eq. 6.50)}$$

From Langmuir adsorption model**,** Hinshelwood developed a model, known as Langmuir-Hinshelwood mechanism, to include heterogeneous reactions, considering the uniform reaction of an adsorbed molecule on the surface. For a monomolecular reaction, the Langmuir-Hinshelwood relation is:

$$r = k * \theta_{\mathrm{A}} = \frac{k * K_{\mathrm{ads}} * C}{1 + K_{\mathrm{ads}} * C} \qquad \text{(Eq. 6.51)}$$

where *k* is the constant rate of the limiting step.

For a bimolecular reaction, the relation is:

$$r = k * \theta_{\mathrm{A}} * \theta_{\mathrm{B}} = \frac{k * K_{\mathrm{ads,A}} * C_{\mathrm{A}} * K_{\mathrm{ads,B}} * C_{\mathrm{B}}}{(1 + K_{\mathrm{ads,A}} * C_{\mathrm{A}} + K_{\mathrm{ads,B}} * C_{\mathrm{B}})^2} \qquad \text{(Eq. 6.52)}$$

The Langmuir-Hinshelwood-Hougen-Watson (LHHW) model provides a more explicit approach, in terms of surface concentration instead of volume concentration. The general equation is:

$$r = \frac{\text{kinetic factor} * \text{ driving force}}{\text{adsorption expression}} \qquad \text{(Eq. 6.53)}$$

Arnold and Roberts (2000) used adaptation of LHHW models for the reduction of chlorinated ethylenes and acetylenes by ZVI in batch system, with an irreversible surface-reaction step. Different rate relations are expressed depending on the rate-determining step (Table **6.10**).

Table 6.10. LHHW models used by Arnold and Roberts (2000) for the reduction of chlorinated ethenes and chlorinated acetylenes by ZVI.

Rate-determining step	Rate equation
Adsorption	$\frac{\mathrm{d}C_{\mathrm{i}}}{\mathrm{d}t} = -\frac{\left(\sum_{\mathrm{j=1}}^{\mathrm{N_j}} k_{\mathrm{ij}}^{\mathrm{a}} S_{\mathrm{t}}\right) C_{\mathrm{i}}}{1 + \sum_{\mathrm{m\neq i}}^{\mathrm{N_m}} K_{\mathrm{m}} C_{\mathrm{m}}} = -k_{\mathrm{obs}} * C_{\mathrm{i}}$
Surface-reaction	$\frac{\mathrm{d}C_{\mathrm{i}}}{\mathrm{d}t} = -\frac{\left(\sum_{\mathrm{j=1}}^{\mathrm{N_j}} k_{\mathrm{ij}}^{\mathrm{s}} S_{\mathrm{t}}\right) K_{\mathrm{i}} C_{\mathrm{i}}}{1 + \sum_{\mathrm{m\neq i}}^{\mathrm{N_m}} K_{\mathrm{m}} \mathrm{C_m}} = -k_{\mathrm{obs}} * C_{\mathrm{i}}$
Desorption	$\frac{\mathrm{d}C_{\mathrm{i}}}{\mathrm{d}t} = -(\sum_{\mathrm{j=1}}^{\mathrm{N_j}} k_{\mathrm{ij}}^{\mathrm{d}} S_{\mathrm{t}})$

k is the kinetic constant, superscript *a* refers to adsorption constant ($\mu M^{-1} h^{-1}$), superscript *s* to surface-reaction constant (h^{-1}) and superscript *d* to desorption constant (h^{-1}); *C* is the aqueous concentration (μM); S_t is the abundance of reactive sites per liter of solution (μM); *K* is an adsorption constant (μM^{-1}); N_i is the total number of primary products formed directly from the parent; N_m is the total number of species that inhibit the reaction of the parent.

Except for the degradation of vinyl chloride in ethylene, and ethylene in ethane which were modeled as adsorption limited reactions, all transformations were modeled as surface-reaction limited reactions (Arnold and Roberts (2000) – Table **6.11**).

Table 6.11. Model-derived kinetic parameters for chlorinated ethylenes and related species in the absence of interspecies competitors (from Arnold and Roberts 2000). Values are for 0.25 g Fe^0/160 mL buffer solution.

Parent	Product	($k^S S_t$) (μM h^{-1})	K (μM^{-1})
PCE	TCE	3.63 (±0.52) 10^{-3}	0.058 (±0.014)
PCE	Dichloroacetylene	2.48 (±0.46) 10^{-2}	0.058 (±0.014)
TCE	trans-DCE	7.72 (±9.68) 10^{-4}	0.065 (±0.009)
TCE	cis-DCE	5.91 (±0.53) 10^{-3}	0.065 (±0.009)
TCE	1,1-DCE	4.42 (±0.49) 10^{-3}	0.065 (±0.009)
TCE	Chloroacetylene	0.33 (±0.03)	0.065 (±0.009)
trans-DCE	VC	5.32 (±15.1) 10^{-2}	0.016 (±0.002)
trans-DCE	Acetylene	4.42 (±0.45)	0.016 (±0.002)
cis-DCE	VC	0.14 (±0.06)	0.029 (±0.003)
cis-DCE	Acetylene	2.18 (±0.15)	0.029 (±0.003)
1,1-DCE	Ethylene	3.72 (±0.25)	0.016 (±0.002)
Acetylene	Ethylene	11.51 (±1.24)	0.109 (±0.022)
Chloroacetylene	Acetylene	6.46 (±0.94)	0.261 (±0.086)
Dichloroacetylene	cis-DCE	1.02 (±1.34)	0.051 (±0.014)
Dichloroacetylene	trans-DCE	2.96 (±1.27)	0.051 (±0.014)
Dichloroacetylene	Chloroacetylene	12.97 (±2.46)	0.051 (±0.014)
Parent	**Product**	**($k^a S_t$) (h^{-1})**	
VC	Ethylene	6.55 (±0.93) 10^{-2}	
Ethylene	Ethane	2.15 (±0.25) 10^{-2}	

Predictive tools based on the molecular properties of each chlorinated solvent can be used to estimate the reactivity depending on the reductant system. These relations, known as quantitative structure activity relationships (QSARs) or linear free energy relationships (LFERs), are developed from one- and two-electron reduction potentials (E_1 and E_2), the lowest unoccupied molecular orbital energy (E_{LUMO}), the energy gap between LUMO and HOMO (E_{GAP}) or the vertical attachment energy VAE, bond strength E_B/carbon-chlorine bond dissociation energy $E_{C\text{-}Cl}$ and attachment rate constant (ARC). Table **6.12** lists the predictive relationship established for COCs dechlorination by zero-valent iron. Other relationships have been proposed for other reductant systems (Perlinger et al. 2000; Tratnyek et al. 2003; Huang et al. 2016a).

Table 6.12. Predictive relationship for the reactivity of COCs by zero-valent iron.

COCs	Relation	Reference
Chloromethanes, chloroethanes, chloroethenes	$\log k_{SA} = -1.5(\pm 0.1)E_{LUMO} - 5.7(\pm 0.2)$ (R^2 = 0.83) $\log k_{SA} = 2.8(\pm 0.2)E_1 - 1.8(\pm 0.1)$ (R^2 = 0.81)	(Scherer et al. 1998)
Chloroethenes (hydrogenolysis)	$\log(k^S S_t) = -15.05(\pm 14.62)E_2 + 6.04(\pm 7.67)$ (R^2 = 0.709)	(Arnold and Roberts 2000)
Chloroethenes (β-elimination)	$\log(k^S S_t) = -30.68(\pm 29.38)E_2 + 17.95(\pm 17.48)$ (R^2 = 0.865)	
Overall reactivity	$\log(k^S S_t) = -3.91(\pm 2.07)E_1 - 2.81(\pm 1.51)$ (R^2 = 0.898)	
TCE, carbon tetrachloride	$\log k_{SA} = -26(\pm 12)E_{LUMO} + 4(\pm 1.3)$ (R^2 = 0.77)	(Miehr et al. 2004)
Chloroethanes	$\ln(1/k_{SA}) = -3.7947\ E_1 + 4.3988$	(Lien and Zhang 2005)

	(R^2 = 0.5983) $\ln(1/k_{SA}) = 0.2226\,E_B - 11.584$ (R^2 =0.8092)	
Chloroethanes	$\log k_{SA} = 8.21(\pm1.20)E_1 - 0.996(\pm0.228)$ (R^2 = 0.903) $\log k_{SA} = -3.48(\pm0.28)E_{LUMO} - 8.73(\pm0.64)$ (R^2 = 0.97)	(Song and Carraway 2005)
Chloromethanes	$\log k_{SA} = -1.95(\pm0.02)E_{LUMO} + 3.42(\pm0.07)$ (R^2 = 1.000) $\log k_{SA} = -2.61(\pm0.17)\mathrm{VAE} - 2.05(\pm0.11)$ (R^2 = 0.996) $\log k_{SA} = 0.73(\pm0.09)\mathrm{ARC} - 3.10(\pm0.81)$ (R^2 = 0.968) $\log k_{SA} = 1.16(\pm0.12)\mathrm{ECD} - 3.89(\pm0.15)$ (R^2 = 0.979)	(Onanong et al. 2007)
Chloroethanes, chloropropanes	$\log k_{SA} = -1.65(\pm0.25)E_{LUMO} + 3.79(\pm1.03)$ (R^2 = 0.860) $\log k_{SA} = -2.26(\pm0.49)\mathrm{VAE} - 0.57(\pm0.56)$ (R^2 = 0.768) $\log k_{SA} = 0.88(\pm0.24)\mathrm{ARC} + 5.28(\pm2.31)$ (R^2 = 0.717) $\log k_{SA} = 0.94(\pm0.16)\mathrm{ECD} - 3.23(\pm0.14)$ (R^2 = 0.835)	
Chloromethanes, chloroethanes	$\log k_{obs} = -0.13(\pm0.12)\mathrm{D_{RX}} + 36(\pm40)$ (R^2 = 0.599) $\log k_{obs} = 14(\pm7)E_1 + 3.9(\pm0.8)$ (R^2 = 0.848)	(Cwiertny et al. 2010)

Units: k_{SA} in L m^{-2} h^{-1}, E_{LUMO} and VAE in electronvolt (eV), E_1 and E_2 in V, k^sS_t in μM h^{-1}, E_B in kcal mol^{-1}, ARC in cm^3 s^{-1}, ECD = Electron Capture Detector response, D_{RX} = gas phase hemolytic carbon-chlorine bond dissociation energy (kJ mol^{-1}).

3.5.2. Degradation pathways

Mechanistic studies of chemical reduction by zero-valent metals have shown a preferential tendency to β-elimination for compounds with α,β-pairs of chlorine atoms (Arnold et al. 1999), while hydrogenolysis and α-elimination are two competitive reactions for compounds with α-position chlorine atoms (Vogel et al. 1987; Fennelly and Roberts 1998; Song and Carraway 2005). For example, reductive β-elimination of chlorinated alkanes results in the formation of chlorinated alkenes, and reductive α-elimination and hydrogenolysis results in the formation of less chlorinated alkanes.

A summary of the general pathway of reduction of chlorinated ethanes and ethylenes is shown in Figure **6.3**. Highly chlorinated ethanes preferentially react via β-elimination rather than hydrogenolysis. The predominant chlorinated intermediate of HCA is PCE (Lien and Zhang 2005), and trace amounts of PCA can be observed with iron nanoparticles (Song and Carraway 2005). Different pathways are proposed to explain the formation of the carbon-carbon double bond. Mechanistic studies via computational or experimental electrochemistry have indicated that the dominant reaction proceeds by two successive single-electron transfer steps, while an alternative pathway involves the formation of

trichloromethylchlorocarbene, pentachloroethyl anion or pentachloroethyl radical as intermediates (Patterson et al. 2001; Huang et al. 2012; Pizarro et al. 2018).

PCA reacts to form mainly TCE and traces of PCE, while 1,1,1,2-TeCA is mainly transformed to 1,1-DCE, with small proportions of TCE obtained (Lien and Zhang 2005; Song and Carraway 2005). PCA can also react rapidly by dehydrochlorination to form PCE (Roberts and Gschwend 1991).

The reductive elimination of 1,1,2,2-TeCA results in the formation of two isomers of DCE, cis-DCE and trans-DCE, in a ratio 4.5:1 for iron metal reactant. The predominant formation of Z-isomer can be explained by the reactivity of the intermediate formed in iron or iron oxide surface. Also, formation of TCE by dehydrochlorination and of 1,1,2-TCA by hydrogenolysis have been observed (Arnold et al. 2002).

1,1,1-TCA and 1,1-DCA reduction only involves α-elimination and hydrogenolysis. Experimental reports have shown that reduction of 1,1,1-TCA occurs via hydrogenolysis to form 1,1-DCA, and via concerted pathways of α-elimination and hydrogenolysis to ethane (Fennelly and Roberts 1998; Song and Carraway 2005). Degradation of COCs in a surface-mediated process results in the formation of transition species like hydrocarbon moieties, in particular alkyls, carbenes, carbenoids and carbynes (Baltruschat et al. 1993; Bent 1996; Müller et al. 1997). Thus, Lien and Zhang (2005) proposed that the formation of surface ethylidyne on Pd/Fe particles can explain the direct reduction of 1,1,1-TCA in ethane.

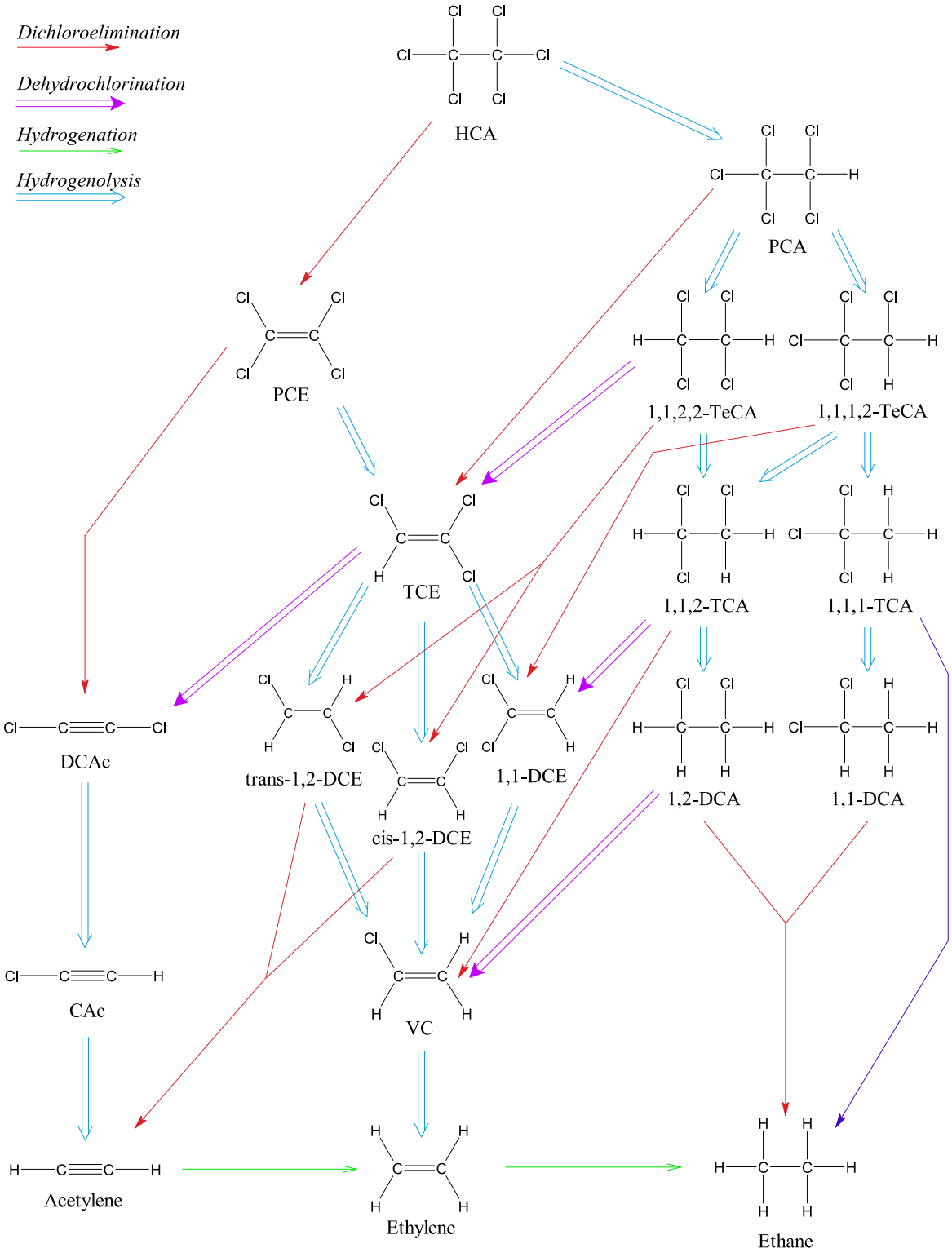

Figure 6.3. Reductive dechlorination pathways of HCA by ZVI.

Due to the presence of an α,β-pair of chlorine atoms, 1,1,2-TCA and 1,2-TCA are susceptible to react mainly via β-elimination. However, production of vinyl chloride from 1,1,2-TCA has not been observed

with iron nanoparticles, so vinyl chloride must react rapidly to form ethane. Similarly, production of ethane from 1,2-TCA has not been proven (Song and Carraway 2005). However, these two pathways are strongly suspected to occur with iron particles, as a same mechanism have been reported with zinc particles (Arnold et al. 1999).

Reduction of chlorinated ethylenes undergoes successive hydrogenolysis pathways. PCE is successively transformed into TCE, DCE isomers (1,1-DCE, cis-1,2-DCE or trans-1,2-DCE), then vinyl chloride and finally ethylene (Vogel et al. 1987; Orth and Gillham 1996). Roberts et al. (1996) highlighted the reductive elimination of trans- and cis-1,2-DCE, resulting in the formation of acetylene as an intermediate of the production of ethylene, and small amounts of vinyl chloride and ethane have been observed. Conversely, 1,1-DCE and vinyl chloride only react to ethylene and ethane. Later, Arnold and Roberts (2000) have shown that PCE and TCE can also react by β-elimination to dichloroacetylene and chloroacetylene respectively. The authors proposed that the production of dichloroacetylene results from a mono-σ-bonded vinyl intermediate at iron surface, whereas the formation of TCE results from a mono-σ-bonded alkyl intermediate.

Dichloroacetylene reacts then via successive hydrogenolysis to chloroacetylene and acetylene, with possible formation of ethylene and ethane as final products (Arnold and Roberts 2000). Dechlorination by bimetallic particles involving indirect reduction with adsorbed atomic hydrogen on the catalyst surface results in a higher formation of saturated hydrocarbons instead of unsaturated hydrocarbons, and less accumulation of chlorinated byproducts. Therefore, ethane is the major degradation end product of reduction of chlorinated ethylenes by bimetallic particles (Schreier and Reinhard 1995; Lien and Zhang 2001, 2007; Schrick et al. 2002; Tee et al. 2005). Coupling reaction of acetylene, dichloroethyl radicals or carbenoids in C_4 compounds, and traces of C_3, C_5 and C_6 compounds, have also been reported (Fennelly and Roberts 1998; Arnold and Roberts 2000).

A summary of the general pathway of reduction of chlorinated benzenes is shown in Figure **6.4**. Reduction of chlorinated benzenes by ZVI undergoes hydrogenolysis. Hexachlorobenzene is firstly transformed into pentachlorobenzene. Pentachlorobenzene reacts to form 1,2,3,4-TeCB and 1,2,3,5-TeCB, and the end product is 1,2,4-TCB. No other chlorobenzenes have been observed by Shih et al. (2009). In a later study, the authors have shown the production of three tetrachlorobenzene isomers, i.e. 1,2,3,4-TeCB, 1,2,3,5-TeCB and 1,2,4,5-TeCB, two trichlorobenzene isomers, i.e. 1,2,3-TCB and 1,2,4-TCB, and the end product is 1,2-DCB (Shih et al. 2011b).

The nature of the catalyst on bimetallic particles has an effect on the byproduct distribution. With Ag/Fe particles, the main dechlorination pathway is the formation of 1,2,4,5-TeCB and 1,2,4-TCB (Xu and Zhang 2000; Nie et al. 2013). With Pd/Fe particles, results obtained by Shih et al. (2009) have shown the production of the three tetrachlorobenzene isomers, 1,2,4-TCB and 1,3,5-TCB, and 1,4-DCB, as end products. With Cu/Fe particles, Zhu et al. (2010) have observed the formation of PeCB, the three TeCB isomers, 1,2,3-TCB and 1,2,4-TCD, and 1,2-DBC as end products, without selectivity via a stepwise process.

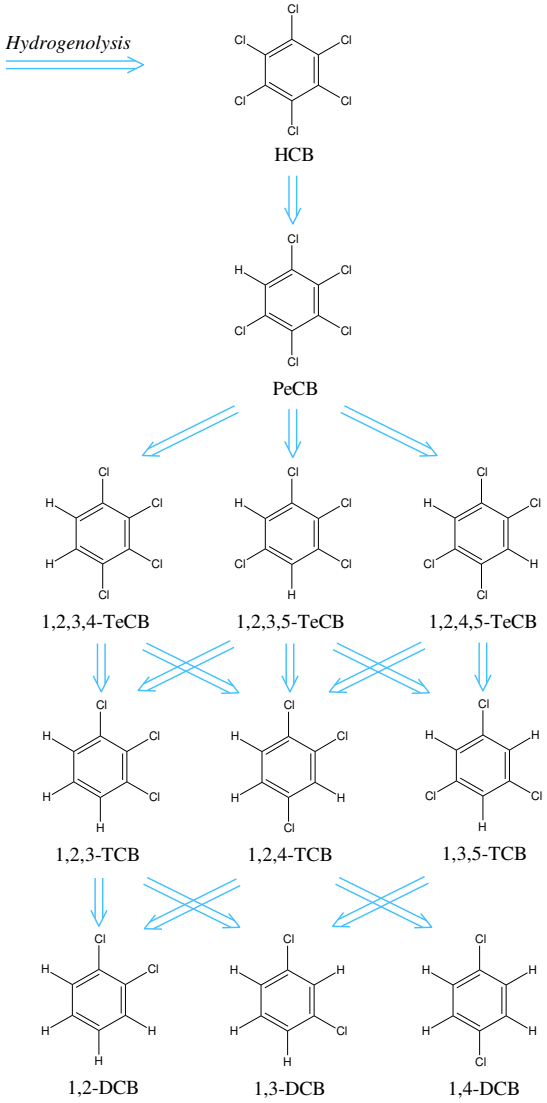

Figure 6.4. Reductive dechlorination pathways of HCB by ZVI. The main dechlorination pathway is influenced by the type of the catalyst metal on iron surface.

Carbon tetrachloride undergoes successive hydrogenolysis via a direct electron transfer mechanism, leading to the formation of chloroform, dichloromethane and methane (Song and Carraway 2006). McCormick and Adriaens (2004) have also observed two other pathways, leading to the formation of CO and methane with the formation of chlorocarbene intermediates. Dichloromethane reacts very slowly with traditional iron particles, and tends to accumulate (Gillham and O'Hannesin 1994; Matheson and Tratnyek 1994). The simultaneous production of dichloromethane and methane can be interpreted by concerted reductive elimination steps involving carbine and charged radical species (Song and Carraway 2006). As for chlorinated ethanes and ethylenes, a complete dechlorination and a higher yield of methane is obtained with reduction by Pd/Fe bimetallic particles (Muftikian et al. 1995; Lien and Zhang 1999). Coupling reactions of two trichloromethyl radicals in HCA are also referenced (He et al. 2015).

3.6. Influence of operating conditions and solution geochemistry

Besides iron intrinsic characteristics, the operating conditions and the solution chemistry are major influencing factors for ZVI reactivity and mobility (Sun et al. 2016). All these factors can affect COCs degradation rates, especially pH, temperature, the use of surfactant and the medium composition.

3.6.1. pH

As indicated in Table **6.5**, protons participate in the chemical reduction of COCs. The reaction rate is generally higher at low pH, as the reaction is thermodynamically more favorable (Table **6.13**).

The effect of pH can be different depending on the compound. Wang and Farrell (2003) have shown by an electrochemical analysis that TCE dechlorination is 50 times higher when pH is lowered from 7 to 3, but only 15 times greater for PCE dechlorination. As reduction with iron particles is a heterogeneous reaction, this result can be attributed to both sorption and surface-reaction step. By electrochemical impedance spectroscopy analysis, the authors have investigated the role of atomic hydrogen on PCE and TCE reduction by using iron. Results suggest different reductive mechanisms: TCE reduction occurred via atomic hydrogen at low pH and via direct electron transfer at neutral pH, whereas PCE reduction occurred via direct electron transfer at low and neutral pH. Thereby, pH value has a greater impact on TCE reduction at low pH. For carbon tetrachloride dechlorination, Jiao et al. (2009) have shown by an electrochemical analysis that the lower the pH value, the faster the dechlorination reaction proceeds.

Later, Luo and Farrell (2013) have studied pH effects on PCE and TCE adsorption energies on iron by a molecular mechanics simulation. A decrease in pH is characterized by a rise in the fractional atomic hydrogen surface coverage, which leads to a decrease of potential energies of TCE and PCE complexes with iron. As this phenomenon is more important for TCE complexes, the authors propose that the complexation equilibrium constant of TCE is increased, resulting in the improvement of TCE dechlorination rate.

Values of reduction constant rates of four COCs at different pH values (ranging from 1.7 to 13) are shown in Table **6.13**. For TCE, a decrease in pH from 8 to 1.7 results in a rate constant six times greater. It is however important to note that the use of buffers can affect the reactivity of ZVI as the nature of the buffer can affect the corrosion rate (He et al. 2018a; Qin et al. 2018b).

Using acidic conditions is also benefit as iron corrosion by-products are more soluble in water in these conditions (Beverskog and Puigdomenech 1996), which can prevent the formation of passive layer at iron surface (see Pourbaix diagram in Figure 6**.1** B). Therefore, pH affects also the structural evolution of the particles (Tang et al. 2017b).

For bimetallic particles, as the main degradation mechanism is hydrodechlorination, there is a relation between pH and degradation. For TCE dechlorination, He and Zhao (2008) have shown that lowering the pH from 9 to 6, the rate-determining step shift from iron corrosion to hydrodechlorination. Indeed, H_2 production is more rapid in acidic conditions. However, some studies have shown that strongly acidic conditions (pH < 3) are detrimental due to the more important iron corrosion, resulting in the accumulation of H_2 bubbles, and the destabilization of the catalyst (Dong et al. 2011; Huang et al. 2016b). The opposite observation was reported for TCE degradation with sulfidated particles, where the constant rate increased from 0.104 h^{-1} at pH 7 to 0.137 h^{-1} at pH 9 (Rajajayavel and Ghoshal 2015). Hence, it is suggested that sulfidated particles would be an efficient reagent for the remediation of groundwater at near-neutral pH (Dong et al. 2018c; Gu et al. 2019).

Table 6.13. Influence of initial pH on constant rate of reaction with ZVI.

Reactant	Pollutant	pH	*k*	Reference
ZVI	CT		k = -0.018 pH + 0.20 (5.5 < pH < 10.0)	(Matheson and Tratnyek 1994)
ZVI (0.077 m² g^{-1})	TCE	1.7	0.59 L h^{-1} m^{-2}	(Chen et al. 2001)
		3.8	0.044 L h^{-1} m^{-2}	
		4.9	0.050 L h^{-1} m^{-2}	
		6.1	0.035 L h^{-1} m^{-2}	
		7.1	0.017 L h^{-1} m^{-2}	
		8.0	0.009 L h^{-1} m^{-2}	
ZVI (0.1582 m² g^{-1})	γ-HCH	4.67	0.0798±0.0054 min^{-1}	(Wang et al. 2009c)
		6.73	0.0125±0.0004 min^{-1}	
		8.30	0.00039±0.00004 min^{-1}	
nZVI (40.3 m² g^{-1})	HCB	3.2	0.12 h^{-1}	(Shih et al. 2011b)
		5.1	0.088 h^{-1}	
		6.8	0.073 h^{-1}	
		9.2	0.052 h^{-1}	
		13.0	0.052 h^{-1}	
			log k = -0.058 pH – 0.755 (3.2 < pH < 9.3)	

3.6.2. Temperature

Temperature is known to have an effect on many physical and chemical properties of COCs, such as their solubility, Henry's law constant, density, viscosity, or interfacial tension (Stephenson 1992; Sleep and Ma 1997; Heron et al. 1998; Knauss et al. 2000; Mackay et al. 2006; Chen et al. 2012; Rodrigues et al. 2017b; Koproch et al. 2018), thus affecting their transport and fate processes. Temperature has also an effect on chemical reactions. A phenomenological law has been proposed in 1889 by Arrhenius to establish the relation between the constant rate *k* and the temperature *T* (K) (Eq. **6.54**).

$$k = A\, e^{-Ea/RT} \qquad \text{(Eq. 6.54)}$$

where *A* is the pre-exponential factor (unit of *k*), *Ea* is the energy activation (J mol^{-1}) and *R* is the universal gas constant (J mol^{-1} K^{-1}). The Arrhenius equation is used to calculate activation energy of a reaction, which represents the minimum energy required to result in a chemical reaction (effective shock between molecules).

Values of reduction constant rates of reduction of four COCs at different temperature are shown in Table **6.14**. For TCE reduction, a rise in the temperature from 10 to 55 °C increase the rate constant by a factor of about 10.

Table 6.14. Influence of temperature on constant rate of reaction with ZVI-based systems.

Reactant	Pollutant	Temperature	*k*	Reference

		(°C)		
Fisher ZVI (0.091 $m^2 g^{-1}$)	TCE	10	0.444 10^{-3} L h^{-1} m^{-2}	(Su and Puls 1999)
		25	1.102 10^{-3} L h^{-1} m^{-2}	
		40	2.494 10^{-3} L h^{-1} m^{-2}	
		55	4.313 10^{-3} L h^{-1} m^{-2}	
Master Builder ZVI (1.164 $m^2 g^{-1}$)	TCE	10	0.0289 10^{-3} L h^{-1} m^{-2}	
		25	0.109 10^{-3} L h^{-1} m^{-2}	
		40	0.156 10^{-3} L h^{-1} m^{-2}	
		55	0.198 10^{-3} L h^{-1} m^{-2}	
Peerless ZVI (0.699 $m^2 g^{-1}$)	TCE	10	0.0304 10^{-3} L h^{-1} m^{-2}	
		25	0.103 10^{-3} L h^{-1} m^{-2}	
		40	0.198 10^{-3} L h^{-1} m^{-2}	
		55	0.270 10^{-3} L h^{-1} m^{-2}	
Aldrich ZVI (0.192 $m^2 g^{-1}$)	TCE	10	0.0016 10^{-3} L h^{-1} m^{-2}	
		25	0.0032 10^{-3} L h^{-1} m^{-2}	
		40	0.0063 10^{-3} L h^{-1} m^{-2}	
		55	0.011 10^{-3} L h^{-1} m^{-2}	
nZVI (33.5 ± 4.2 $m^2 g^{-1}$)	PCE	15	0.011 h^{-1}	(Lien and Zhang 2007)
		25	0.023 h^{-1}	
		40	0.064 h^{-1}	
		50	0.081 h^{-1}	
Pd/Fe nanoparticles (33.5 ± 4.2 $m^2 g^{-1}$)	PCE	5	1.14 h^{-1}	
		15	1.23 h^{-1}	
		25	2.07 h^{-1}	
		40	6.71 h^{-1}	
ZVI powder (0.1582 $m^2 g^{-1}$)	γ-HCH	25	0.0125±0.0004 min^{-1}	(Wang et al. 2009c)
		35	0.0146±0.0006 min^{-1}	
		45	0.0271±0.0008 min^{-1}	
nZVI (40.3 $m^2 g^{-1}$)	HCB	5	0.050 h^{-1}	(Shih et al. 2011b)
		25	0.075 h^{-1}	
		45	0.12 h^{-1}	

3.6.3. Surfactant

A surfactant is an amphiphilic compound, having both a hydrophilic and a lipophilic group in its structure. Surfactants have a strong tendency to accumulate at the interface between two distinct phases, causing alterations of interfacial properties according to the molecular structure, pH and temperature (Rosen and Kunjappu 2012). When dissolved in water, surfactants adsorb to the different interfaces (air-water, COC-water and solid-water) and reduce the interfacial tension. Once the interface is saturated, the interfacial tension stabilizes at its minimal value. Thereafter, a spontaneous formation of an organized structure in solution, called micelles, is observed for higher concentrations in surfactant, in order to minimize the contact surface between water and lipophilic groups. Beyond this concentration called critical micelle concentration (CMC), other physicochemical properties begin to change, such as solubilization. Lipophilic compounds like COCs can then be trapped within the micelle, which will result in the rise of the apparent solubility (sum of the free solute dissolved in water and trapped in the micelle) (Jafvert 1994; Cho and Park 2006; Mao et al. 2015).

Surfactants are generally categorized into two large groups: ionic (cationic or anionic) and neutral (nonionic or zwitterionic) surfactants. Table **6.15** lists the main surfactants used for the enhancement of the remediation of COCs.

Table 6.15. List of surfactants frequently used for the enhancement of COCs remediation.

Name	Formula	Type	*M* (g mol^{-1})	CMC (mM)
Brij30	$CH_3(CH_2)_{11}(OCH_2CH_2)_4OH$	Nonionic	362.6	0.035
Brij35	$CH_3(CH_2)_{11}(OCH_2CH_2)_{23}OH$	Nonionic	1199.6	0.090
Brij36	$CH_3(CH_2)_{11}(OCH_2CH_2)_{10}OH$	Nonionic	626.9	0.20
Brij56	$CH_3(CH_2)_{15}(OCH_2CH_2)_{10}OH$	Nonionic	683.0	0.023
Brij97	$CH_3(CH_2)_{17}(OCH_2CH_2)_{10}OH$	Nonionic	711.0	0.35
CPC	$C_{21}H_{38}NCl$	Cationic	340.0	0.90
CTAB	$(C_{16}H_{33})N(CH_3)_3Br$	Cationic	364.5	0.92-1.00
DPC	$C_{17}H_{30}NCl$	Cationic	283.9	1.63
DTAC	$C_{15}H_{34}NCl$	Cationic	263.9	20
HDTMA	$CH_3(CH_2)_{15}N(CH_3)_3^+$	Cationic	284.6	0.9
SDBS	$C_{12}H_{25}C_6H_4SO_3Na$	Anionic	348.5	1.5
SDS	$C_{12}H_{25}SO_4Na$	Anionic	288.4	8.2
Triton X-100	$C_8H_{17}C_6H_4(OCH_2CH_2)_xOH$	Nonionic	602.8-646.9	0.22-0.24
Tween 80	$C_{64}H_{124}O_{26}$	Nonionic	1309.7	0.012

Brij30 = PEO(4) lauryl ether, Brij35 = PEO(23) lauryl ether, Brij36 = PEO(10) lauryl ether, Brij56 = PEO(10) cetyl ether, Brij97 = PEO(10) oleyl ether, CPC = cetyl pyridium chloride, CTAB = cetyl trimetyl ammonium bromide, DPC = 1-dodecylpyridinium chloride, DTAC = dodecyl trimethyl ammonium chloride, HDTMA = hexadecyltrimethylammonium, SDBS = sodium dodecyl benzene sulfonate, SDS = sodium dodecyl sulfate.

It is worth mentioning that the presence of iron particles causes the appearance of a solid-liquid interface on which surfactants can adsorb, leading to modification of iron surface properties. A thin and compact shell of surfactants can be observed on the surface of the particles (Soukupova et al. 2015). Therefore, a number of processes may be affected, e.g. nanoparticle aggregation, mass transport and sorption.

Loraine (2001) has pointed out that concentration of SDS and Triton X-100 (TX-100) surfactants above their respective CMC decreased PCE and TCE surface concentration on iron, due to the increase of solubilization in the micelles. The presence of SDS at concentrations less than its CMC had no impact on PCE and TCE reduction rates. TX-100 can increase PCE removal while TCE removal was not affected. The author suggests that TX-100 may act as a hydrogen donor to favor hydrogenolysis pathway, which is more important for PCE reduction than for TCE reduction (Arnold et al. 1999).

Cho and Park (2006) have observed that PCE dechlorination rates by ZVI increased with nonionic TX-100 and cationic HDTMA surfactants at one-half and two times their respective CMC, thanks to a stronger affinity between PCE and the modified hydrophobic surface of iron particles. PCE removal was higher with anionic SDBS surfactant, but the enhancement was attributed to an increase of sorption on iron instead of effective chemical reduction.

Harendra and Vipulanandan (2008, 2011) have studied the dechlorination of PCE solubilized in different surfactants by Ni/Fe particles (200 g L^{-1}). The authors have shown that more than 500 mg L^{-1} of PCE can be completely degraded in less than 3 h with a biosurfactant (UH-surfactant, 3.2 g L^{-1}) and in less than 9 h with CTAB (2.8 g L^{-1}). Degradation with SDS (3.5 g L^{-1}) and TX-100 (1.5 g L^{-1}) is incomplete even after more than 15 h. Reactions are pseudo-first order, except with TX-100 (1.93) and UH-biosurfactant (1.8).

Shin et al. (2008) have shown that cationic surfactants CTAB, PCP and CPC enhanced TCE reduction by ZVI at concentration lower than their respective CMC. Nonionic surfactants Brij30, Brij35, Brij36, Brij56 and Brij97, and anionic surfactant SDS inhibited degradation. The authors claim that cationic surfactants enhanced TCE adsorption on iron due to the electrostatic interactions between electronegative chlorine group and positive head group of the surfactant. For *in situ* application, low amounts of cationic surfactants have to be used, as they can potentially contaminate groundwater.

Zhang et al. (2011) have studied the degradation of soil-sorbed TCE by Pd/Fe nanoparticles stabilized with carboxymethyl cellulose with cationic HDTMA, nonionic Tween 80 surfactants and anionic SDS surfactants. They concluded that both the type of surfactant and soil characteristics had a strong impact on degradation rates. For a soil with a high organic matter content, degradation rates are strongly limited by desorption kinetics. The authors have shown that SDS is more effective for TCE desorption and degradation in water, both at and above its CMC. However, inhibitory effects were observed for cationic and nonionic surfactants.

Reduction of chlorinated benzenes in presence of surfactant has been studied. Nie et al. (2012) have shown that HCB dechlorination with bimetallic Ag/Fe particles (dechlorination rate of 59.5% after 20 minutes without surfactant) is clearly promoted by the nonionic surfactant TX-100, with a dechlorination rate improved to 94.1% with 20 mg L^{-1} TX-100, and 98.5% with 100 mg L^{-1} TX-100. Cationic surfactant hexadecylpyridinium bromide hydrate (HBH) has to be used at low concentrations, with an increase to 88.6% at 20 mg L^{-1} HBH, but the rate decreases with increasing the concentration beyond 50 mg L^{-1}, showing an inhibitory effect when 400 mg L^{-1} were added (41.3% of dechlorination). With anionic surfactant SDBS, the rate increased with increasing the concentration, and the dechlorination rate reached 91.7% with 400 mg L^{-1} SDBS.

Zheng et al. (2009) have shown that TX-100 also improved HCB dechlorination with Cu/Fe microparticles, especially due to the improvement of HCB mass transfer. Yuan et al. (2010) have shown that the dechlorination rate of chlorinated benzenes with TX-100 and cationic myristylpyridinium bromide (MPB) increased with increasing hydrophobicity ($n_{Cl} > 4$), due to the hydrophobic-hydrophilic variation at the surface of Cu/Fe particles. In field experiment, the dechlorination rate with surfactant is however impacted by the presence of organic matter (humic acid) and corrosion inhibitors (Otto et al. 2003; Yuan et al. 2010b).

It is also possible to combine the use of anionic and nonionic surfactants to obtain synergetic effects for the desorption, solubilization and the chemical reduction of COCs by ZVI-based particles (Yang et al. 2005; Zhao et al. 2006; Wu et al. 2017, 2018).

3.6.4. Medium composition

The presence of ionic species affects the ionic strength of a solution, as well as the various interactions. Oleszek-Kudlak et al. (2004) have studied the influence of sodium chloride NaCl, potassium chloride KCl and calcium chloride $CaCl_2$ on HCB aqueous solubility at 25 °C and observed a decrease in solubility with salt addition. This phenomenon is known as the salting-out effect and depends on the electrolyte valence. Setschenow equation (Eq. **6.55**) gives the solubility of the nonelectrolyte in an aqueous salt solution:

$$\log\left(\frac{s_W}{s}\right) = k_S\, C_S \qquad \text{(Eq. 6.55)}$$

where s_W is its solubility in pure water, s its solubility in the salt solution of concentration C_S (mol L^{-1}) and k_S is the salting coefficient (L mol^{-1}).

The mobility of surface-modified nZVI particles is impacted by the ionic strength and the medium composition (Saleh et al. 2008; Laumann et al. 2013). Iron reactivity is also impacted by the presence of dissolved ionic compounds (Table **6.16**), mainly because of the change in iron corrosion rates and pathways (Pullin et al. 2017a; Velimirovic et al. 2018).

Table 6.16. Degradation rate constants and efficiencies of HCB by nZVI particles various electrolytes (from Su et al. 2012).

Salts	Concentration (mM)	k (h^{-1})	Degradation efficiency after 72 h (%)
Without salts	0	0.075	39
$NaHCO_3$	0.8	0.076	42
	7.7	0.076	42
$NaNO_3$	0.8	0.060	39
	7.7	0.050	30
NaCl	0.8	0.081	41
	3.8	0.107	48
	7.7	0.170	67
Na_2SO_4	0.8	0.078	43
	3.8	0.081	50
	7.7	0.087	58
$MgSO_4$	0.8	0.076	42
	7.7	0.089	59
$FeSO_4$	0.8	0.073	37
	7.7	0.071	28
$CuSO_4$	0.8	0.257	89
	7.7	0.298	100

The presence of aqueous silica can decrease the corrosion of iron particles due to the formation of Si surface complexation (Rushing et al. 2003; Keith et al. 2005). The presence of bicarbonate ions has shown no significant effect on the dechlorination of HCB (Su et al. 2012) and 1,1,1-TCA (Li et al. 2017a). However, Bi et al. (2009) have demonstrated that bicarbonate can either be beneficial or inhibitor – depending on its concentration – on the degradation of 4-chloronitrobenzene and 4-chloraniline by granular iron. The presence of nitrate and hexavalent chromium could affect the reactivity of ZVI particles towards COCs (Schlicker et al. 2000; Su et al. 2012; Kaifas et al. 2014; Li et al. 2017a), causing a side reaction which generates competitive reaction and the formation of passivating precipitate layers γ-Fe_2O_3 instead of non-passivating Fe(II,III) oxide Fe_3O_4 (Eqs. **6.56-59**). It has been shown that the presence of Cr(VI) as a co-contaminant will dramatically inhibit the electron efficiency of COCs dechlorination, e.g. TCE dechlorination, due to the formation of a Fe/Cr hydroxides passive layer (Lu et al. 2012; Zou et al. 2019).

$$2\ CrO_4^{2-} + 2\ Fe^0 + 4\ H^+ \rightarrow\ \gamma\ Fe_2O_3 + Cr_2O_3 + 2\ H_2O \qquad \text{(Eq. 6.56)}$$

$$2\ CrO_4^{2-} + 2\ Fe^0 + 4\ H^+ \rightarrow\ \gamma\ Fe_2O_3 + Cr_2O_3 + 2\ H_2O \qquad \text{(Eq. 6.57)}$$

$$3\ NO_3^- + 8\ Fe^0 + 6\ H^+ + 3\ H_2O \rightarrow\ 4\ \gamma\ Fe_2O_3 + 3\ NH_4^+ \qquad \text{(Eq. 6.58)}$$

$$NO_3^- + 8\ Fe_3O_4 + 2\ H^+ + H_2O \rightarrow\ 12\ \gamma\ Fe_2O_3 + 3\ NH_4^+ \qquad \text{(Eq. 6.59)}$$

The presence of sulfate and chloride ions is beneficial to iron corrosion, due to the formation of new reactive sites or the regeneration of passivated sites (Lipczynska-Kochany et al. 1994; Domínguez et al. 2016). However, Lu et al. (2006) have reported an inhibitory effect of chloride ions for HCB degradation, with only 65% of HCB reduced for 0.42 M of Cl^-, and 40% for 0.84 M of Cl^-, compared to a complete dechlorination of HCB in 3 h without chloride ions. Adsorption on the surface can occur with high concentration (> 3 g L^{-1}) of NaCl, which can inhibit the remediation process (Hwang et al. 2015). In addition, in excessive presence of Fe^{2+} and Cl^- (C > 1 mol L^{-1}), akaganéite β-FeOOH can be formed preferentially on the surface of the particles (Rémazeilles and Refait 2007).

Depending on the standard potential of metal cations relative to iron, different observations on the reactivity of ZVI particles have been reported, such as diffusion, encapsulation, sorption and/or reduction at iron surface (Li and Zhang 2007; Zou et al. 2016; Li et al. 2017c; Ling et al. 2017). Sorption and formation of surface-complex occur for metal cations with a close or more negative standard potential than that of iron, such as Ba^{2+}, Cd^{2+}, Cs^+ or Zn^{2+}, whereas adsorption and reduction occur for metal cations with a higher potential, such as Ag^+, Ni^{2+}, Cu^{2+} or Hg^{2+}. For metal cations with a slightly more positive potential, a combination of adsorption and reduction is reported. Magnesium and sodium ions have no effect on iron reactivity as their standard potential is lower than that of iron (Su et al. 2012). Copper and nickel ions enhance rate constants and degradation efficiencies due to solid materials deposit that enhance reactivity (Schrick et al. 2002; Lien et al. 2007; Zheng et al. 2009; Zhu et al. 2010). The effect is more important in the presence of Ni^{2+} thanks to the catalytic production of atomic hydrogen H^* on the reduced-Ni on ZVI surface (Dries et al. 2005; Doong and Lai 2006; Shih et al. 2011a; Wu et al. 2015). Chen et al. (2016) have observed that HCB removal by iron particles on activated carbon support was enhanced in presence of ions that facilitate iron corrosion, such as bicarbonate, chloride, ferrous and copper ions.

In addition to ionic species, natural organic matter (NOM) occurring in soils and groundwater is known to influence the chemical degradation by ZVI, in terms of enhancement of solubilization, sorption and electron transfer (Chiou et al. 1987; Weber 1996; Watanabe et al. 2009; Louie et al. 2016). Tratnyek et al. (2001) have shown that the reduction of TCE and carbon tetrachloride by ZVI was inhibited by NOM (Ogeechee HA, Coal Creek HA and OGI Soil HA at 5 mg L^{-1} each) due to competitive adsorption on iron surface, but the presence of quinone compounds (juglone and AQDS) increased the reduction rate due to mediated electron-transfer. However, they suggest that the effects will not be much significant in field applications as the observed effects were low in laboratory experiments. Doong and Lai (2005) have shown that low concentration of humic acids (< 50 mg L^{-1}) decrease PCE dechlorination rate by Pd/Fe particles; normalized constant rates of dechlorination decrease from 33.47 L m^{-2} h^{-1} without humic acid to 16.86 L m^{-2} h^{-1} at 5 mg L^{-1} and 1.69 L m^{-2} h^{-1} at 50 mg L^{-1} of humic acid. Similar observations for 1,1,1-TCA degradation by biochar supported Ni/Fe nanoparticles were reported, with the inhibitory effect explained by the adsorption of humic acid on active surface site (Li et al. 2017a). Doong and Lai (2006) have also studied the effect of metal ions in the absence and the presence of humic acid, with a decrease of constant rates in the presence of humic acid (Table **6.17**). Generally, the presence of macromolecules, which are abundant in the subsurface, results in a decrease in iron reactivity due to the blocking of reactive site through adsorption, complexation or a combination of both (Bhattacharjee et al. 2016; Bhattacharjee and Ghoshal 2018b).

Table 6.17. Dechlorination rate constants of PCE by ZVI in the presence of divalent metal and humic acid (from Doong and Lai 2006).

System	Without humic acid		With humic acid	
	k_{obs} (h^{-1})	k_{SA} ($L\ m^{-2}\ h^{-1}$)	k_{obs} (h^{-1})	k_{SA} ($L\ m^{-2}\ h^{-1}$)
ZVI	9.6 (± 1.7) 10^{-3}	3.43 (± 0.61) 10^{-3}	1.5 (± 0.06) 10^{-3}	0.54 (± 0.02) 10^{-3}
ZVI + Cu(II)	22.9 (± 6.5) 10^{-3}	8.24 (± 2.32) 10^{-3}	4.8 (± 0.7) 10^{-3}	1.71 (± 0.25) 10^{-3}
ZVI + Co(II)	16.7 (± 3.5) 10^{-3}	5.96 (± 1.23) 10^{-3}	6.1 (± 0.6) 10^{-3}	2.15 (± 0.22) 10^{-3}
ZVI + Ni(II)	809 (± 16) 10^{-3}	289 (± 6) 10^{-3}	256 (± 41) 10^{-3}	91 (± 16) 10^{-3}

Porphyrins that are naturally produced in subsurface, such as vitamin B_{12} (cobalamine), are good catalysts for the reductive dechlorination of COCs, and work as electron transfer mediators in the presence of an electron donor. If titanium(III) citrate is generally used as the reductant (Burris et al. 1996, 1998; Glod et al. 1997; Dror and Schlautman 2004), an enhanced reductive dechlorination by nZVI particles with vitamin B_{12} is also observed (Amir and Lee 2011). Hence, the addition of vitamin B_{12} model compounds (cobaloximes) has been proposed for COCs catalytic degradation (McCauley et al. 2002; Pizarro et al. 2018).

4. Injection of reductants

In situ chemical reduction efficiency is highly dependent on the intimate contact between contaminants and reductant (Noubactep et al. 2012). The injection method of reductant is therefore a decisive factor of treatment (Comba et al. 2011b). The selection of injection method depends on the selected reductant. Indeed, reductant can be in liquid (sodium dithionite), pure phase (edible oils), emulsion and foam (calcium polysulfide), gas (hydrogen) or particulate form (zero-valent iron). Thus, injection methods are fundamentally different (Tratnyek et al. 2014).

4.1. Injection of dissolved reductants

For moderately permeable phreatic zone, dissolved reductant injection can be performed without major difficulties via conventional injection wells, involving the extraction of contaminated water and the replacement by clean water (McCarty 2010). Flow rates and injection pressures are calculated from the hydraulic flow rate of groundwater, the concentrations to be achieved (determined by the stoichiometry), natural reductant demand (NRD) and contact time (determined by degradation kinetics).

For high hydraulic conductivity, contact time between pollutant and reductant may not be sufficient. In this case, it is possible to pump the water downstream and re-inject it upstream (recirculation or injection/extraction "push-pull") (Hyman and Dupont 2001; FRTR 2007; Colombano et al. 2010).

Injection of reducing agents (Fig. **6.5**) may be improved by hydraulic and pneumatic fracturing or by *in situ* soil mixing in the case of permeable zone (Brown 2010). Fracturing consists of injecting air or water at high pressure in order to improve permeability (Tratnyek et al. 2014). Deep soil mixing involves reductant injections via hollow augers for an *in situ* mechanical mixing with soil, thereby generating attrition, expansion and unclogging phenomena (Olson et al. 2012).

4.2. Injection of gases

Gas injection can be accomplished by *in situ* sparging. It is recommended to use hollow-fiber membranes to reduce as much as possible the size of the bubbles and the contact surfaces, hence promoting dissolution of reductive gases (Leeson et al. 2002; Johnson and Johnson 2012).

4.3. Injection of particular solids

Zero-valent iron particles are primarily injected using aqueous suspensions, under gravity feed or pressurized conditions (e.g. direct push, controlled-pressure delivery). Generally, the particle concentration in the slurry ranged from 1 to 30 g L^{-1} (Mueller et al. 2012); it is recommended to use a concentration higher than 5 g L^{-1} to improve the efficiency (Kim et al. 2017b).

The injection of nZVI particles can be problematic. Indeed, particles may agglomerate, settle on the solid matrix and create clogging (Phenrat et al. 2007, 2010). Therefore, iron transport distances are relatively small, a few meters at most (Bennett et al. 2010; Johnson et al. 2013). To increase these distances, vectorization of nZVI particles can be promoted by coated polymers (Phenrat et al. 2008, 2009a; Kaifas 2014), and delivery of non-aqueous phase liquids, emulsion and foam (Wang and Mulligan 2004; Quinn et al. 2005; Berge and Ramsburg 2009; Shen et al. 2011). The main difficulty concerning the use of iron particles is related to the creation of a homogeneous reactive zone. Generally, the design of a pilot test delivery is the result of a compromise among several needs, especially the reactivity, the slurring viscosity, the discharge rate and the monitoring setup (Luna et al. 2015).

The injection of nZVI is governed by Darcy's Law, and the maximum distance traveled (r_{max}) can be predicted by using Eq. **6.60**:

$$r_{\max} = \sqrt{\frac{V}{\pi b n R} + r_{\text{well}}^2} \qquad \text{(Eq. 6.60)}$$

where V is the volume injected, b is the aquifer thickness, n is the effective porosity, R is the retardation factor and r_{well} is the radius of the well (Bennett et al. 2010). However, there is still a lack in comprehensive numerical model to predict the transport and remediation associated with nZVI particles. Currently, only a few comprehensive numerical models has been developed (Tosco and Sethi 2010; O 'Carroll et al. 2013; Tosco et al. 2014a; Chowdhury et al. 2015; Bianco et al. 2016; Babakhani et al. 2017; Tsakiroglou et al. 2018), and the main model to predict nanoparticle transport and remediation is based on the colloid filtration theory (CFT) (Krol et al. 2013), which is incorporated into the advection-dispersion equation:

$$\frac{\partial C}{\partial t} = D_{\text{H}} \frac{\partial^2 C}{\partial x^2} - v_p \frac{\partial C}{\partial x} - K_{\text{att}} C \qquad \text{(Eq. 6.61)}$$

where C is the content in nZVI in the solution (g m^{-3}), D_H is the hydrodynamic dispersion (m^2 s^{-1}), v_p is the pore water velocity (m s^{-1}), t is the time (s), and K_{att} is the rate at which nZVI is deposited on available collector sites (s^{-1}).

$$K_{\text{att}} = \frac{3(1-\theta_{\text{W}})}{2\, d_{50}} \alpha \eta_0 v_{\text{p}} \qquad \text{(Eq. 6.62)}$$

where d_{50} is the median collector grain size (m), θ_w is the volumetric water content, η_0 is the theoretical collision efficiency and α is the sticking efficiency, calculated as:

$$\alpha = -\frac{2}{3} \frac{d_{50}}{(1-\theta) L \eta_0} \ln\left(\frac{C}{C_0}\right) \qquad \text{(Eq. 6.63)}$$

where L is the length of porous media (m), and C/C_0 is the maximum normalized effluent concentration. Other models incorporate a Langmuir-type adsorption isotherm in the traditional advection-dispersion

equation (Zhang et al. 2017). It is also important to note that in porous media, the mobility of iron particles can be affected by the presence of biofilm (Basnet et al. 2016; Crampon et al. 2018).

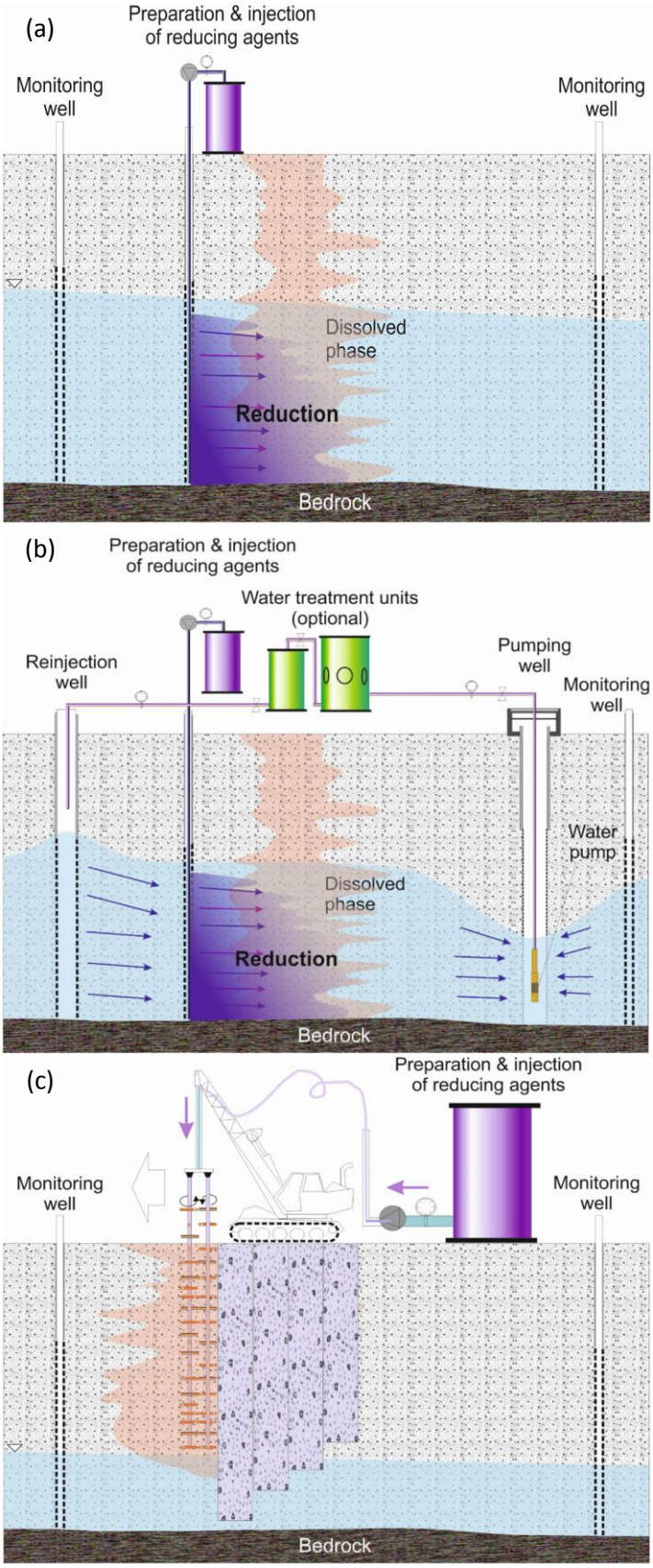

Figure 6.5. Schematic illustration of *in situ* chemical reduction (a) with traditional injection, (b) with recirculation system and (c) with deep soil mixing (adapted from Colombano et al. 2010).

All the previous sections in this chapter have highlighted the factors to be taken into account in order to ensure the proper functioning of chemical reduction for *in situ* application, from the main properties of COCs to the kinetics and degradation pathways, with the influence of physicochemical parameters. Geological and hydrogeological characteristics are also important but are very specific to each polluted site.

5. Case study

At every site where COCs has contaminated the local groundwater, there are two principal components to the problem: a subsurface source of residual or mobile DNAPL, and an associated dissolved-phase plume in groundwater (McCarty 2010; Kueper et al. 2014; Suchomel et al. 2014). Most of the contaminant mass is in the source zone, although the plume usually occupies a much larger volume of the subsurface. The COCs phase in the vadose and groundwater zones often contains sufficient chemical mass to cause dissolved plumes to persist for centuries (Pankow and Cherry 1996). Remediation of COCs sources can generally be removed at high percentage (McCarty 2010), essentially, where COCs sources residuals are situated above the water table; in low-permeability soils, remediation strategies are still challenging. However, COCs remediation of the dissolved-phase plume is still under investigation probably because of the plume lengths, the heterogeneity of the groundwater contaminated zones, the wide range of the metabolite concentration as well as the lack/effectiveness/cost of monitoring.

We will present hereafter a demonstration/development of field application of ISCR on plume treatment using two strong reducing agents separately – sodium dithionite (DT) and zero-valent iron nanoparticles (nZVI) – and together as a combination of the two (Betelu and Ignatiadis 2013; Noel et al. 2013; Ignatiadis et al. 2014, 2015, 2016; Betelu et al. 2015). The depollution technique is called Reductive Chemical DeChlorination (RCDC). This study was accomplished within the framework of DECHLORED, a project partly financed by ADEME Eco-industries 2011 program. It aimed at developing and evaluating/proving the efficiency of three defined emerging *in situ* RCDC process. For this purpose, four key steps were identified: (i) define, at laboratory scale, the operating conditions for the process application, (ii) determine performances, (iii) draw up the list of the equipment and the technical conditions of *in situ* implementation and (iv) make a complete assessment of processes application.

A multiscale approach was thus used during development of the technology, ranging from bench-scale laboratory tests using batches and columns as well as model molecules to full field-scale treatability tests. Each successive scale experiment allowed the identification of the effects related to each scale; it also enabled better design of the next larger scale experiment.

RCDC demonstration was performed in Néry-Saintines, 60, Oise, France, a large polluted area of more than 1 km². It is an old quarry, used as illegal waste deposit before 1978. The contaminated site was carefully selected because it presented a well-documented pollution in a sandy aquifer of Cuisian period with a majority of COCs and their metabolites provided by analyses since 1980. The use of state-of-the-art database led us to design and implement the pilot (50 m width × 50 m length × 22-23 m depth). Data provided by new physical and chemical monitoring *in situ* led us firstly to better understand the three-dimensional dynamics of the chlorinated solvent plume in the selected zone as well as to illuminated natural attenuation. It then led us to evaluate the efficiency of the three defined emerging *in situ* RCDC process.

5.1. Laboratory experiments

For laboratory experiments, performed by using bench-scale laboratory tests – mainly batches and columns –, PCE was chosen as the target compound as it is one of the most widespread chlorinated pollutants in groundwater.

First, batch experiments carried out in hermetically closed cells allowed the setting up of protocols making it possible to study the feasibility of RDC for PCE. Tests were carried out using sodium dithionite (Silex International, Engis, Belgium) and nZVI particles, NANOFER 25 and NANOFER 25S (aqueous suspension of nZVI particles from NANO IRON s.r.o., Rajhrad, Czech Republic), while varying operating parameters: nature and contents of reagents, temperature (from 12 to 25 °C), concentrations in pollutants, reagent/pollutant molar ratios, treatment duration, physical and chemical parameters.

Columns experiments were then conducted in designed Kynar® columns (Fig. **6.6**, height of 50 cm; diameter of 15 cm) fully equipped with sophisticated systems for non-destructive monitoring of time changing physical parameters and chemical compositions (Fig. **6.7**). The entire system – filled with reference sand from Fontainebleau, France, and with Cuisian sand from the selected polluted site – was placed in air-conditioned cupboard under different operating conditions. Monitoring was complemented by probes (temperature, pH, ORP, conductivity, dissolved oxygen). Gas chromatography (GC) led to monitor PCE and its degradation products migration and dispersion over the entire columns. Ion chromatography (IC) was used for the quantitation of Cl^- at the column outputs to correlate RCDC.

Figure 6.6. Complete experimental device of percolation (feed bottles with reagents and pollutants, pumps, columns, flow-through-system carrying the monitoring probes), placed in air-conditioned cupboard.

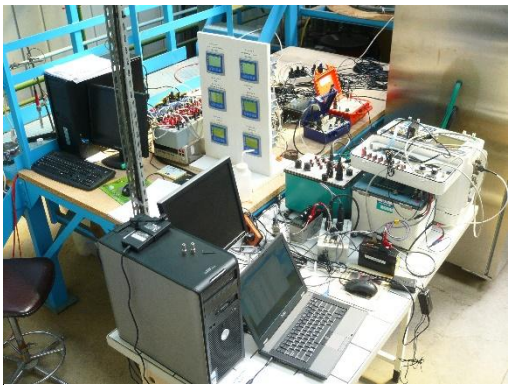

Figure 6.7. Setup and apparatuses for the monitoring of the physical and chemical parameters of the column output water and geophysical electrical measurements into the column (and over the length of the column).

Results have shown the persistence of PCE in deionized water and allowed us to evaluate its solubility (169 ± 7 mg L^{-1} at 12 °C). The association DT+nZVI was established to be more powerful than DT or nZVI alone, probably due to a synergetic concerted mechanism. GC analyses suggested that the combination DT+nZVI led to minimize the formation of chlorinated intermediate species, which represents a significant advantage for *in situ* groundwater treatments.

Column experiments enabled us to:

- evaluate the applicability of the selected operating conditions close to those being able to be met on the aquifers or soils;
- improve the understanding of reactant efficacy, and also their transformation and persistence;
- model these flow-through systems (1D or 2D column set up) by numerical modeling softwares (PHREEQC® and MARTHE® reactive transport simulations).

Results also recommended combining of geophysical measurements with electroanalytical measurements to monitor RCDC process, to give an advantageous method for monitoring *in situ* remediation.

5.2. In situ implementation

5.2.1. The large area

Fig. **6.8** shows the geographic location of the polluted site. It is a large area of more than 1 km² composed of a network of 12 piezometers (Fig. **6.8a**). The zone is constantly fed (open system) and the pollution conveyed by the water table of Cuisian sands. A conceptual scheme of the polluted site as a large area is given in Fig. **6.8b.**

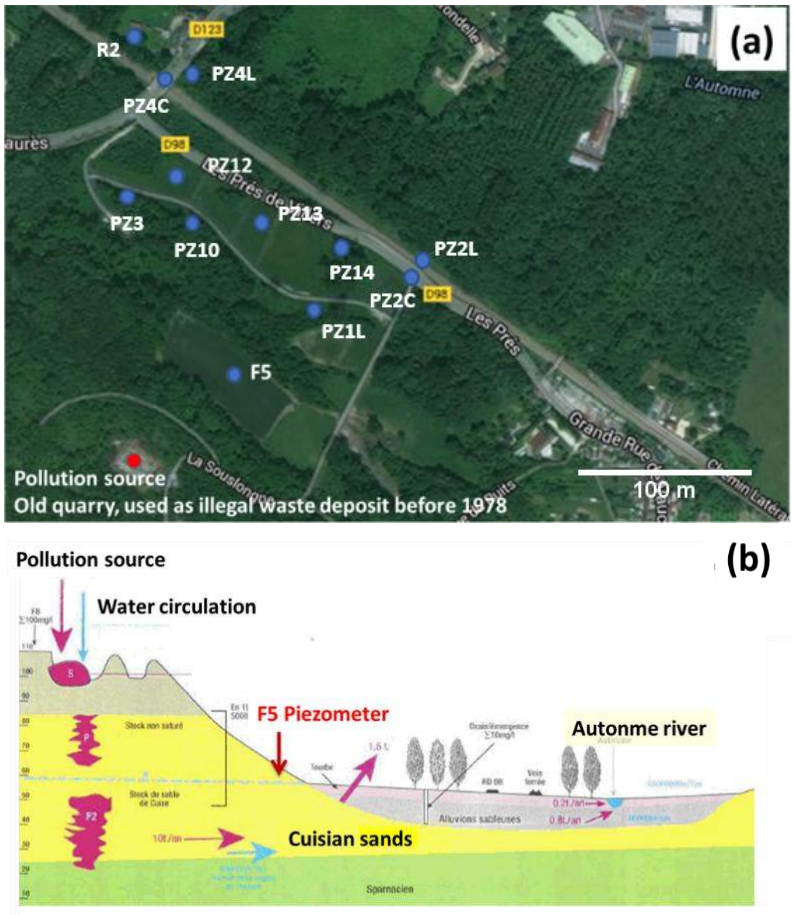

Figure 6.5. (a) Geographic location of the polluted site as a large area with the small area of the pilot implementation included inside, with the distribution of some piezometers at different locations within the polluted area where sampling was carried out for content analyses between 1999 and 2013. (b) Conceptual scheme of the polluted site.

Before RCDC implementation, the physical and chemical parameters of the groundwater of the polluted site (i.e. the natural attenuation monitoring) were investigated:

- during 15 years (1999-2013) from several tens of piezometers (PZs) distributed in a large area of more than 1 km². This preliminary work enabled to choose the convenient emplacement of the RCDC pilot.
- during 6 months (July-December, 2014) locally, from 12 piezometers, sampled at two depths (-10 and -20 m), in a smaller area (50 x 50 m²) where the pilot was implemented.

The objective of this preliminary study was to (i) improve understanding on the mechanisms and kinetics of the natural attenuation process that have occurred in the groundwater of this old polluted site, (ii) evaluate if natural attenuation can or not be perceived as an attractive option and (iii) compare the two processes, the natural attenuation and the forthcoming RCDC.

For both large and small areas, the analytical methodology is composed of:

- field measurements or analyses of the non-conservative parameters/species: pH, ORP, temperature, conductivity, dissolved oxygen, and some ionic species such as chloride, bicarbonate, dissolved iron, sulfide (present in deeper sediments), sulfate and phosphate ions;
- water sampling for the analysis in laboratory of the conservative elements: main and traces elements, pollutants (COCs), and carbon source;
- GC for dissolved COCs, ion chromatography for Cl^- ion, potentiometric titration for alkalinity, sulfide, and Merck kits.

5.2.2. Investigation of the natural attenuation in the large area

Using the network of 12 piezometers (localized in Fig **6.8a**), intensive sampling was carried out by ADEME for content analyses between 1999 and 2013. The results were investigated such as to select the most appropriate location for the *in situ* implementation of the RCDC pilot and to show the mechanism and the limiting steps of the natural attenuation. Figures **6.9-12** show the spatiotemporal evolution of the nature and abundance of chlorinated ethylenes in the groundwater. Other contaminants, not discussed here, includes chloroethanes and chloromethanes.

Figure **6.9** presents the results of chloride analyses carried out in seven monitoring PZs on Néry-Saintines site between 2000 and 2013. PZ F5 is located nearest to the contamination source area, while PZ14, PZ13, PZ12, PZ4C and R2 are located at the North of F5, in the tablecloth flow direction. The natural geochemical chloride ion background in the aquifer water was measured as a reference value from a drinkable water piezometer (AEP Néry), close to the site but not impacted by the pollution. This reference average value is of 15 mg L^{-1}. All Cl^- content measured in the PZs located in the North of the polluted site were higher than the reference value, with variable chloride contents ranging between 30 and 340 mg L^{-1}, according to the time and to the PZ position. Chloride ion is the principal produced component (evolution from 20 mg L^{-1} in a non-impacted area to 300 mg L^{-1}), as well as bicarbonate (150 to 650 mg L^{-1}). These measurements are an evidence of the natural attenuation in the Cuisian sand aquifer.

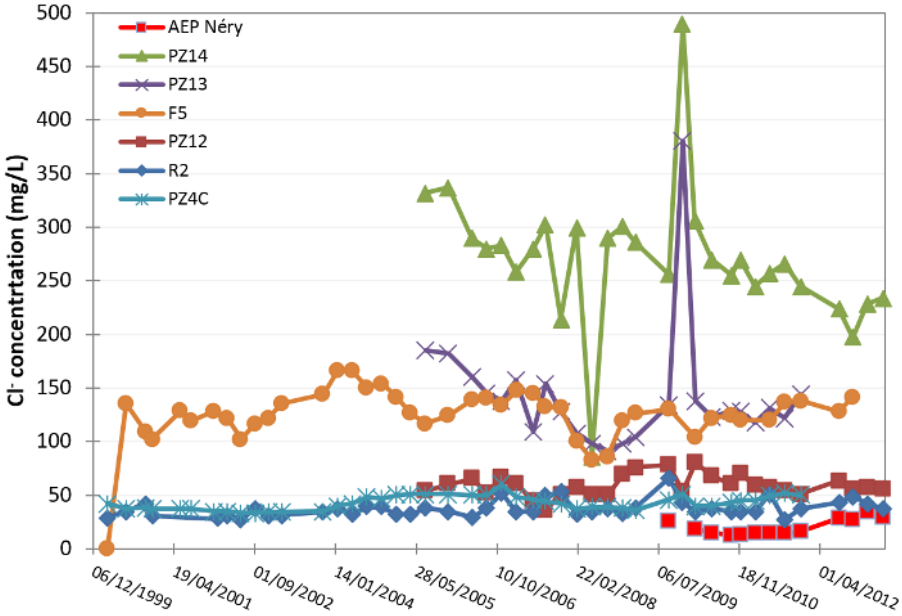

Figure 6.9. Cl^- concentration at locations within the area between 1999 and 2012. Chloride spatiotemporal content evolution at some piezometers inside and outside the polluted zone. Piezometer AEP Néry is located close to the polluted site, but in a non-impacted area.

Figure **6.10** presents the evolution of COCs concentration from piezometer F5 (upstream of the pilot implementation) from 2000 to 2013. The occurrence of the five main pollutants confirmed the existence of a natural attenuation between 2000 and 2012. PCE was degraded as its concentration decreased from *ca* 3000 µg L^{-1} in 2001 to 500 µg L^{-1} in 2013. TCE concentration was constant from 2002 to 2008, and then increased from 2009. 1,1-DCE was the most concentrated breakdown product, with an average concentration of 6000 µg L^{-1}.

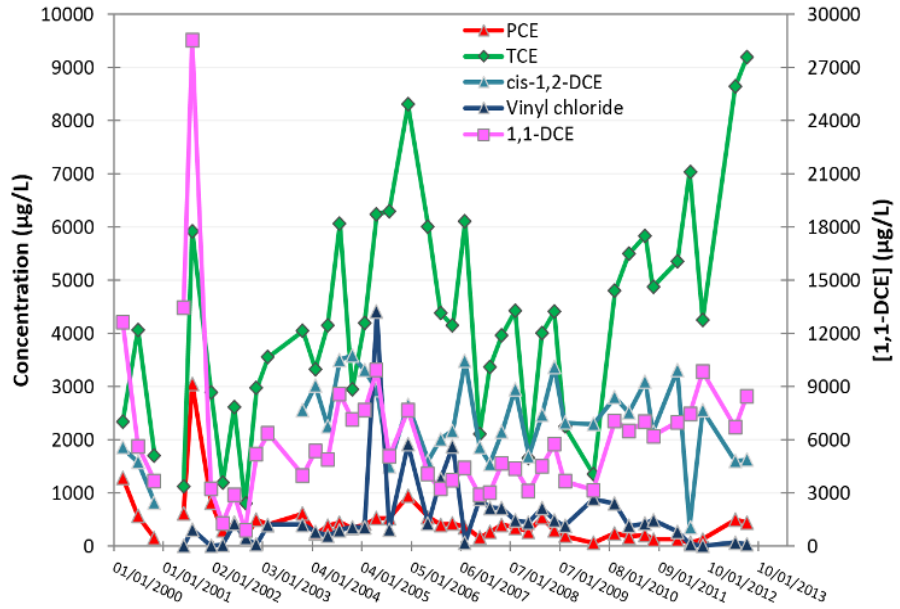

Figure 6.10. COCs content evolution at piezometer F5 inside the polluted zone between 2000 and 2013.

Figure **6.11** presents the COCs content evolution at piezometer PZ14 from 2005 to 2013. The natural attenuation of the plume in this direction was completely achieved before 2008.

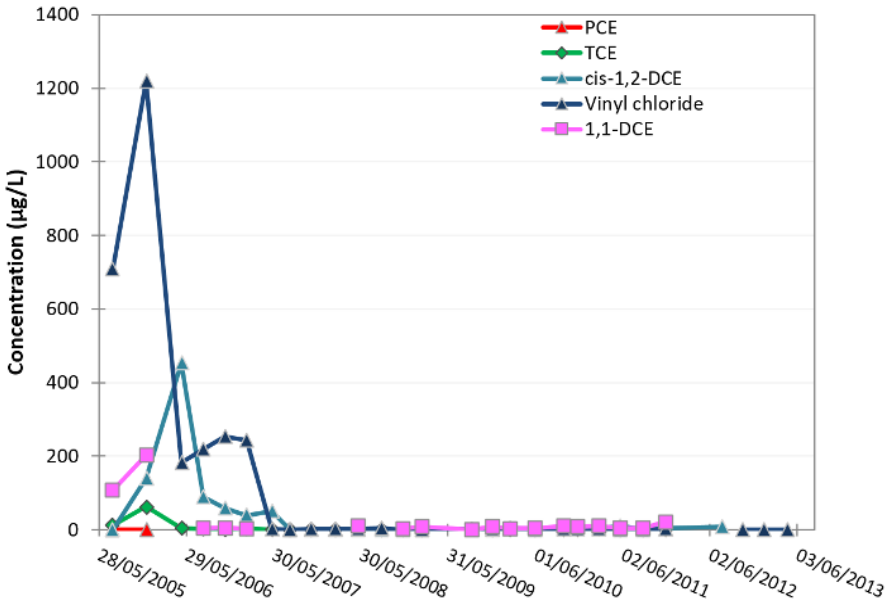

Figure 6.11. COCs content evolution at piezometer PZ14 inside the polluted zone between 2005 and 2013.

Figure **6.12** presents the COCs content evolution at piezometer PZ13 from 2005 to 2013. This piezometer, located downstream from F5, showed elevated COCs concentrations breakdown products, with the highest content recorded around spring 2008. PCE was quasi absent, while TCE content remained lower than 10 µg L^{-1}. Chloride ion content was variable, *ca* 150 mg L^{-1}, while remaining in the range 100-200 mg L^{-1}. This concentration, abnormally high for the Cuisian sandy aquifer, confirmed the natural attenuation.

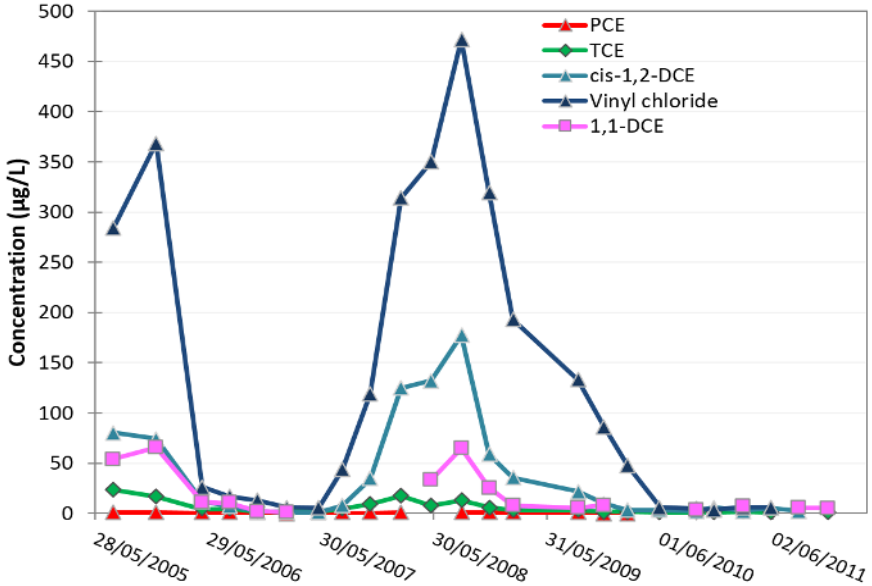

Figure 6.12. COCs content evolution at piezometer PZ13 inside the polluted zone between 2005 and 2011.

The processing of the ADEME database acquired from tens of piezometers during 13 years (2000-2013) led field evidence on rates and limitations on natural attenuation, e.g. the existence of a slow natural attenuation process in agreement with the sequential reductive dechlorination of PCE through TCE, cis-DCE, VC and ethylene (Vogel and McCarty 1985; Freedman and Gossett 1989; de Bruin et al. 1992; DiStefano et al. 1992; Maymó-Gatell et al. 1995, 1999).

The presence of cis-1,2-DCE (up to 1700 µg L^{-1}) clearly indicated the occurrence of reductive dechlorination; the presence of VC showed that biodegradation resulted in an almost complete dechlorination of PCE. Nevertheless, data exhibited high TCE concentrations in the groundwater – in the range from 1500 to 4500 µg L^{-1}, and up to 9000 µg L^{-1} –, demonstrating the significance of the contamination and the low degradation rates.

Because the principal witness of COCs impact is piezometer F5, located downstream from the Western zone of the old quarry, the pilot was implemented in a convenient location, in the direction of the water flow, in parallel with the F5 piezometer, in a topographically accessible place to the installing and handling the work apparatuses. Before any implementation of the network, geological and hydrogeological investigations allowed dimensioning the pilot area, namely the small area.

5.2.3. The small area

The small area was implemented is a 50 m x 50 m zone (2500 m², Fig. **6.13**). A review of topographic maps indicates that the site slopes gently northward with high bedrock ridges to the East. The ridge trends in the North-South direction. The average ground surface elevation at the site is 45 m above sea level. Locally, the site is underlain by very fine sand, between 10 and 15 m deep, silt, gravel, clays (Cuisian sands), natural organic matter and other organic compounds, e.g. BTEX, methanol and ethanol. Coring showed a roof of the Sparnacian clays in the range from 22.6 m to 23.1 m. Groundwater pumping tests in wells were measured to characterize the groundwater flow. Results of these measurements indicated that groundwater flows to the North-East, and the horizontal flow velocities were estimated to be higher than 40 cm d^{-1}.

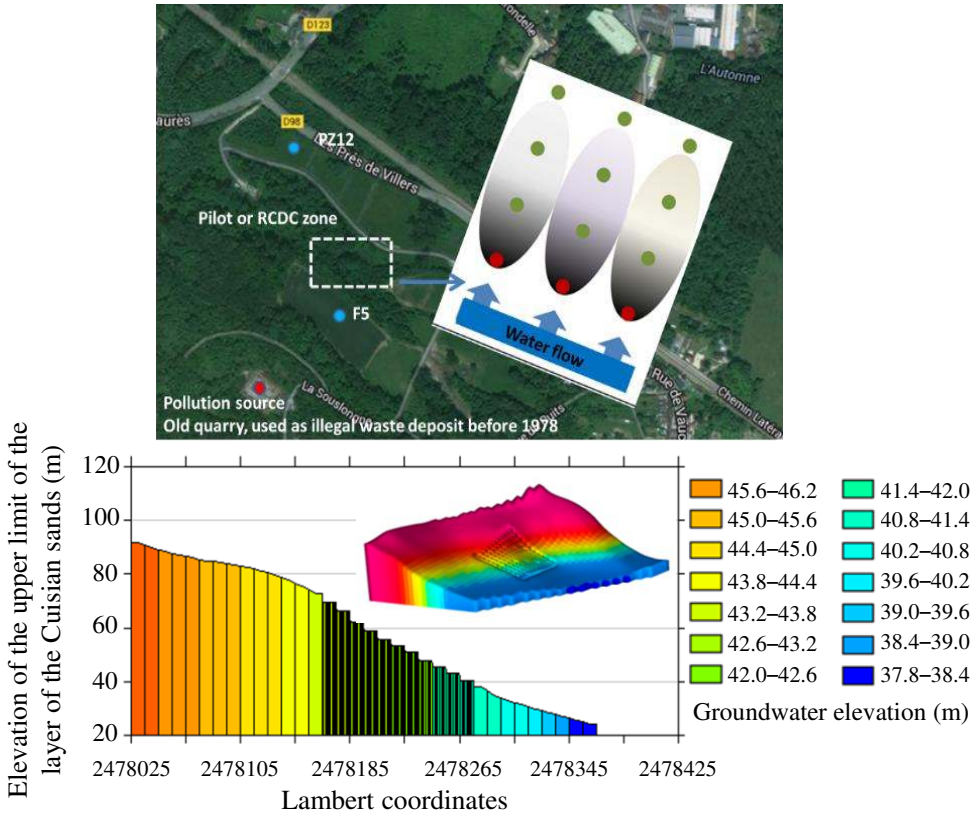

Figure 6.6. Localization and implementation of the demonstration site, with a 3D modeling of the topography.

A network of 12 piezometers (PZs) of an average depth of 22-23 m was installed in order to define the initial conditions and later to perform and monitor the chemical treatment. They were disposed along a transect intercepting perpendicularly to the polluted groundwater flow. Three of them, schemed in red in Fig. **6.13**, were designed as injection wells (I1, I2 and I3 in Figs. **6.14-6.15**) and were equipped for simultaneous injection over four different levels, from 0 to -25 m. The other nine PZs – respectively distanced at 5, 10 and 25 m from the injection wells – were designed as monitoring wells (control piezometers, cPZs) and fully equipped with probes (C11, C12, C13; C21, C22, C23; and C31, C32, C33 in Figs. **6.14-6.15**).

The groundwater quality was carried out in depth between August 18 and August 21, 2014. Series of *in situ* measurements and sampling were achieved in each PZ, at a high point (H) at -10 m depth and at a low point (B) at -20 m depth. The sampling was carried out by the use of inflatable packers in order to isolate a zone when the sampling is operated in the other point. This initial pollution state of the pilot zone was carried out in order to be used as reference before any injection of reductant, for the comparison of the total COCs content, as well as the nature, abundance and relative distribution of COCs within the pilot area.

5.2.4. Investigation of the natural attenuation in the small area

Figures **6.14** and **6.15** summarize, in two dimensions, the physical and chemical parameters as well as the COCs distribution in the groundwater of the small area.

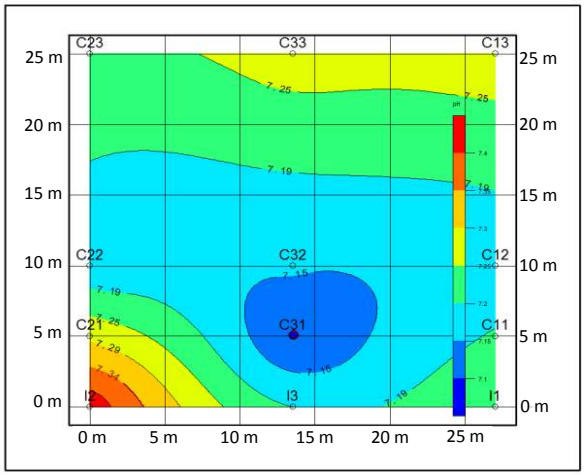

pH, ranging from 7.1 to 7.4, with the lowest values located at $[tCOCs]_{max}$

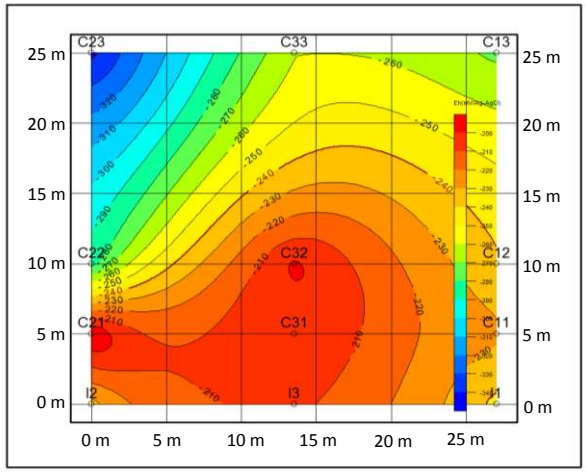

ORP, ranging from -200 to -340 mV vs Ag-AgCl, is proof of mild anaerobic media

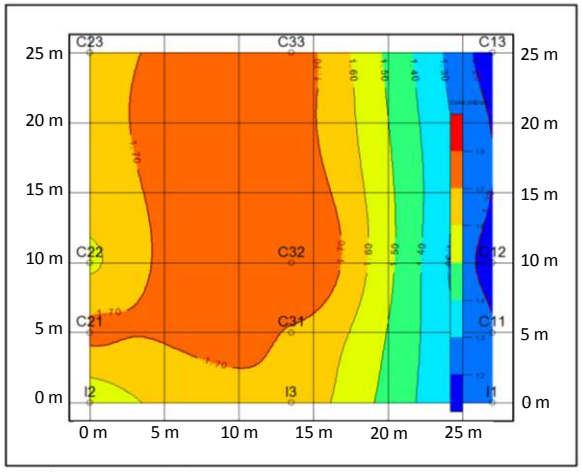

Conductivity, ranging from 1.2 to 1.7 mS cm^{-1}, is correlated with $[Cl^-]$

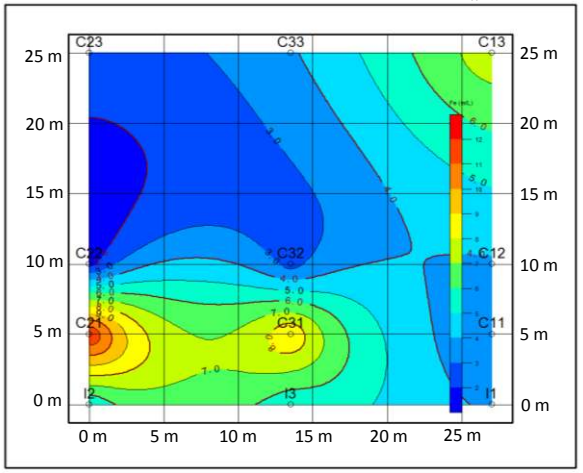

$[Fe^{2+}]$, ranging from 2 to 10 mg L^{-1}, is proof of anaerobic media

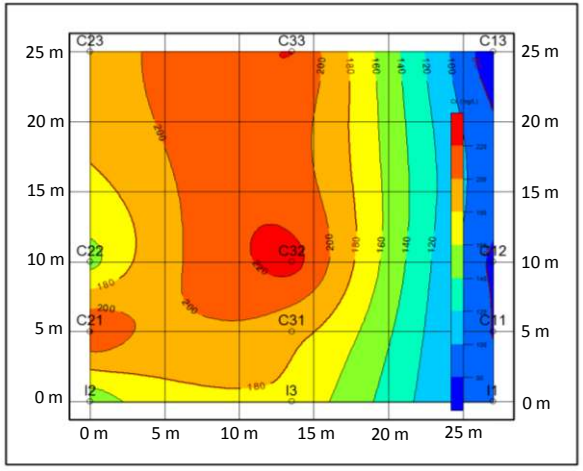

$[Cl^-]$, ranging from 80 to 220 mg L^{-1}, is proof of the natural attenuation

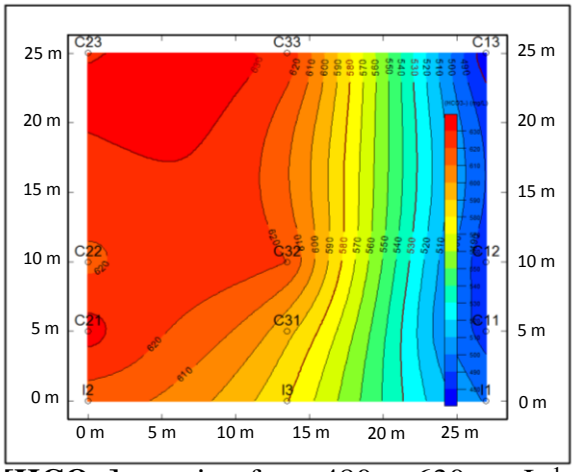

$[HCO_3^-]$, ranging from 480 to 630 mg L^{-1}, is proof of the biodegradation of organic compounds

Figure 6.14. State of the site before treatment: Interpolation of the major physical and chemical parameters in the water sampled in the three injecting wells (I1, I2 and I3) at two levels (average value of -10 and -20 m) and in the monitoring wells (C11, C12, C13; C21, C22, C23; and C31, C32, C33) at two levels (average value of -10 and -20 m). The axes are in meters.

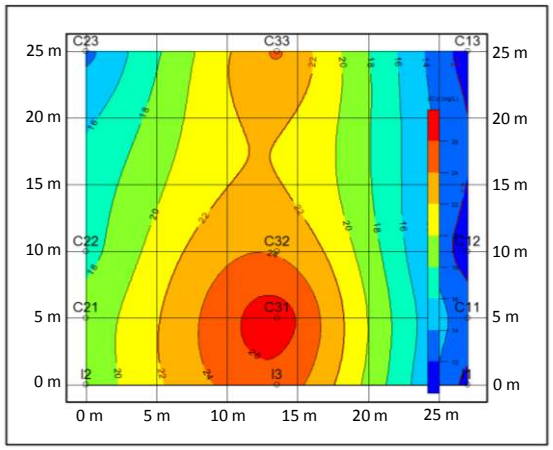

[tCOCs], ranging from 12 to 26 mg L^{-1}, with the highest content at the center

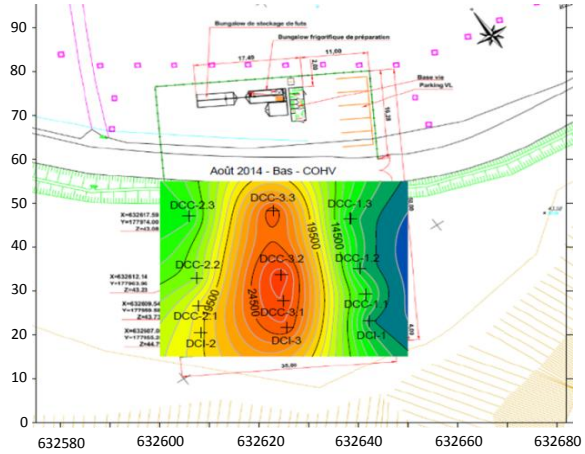

[tCOCs], ranging from 12 to 26 mg L^{-1}, at the level -20 m

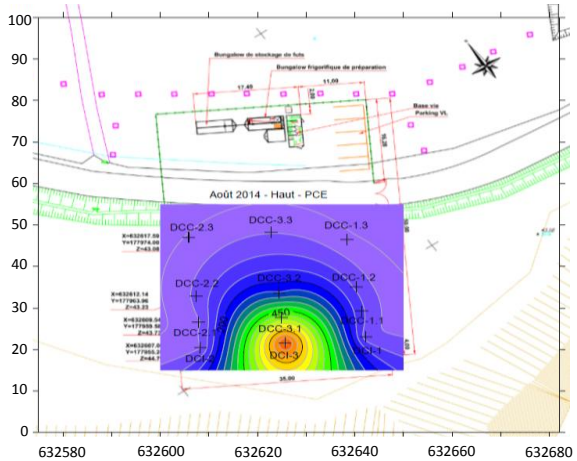

[PCE], ranging from 5 to 870 µg L^{-1}, at the level -10 m

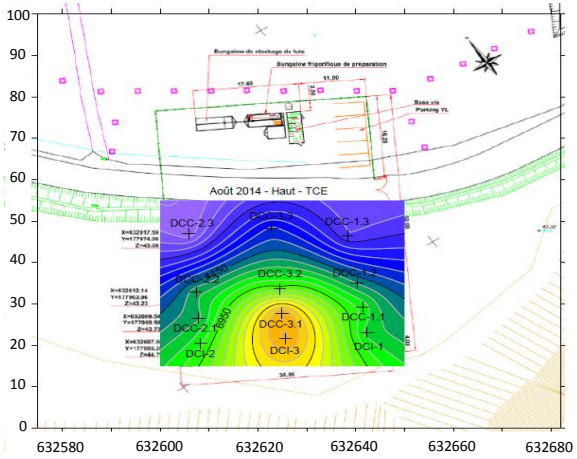

[TCE], ranging from 140 to 13000 µg L^{-1}, at the level -10 m

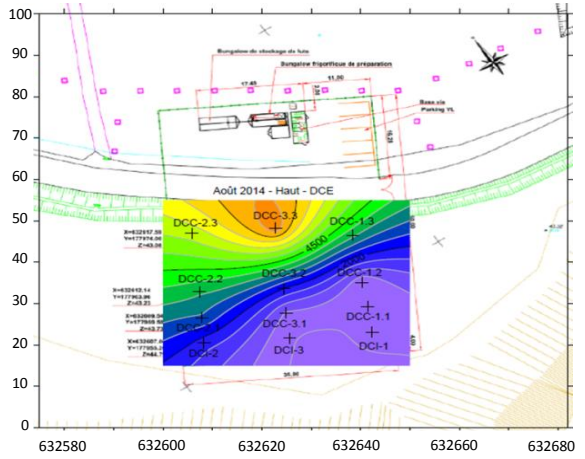

[cis-1,2-DCE], ranging from 250 to 7500 µg L^{-1}, at the level -10 m

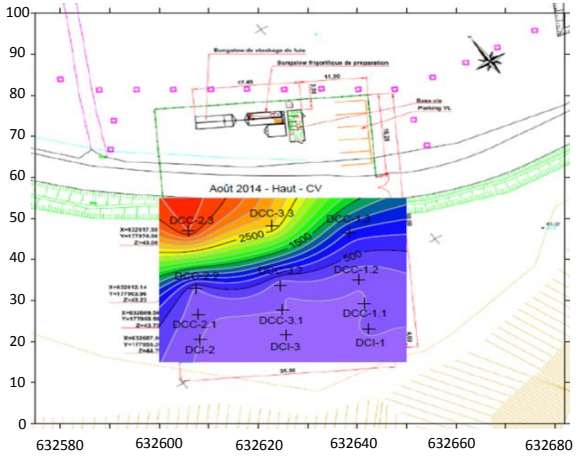

[VC], ranging from 100 to 3700 µg L^{-1}, at the level -10 m

Figure 6.15. State of the site before treatment: Interpolation of tCOCs, PCE, TCE, cis-1,2-DCE and VC contents in the water sampled in the three injecting wells (I1, 12 and 13), as the case might be, at levels -10 and -20 m, or -10 m or -20 m, and in the monitoring wells (C11, C12, C13; C21, C22, C23; and C31, C32, C33), as the case might be, at levels -10 and -20 m, or -10 m or -20 m. The axes are in meters.

The area was selected such as to provide adequate coverage of the contamination for further demonstration of the pilot efficiency. Results showed that the entire investigated area was contaminated by COCs at all depth range. The highest concentrations of total COCs in groundwater were detected in the upper zone of the future pilot (South-West). PCE and TCE were confirmed to be the main pollutants of concern on the site. Their contents, ranging from 5 to 870 µg L^{-1} for PCE and from 140 to 13000 µg L^{-1} for TCE, decreased sharply in the direction of the groundwater flow, due supposedly to natural attenuation. This process is further supported by the presence of cis-1,2-DCE and VC, for which the highest concentrations (up to 3700 µg L^{-1} in PZ C23) were found at the North-West, in the direction of the groundwater flow. In the area, pH was neutral in the range from 7.1 to 7.4, i.e. the optimal pH range for reductive biodechlorination (Aziz et al. 2013). Redox potential ranged from -200 to -340 mV/Ag-AgCl, indicating mild anaerobic groundwater conditions and the depletion of dissolved oxygen. In agreement with Pourbaix (1963), the redox potential decreases with pH. Nevertheless, it decreased in the order of magnitude of 100 mV when the pH only varied in the order of magnitude of 0.3 unit. The main results indicated that the lower the redox potential, the higher the chloride content, the higher the conductivity, the lower the dissolved Fe^{2+} content, and the higher the alkalinity. Alkalinity reflects the buffering capacity of the aquifer. An increase in alkalinity in association with a stable pH value indicate that the buffering capacity of the aquifer is sufficient to neutralize the metabolic acids produced by the degradation of substrates. Here, the elevated alkalinity values, ranging from 480 to 630 mg L^{-1} at neutral pH, are the proof of the biodegradation of organic compounds, e.g. natural organic matter (NOM) or additional anthropogenic contaminant such as BTEX, which produce CO_2 that dissolves in HCO_3^-. This result is therefore an indicator of a microbial activity, for which the organic matter is the electron donor. The high alkalinity content in combination with the facts that (i) mild redox potential were measured and (ii) no efficient reduction occurred, also demonstrated that no methanogenesis was happening (Wiedemeier et al. 1998; Suthersan 2002). The presence of dissolved Fe(II) demonstrated that sulfate reduction to sulfide (sulfanogenesis) was not occurring, i.e. there was no precipitation of Fe(II) in FeS.

The natural attenuation can be explained by (i) the presence of an indirect biologically mediated process and (ii) the direct reductive dechlorination of COCs, which act as electron acceptors. The first scenario involves a biologically mediated abiotic degradation (Scherer et al. 2014). Indeed, the oxidation of organic matter can also be associated to the reduction of other electron acceptors than COCs. Here, the presence of dissolved Fe^{2+} ranging from 2 to 10 mg L^{-1} is an indicator of the presence of iron-reducing bacteria (IRB) that use Fe(III) oxide-hydroxides as electron acceptors (Wiedemeier et al. 1998, 1999). Fe(II) species can reduce the aquifer minerals, e.g. magnetite and clays, and surface-complexed Fe(II) or metastable iron oxide-hydroxides can be responsible for the mediated abiotic reductive dechlorination (Jeong et al. 2011). This hypothesis agrees with the decrease in Fe^{2+} content observed in the North-West, in association with the decrease in PCE and TCE contents and the increase in cis-1,2-DCE and VC contents. The second scenario requires the presence of specific dehalorespiring bacteria strains that are effective for the degradation of chlorinated ethylenes. Those microorganisms use the carbon substrate, or H_2 resulting from its fermentation, for COCs reductive dechlorination in a sequential electron transfer (Stroo et al. 2014).

The synergy of the data collected is sufficient to document the occurrence of natural attenuation and its level of occurrence. The sequential degradation of PCE to VC was observed inside the small area; however, the complete reduction to ethylene is a slower process (Middeldorp et al. 1999), which can explain the accumulation of VC in the upper part (PZs C23 and C33) of the pilot area.

5.2.5. Synthesis on the natural attenuation and state of the two areas before treatment

The objective of the preliminary study regarding the large and the small areas was to improve the understanding of the mechanisms and kinetics of natural attenuation occurring in the groundwater of this aged polluted site. The pollution in the sandy aquifer (Cuisian period) stands today as a majority of COCs, mainly chlorinated ethylenes. The data basis composed of geochemical analyses from this site since 1999 was assessed.

The nature, abundance and relative distribution of COCs and their metabolites were measured, and their spatiotemporal evolution were investigated and interpolated. Temperature, pH, redox potential, conductivity, content in chloride, bicarbonate, dissolved iron, sulfate, phosphate and sulfide were considered, interpolated and mapped. Thus, this study has shown the slow natural attenuation process, its mechanisms (reduction pathways) and limiting steps (nature and abundance of metabolites). Chloride ion was the principal produced component (evolution from 15 mg L^{-1} in a near not impacted zone to 340 mg L^{-1}), as well as bicarbonate (150 to 650 mg L^{-1}) resulting from CO_2 dissolution after its production by the biodegradation of organic compounds.

Within the future pilot zone, the total COCs content at this location was about 30 mg L^{-1}. The weight fractions of COCs were: 0.3-1.0% for PCE, 25-45% for TCE, 0.3-0.4% for trans-1,2-DCE, 0.5-15.0% for cis,1,2-DCE, 40-50% for 1,1-DCE, 0.7-30.0% for VC, 0.8-1.3% for 1,1-DCA, 0.2-0.4% for DCM, 3.5-6.0% for TCM, and 0.3-0.4% for CT.

The existence of mild anaerobic conditions, the production of Fe(II), the existence of a source of fermentable substrates (organic matter as well as BTEX), and the high concentration of chloride ions are among the qualitative indicators evidencing the natural attenuation of chlorinated solvents through dehalorespiring bacteria and/or a biologically mediated abiotic dechlorination by Fe(II) species.

5.3. Treatment on the demonstration site

5.3.1. Treatment principle and calculation of reagent concentrations to be injected

The pilot demonstration aimed at investigating three different chemical treatments: (i) line 1 = treatment with dithionite alone, (ii) line 2 = treatment with nZVI alone and (iii) line 3 = treatment with dithionite + nZVI. The objective was to investigate, verify and consolidate the obtained results in laboratory at a larger scale*, in situ*. The three treatment injections were thus sufficiently spaced in space (13.5 m) and time (sequential treatment) to avoid any interactions between the reactive zones.

Reagents were injected into the sandy water table by means of the three different injection wells (DCI1, DCI2 and DCI3) at four levels in each one. The sampling and the monitoring were carried out thanks the other nine piezometers (DCC11, DCC12, DCC13; DCC21, DCC22, DCC23; and DCC31, DCC32, DCC33) downstream from the injection wells (Fig. **6.16**). They were equipped with multiparametric probes which provided temperature, pH, redox potential and conductivity. Two zones with strainers were separated by a full tube of 1 m length for sampling at two levels, top (H for “Haut”, Top) and bottom (B for “Bas”, Bottom).

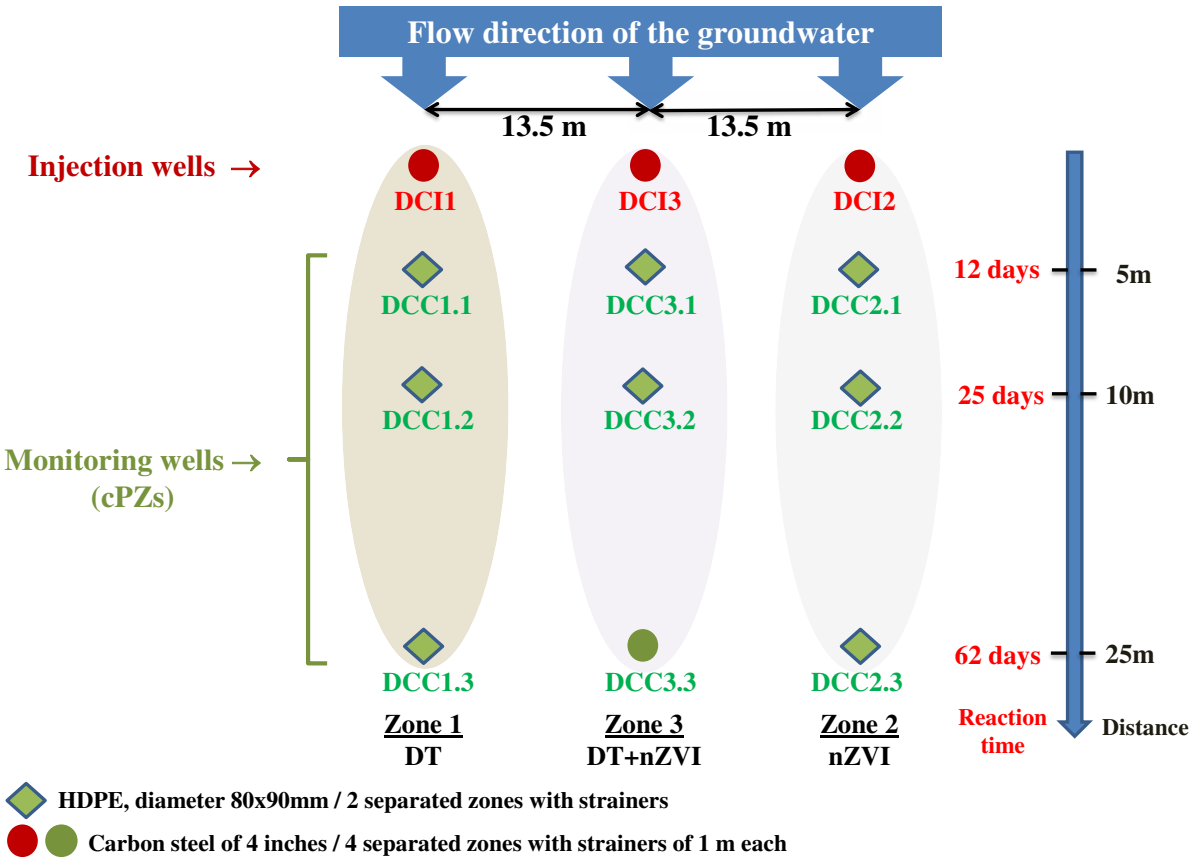

Figure 6.16. Concept of the demonstration pilot on Néry-Saintines site.

The calculation of the concentration and the flow of the solutions to be injected were carried out starting from the calculation of the pollutants mass throughput entering the system composing the pilot zone. Water-table flow Q on the right of the pilot was deduced from Eq. **6.64**:

$$Q = K.e.L.i \qquad \text{(Eq. 6.64)}$$

where Q is the water-table flow ($m^3\ s^{-1}$), K is the permeability coefficient of the Cuisian sands formation ($m\ s^{-1}$), e is the thickness of the saturated zone ranging between 20.40 m (injector DCI-2) and 21.10 m (injector DCI-1) (m), L is the length of the orthogonal section to the flow direction (m, see Fig. **6.17**) and i is the gradient of average hydraulic load, estimated at 2.9%. The flow obtained lies between 8.77 10^{-4} and 8.92 10^{-4} $m^3 \cdot s^{-1}$, an annual throughput of about 27668 to 28135 m^3.

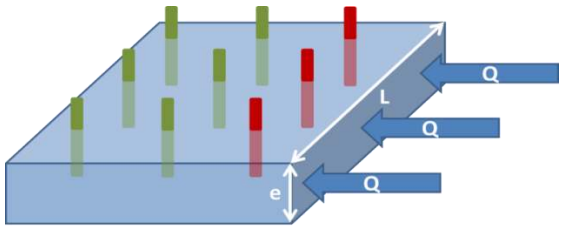

Figure 6.17. Geometrical configuration of the treatment device. The frontage feed in pollutant of the pilot is calculated by multiplication of the thickness *e* by the length of the frontage *L*.

Pollutant mass flow was calculated from Eq. **6.65**:

$$q = Q.C \qquad \text{(Eq. 6.65)}$$

where q is the pollutant mass flow (g h^{-1}), Q is the water-table flow (m^3 h^{-1}) and C is the average pollutant concentration (g m^{-3}). Thus, the value of pollutant mass flow obtained on the level of the section to be treated was about 29 g h^{-1}.

Figure **6.18** presents the injection units of nZVI and DT. The necessary quantity of reagents was calculated taking account of the pollutant mass flow as well as the efficient mass ratio reactant/pollutant obtained during the preliminary tests in laboratory. The calculation methods are confidential and are not presented here. The treatment duration was fixed at 62 days.

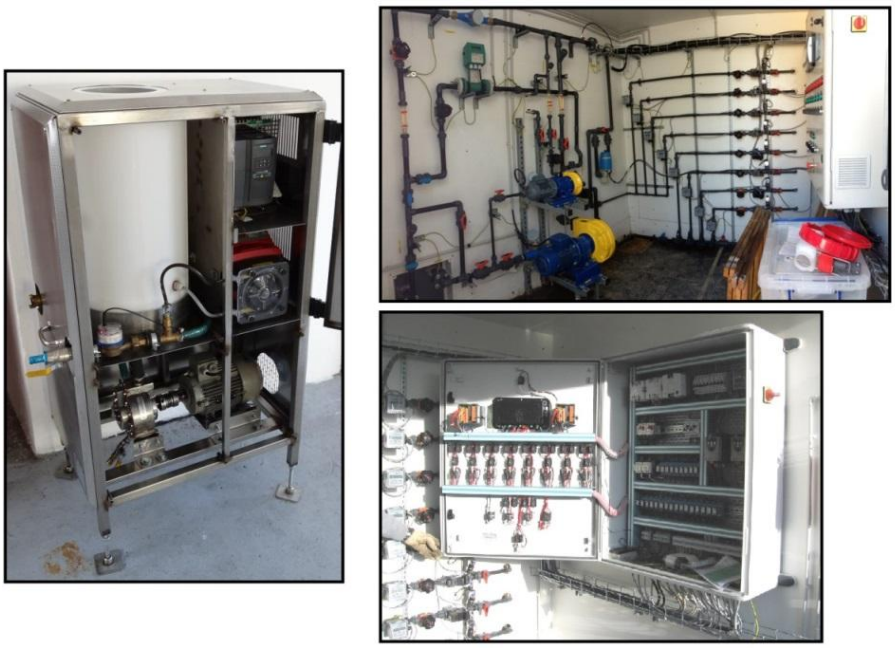

Figure 6.18. Injection units of nZVI (left) and DT (right), with automate.

5.3.2. Line 1: dithionite solution alone

Dithionite solution (150 g L^{-1}) was injected from May 18 to June 18, 2015, with an average flowrate of 36 L h^{-1}, diluted on line with fresh water to reach a flowrate of 200 L h^{-1}. Thus, an average of 5.4 kg of dithionite was injected each hour during one month at a constant flowrate of 200 L h^{-1}. The injection took place simultaneously at four levels into DCI1.

Evolution of the total content of COCs

The reduction percentage of the total content of COCs (tCOCs) obtained at two sampling levels (high and low, H and B) of each control (DCC1.1, DCC1.2, DCC1.3) compared to the initial results obtained in August 2014 are presented in Fig. **6.19.** The reduction rates are based on (i) the sampling day, (ii) the distance of the control piezometer from the injector and (iii) the level ('H' or 'B').

The abatement percentage ranged from 0 to 90% in the area. DCC1.1, located at 5 m from the injector, has the higher abatement, ranging from 55 to 90%. DCC1.2 and DCC1.3, located respectively at 10 m and 25 m from DCI1, had lower abatement percentage, ranging from 6 to 44% for DCC1.2 and 0% and 27% for DCC1.3. At the end of the treatment (i.e. July 8), the global impact appears insignificant on the two cPZ, DCC1.2 and DCC1.3, whereas the strong reductive conditions were responsible for a 90% of the reduction percentage.

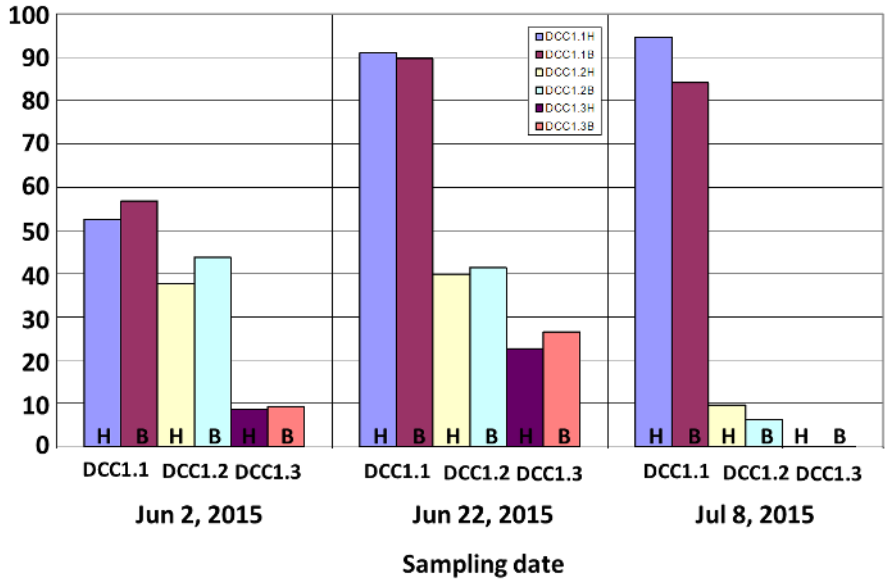

Figure 6.19. Reduction percentage of total content of COCs compared to the reference of August 18, 2014, at the two sampled levels of each control piezometer of the line 1.

Evolution of alkalinity expressed as bicarbonate and of chloride content

Table **6.18** presents alkalinity expressed as bicarbonate concentration and chloride concentration in the sampled water at two levels (H and B) of each control piezometer of line 1.

Table 6.18. Alkalinity expressed as bicarbonate concentration (mg L^{-1}) and chloride concentration (mg L^{-1}) in the sampled water at two levels (H and B) of each control piezometer of line 1.

Date	Element	DCI1H	DCI1B	DCC1.1H	DCC1.1B	DCC1.2H	DCC1.2B	DCC1.3H	DCC1.3B
Aug 18, 2014	Alkalinity	501.9	495.6	495.6	494.1	487.5	475.8	467.7	478.1
	Chloride	77.7	87	81.7	77	81.3	70	64.3	67.3
Jun 2, 2015	Alkalinity	-	-	556.5	571.1	512.5	519.9	458.8	463.7
	Chloride	-	-	106	142	82	88	70	108
Jun 22, 2015	Alkalinity	-	-	512.5	537	495.5	500.3	461.3	461.3
	Chloride	-	-	2500	500	276	270	76	66
Jul 8, 2015	Alkalinity	-	-	> 2000	> 2000	540.9	543.8	457.9	451.5
	Chloride	-	-	500	500	104	102	70	80

Bicarbonate (HCO_3^-), already rather high, marginally increased, except in DCC1.1H and B. This increase was rather assigned to dithionite degradation products. Chloride content (Cl^-), already rather high in line 1 (compared to Néry drinking water), increased especially at the first two controls (DCC1.1 and DCC1.2). It remains in the same order of magnitude in DCC1.3. As the increases were mainly due to dithionite solutions, which contains chloride ions, the follow-up of Cl^- can be used to trace the dithionite arrival on the level of a cPZ. The acquired data clearly confirmed that dithionite did not reached DCC1.3.

Evolution of TCE, cis-1,2-DCE, 1,1-DCE and VC content

Table **6.19** presents the individual evolutions of TCE, cis-1,2-DCE, 1,1-DCE and VC content in the cPZs of line 1. In DCC1.1, a decrease in the four compounds was observed between June 2 and July 8. At both levels, an abatement of more than 80%, and up to 95%, for TCE, cis-1,2-DCE, 1,1-DCE and VC, was obtained.

Table 6.19. TCE, cis-1,2-DCE, 1,1-DCE and VC concentration (in µg L^{-1}) in the sampled water at two levels (H and B) of each control piezometer of line 1.

Date	Individual COC	DCI1H	DCI1B	DCC1.1H	DCC1.1B	DCC1.2H	DCC1.2B	DCC1.3H	DCC1.3B
Aug 18, 2014	TCE	5700	4200	6300	5700	4900	4800	1500	980
	cis-1,2-DCE	220	260	80	120	54	180	3600	4100
	1,1-DCE	6000	4200	6100	5500	4900	4600	4200	4500
	VC	130	110	100	110	120	150	840	800
Jun 2, 2015	TCE	-	-	4600	3800	4800	4400	1900	2700
	cis-1,2-DCE	-	-	53	52	74	100	2300	1700
	1,1-DCE	-	-	3300	4000	3200	3100	1900	2000
	VC	-	-	50	50	50	50	640	720
Jun 22, 2015	TCE	-	-	640	690	4800	4800	1500	1900
	cis-1,2-DCE	-	-	7	8.2	75	100	2400	2000
	1,1-DCE	-	-	410	440	650	370	3300	2900
	VC	-	-	5	6.8	29	25	450	530
Jul 8, 2015	TCE	-	-	26	1100	3600	3600	1800	1600
	cis-1,2-DCE	-	-	11	17	89	120	2600	3100
	1,1-DCE	-	-	370	500	5200	5200	5600	5300
	VC	-	-	5	6.2	58	62	440	580

In DCC1.2, the reduction of the tCOCs was related to 1,1-DCE and, in a lesser extent, to VC, with an abatement reaching 80-90% and 42-50%, respectively, between June 2 and June 22. From June 22, TCE content was decreased by 25%. This phenomenon was accompanied by an increase in cis-1,2-DCE content by 18-20%, of 1,1-DCE content by 700-1300% and of VC content by 100-150%. This result highlights the rapid dechlorination rate of both TCE and cis-1,2-DCE by dithionite (both undergo reductive dechlorination), while both 1,1-DCE and VC accumulated.

In DCC1.3, two different behaviors were observed depending on the sampling depth. At -10 m, TCE and cis-1,2-DCE content remained unchanged, and only 1,1-DCE and VC appeared impacted. From June 2 to July 8, 1,1-DCE content increased drastically whereas VC content decreased by 31%. At -20 m, TCE content decreased by 60%. In the same time, cis-1,2-DCE and 1,1-DCE content increased by 80 and 165%, respectively, while VC content decreased by 20%.

By limiting the comparison to the data of June 2 and July 8, 2015, results show that the use of dithionite clearly decreased COCs content up to 100% in the first cPZ DCC1.1 “H” and “B”. These results are in good agreement with those obtained at laboratory scale. They also highlight the applicability of dithionite treatment, whose injection is facilitated in groundwater by using a soluble reductant.

However, the lower abatement for TCE and cis-1,2-DCE and the accumulation of 1,1-DCE and VC observed in DCC1.2 clearly shows a limitation in the treatment due to an insufficient dithionite quantity (i.e. COCs reduction is effective when dithionite is abundant). This phenomenon can first be explained by the dilution of dithionite by the widening of its plume, since the speed of water-table was higher than 40 cm d^{-1}. It is also explained by the oxidation of dithionite due to the presence of trace elements, organic matter, clays and other contaminants in the ground. This hypothesis was straitened by the strong reducing conditions that remained in DCC1.1 after the treatment (July 8), in agreement with the redox potential (-650 mV/Ag-AgCl) and the high reductive percentage, and the insignificant impact of the treatment in DCC1.3, because dithionite did not reach this cPZ.

The later phenomenon agrees with the fact that only VC decrease in DCC1.3, essentially between June 2 and June 22. This highlights a temporary bio-oxidative process in agreement with the lack of the reductive chemical treatment and the probable presence of very low dissolved oxygen content in the groundwater (due to sampling and measurements). "Mild" oxidizing conditions (-175 mV/AgAgCl) straitened that hypothesis, while neither pH (7.25) nor temperature (12.2 °C) did vary. Moreover, aerobic and anaerobic oxidation mainly concerns VC (Hartmans and De Bont 1992; Bradley and Chapelle 1996; Verce et al. 2000, 2001; Coleman et al. 2002; Danko et al. 2004; Elango et al. 2006; Gossett 2010; Mattes et al. 2010).

This highly efficient metabolic process allows the microorganisms that carry it to integrate these molecules into their metabolism to lead either to their use as a carbon source for the synthesis of more complex molecules (anabolism), or to their use as a source of energy degrading them to CO_2 (catabolism) (Mattes et al. 2010). Nevertheless, because (i) the removal of VC was not efficient (20%) and (ii) TCE dechlorination pursued in agreement with the accumulation of the degradation products, there was ample time for anaerobic reactions to proceed once the oxygen was consumed. Dehalorespiration process is thus assumed to be responsible of TCE dechlorination between June 2 and July 8. Nevertheless, the increase in 1,1-DCE content remains questionable.

5.3.3. Line 2: nZVI alone

New and confidential injection techniques were used to inject nZVI particles at four levels in the injection well DCI2. Injections were sequential (at each level) and continuous during a day per level between March 19, 2015 and March 24, 2015, as follows:

- Level 1: March 19, 2015: injection of 1 canister of nZVI solution: water flowrate of 240 L h^{-1} and nZVI solution flowrate of 84 mL·min^{-1}; i.e. continuously 16.8 mL of nZVI per liter of water;
- Level 2: March 20, 2015: injection of 1 canister of nZVI solution: water flowrate of 237 L h^{-1} and nZVI solution flowrate of 84 mL·min^{-1}; i.e. continuously 21.2 mL of nZVI per liter of water;
- Level 3: March 23, 2015: injection of 1 canister of nZVI solution: water flowrate of 327 L h^{-1} and nZVI solution flowrate of 84 mL·min^{-1}; i.e. continuously 15.4 mL of nZVI per liter of water;
- Level 4: March 24, 2015: injection of 1 canister nZVI solution by using a suppressor.

The injection resulted in the installation of a vertical barrier limiting itself to injector DCI2 and its immediate vicinity.

Evolution of the total content of COCs

Figure **6.20** presents the reduction percentage of tCOCs obtained at the two levels (H and B) of each cPZ (DCC2.1, DCC2.2, DCC2.3), compared to the results achieved during the reference sampling of August 2014. Let us consider that analyses were carried out three months after the first injection. COCs abatements ranged between 5 and approximately 60% according to the sampling date, the cPZ and the sampling level. In comparison, the abatements ranged only from 2 to 10% in laboratory batch experiments.

Significant results in the range from 30 to 60% were obtained on June 2 for DCC2.2 and DCC2.3 and on June 22 for DCC2.3, evidencing that the abatements were ascribable with the injection of nZVI solutions. The progressive decrease in the abatements, as illustrated/highlighted for DCC2.2, is in agreement with the relative loss in reactivity of iron particles.

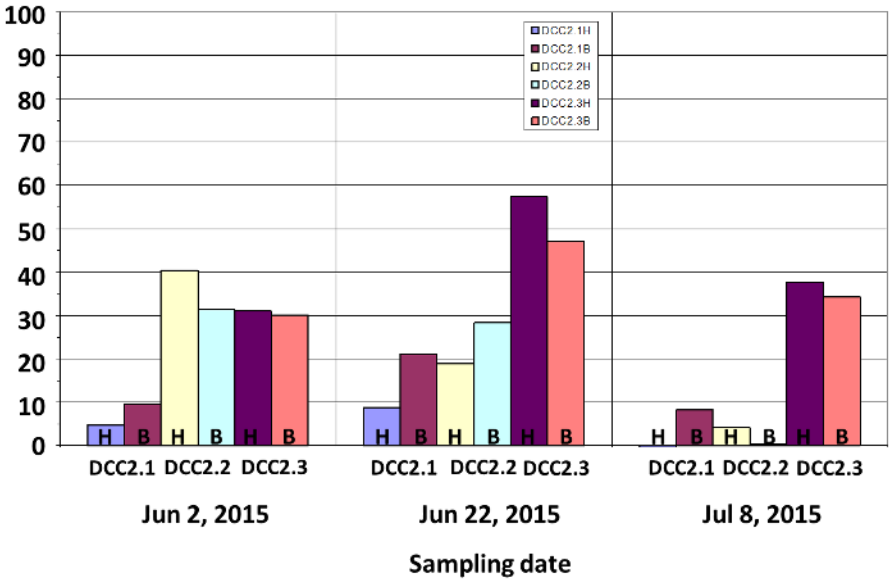

Figure 6.20. Reduction percentage of tCOCs compared to the reference of August 18, 2014, at the two levels of each control piezometer of the line 2.

Evolution of alkalinity expressed as bicarbonate and of chloride content

Table **6.20** presents alkalinity expressed as bicarbonate concentration and chloride concentration in the sampled water at two levels (H and B) of each control piezometer of line 2.

Table 6.20. Alkalinity expressed as bicarbonate concentration (mg L^{-1}) and chloride concentration (mg L^{-1}) in the sampled water at two levels (H and B) of each control piezometer of line 2.

Date	Element	DCI2H	DCI2B	DCC2.1H	DCC2.1B	DCC2.2H	DCC2.2B	DCC2.3H	DCC2.3B
Aug 18, 2014	Alkalinity	623.7	603.9	623.7	645.1	614.4	619.2	618.6	640.5
	Chloride	127.0	162.0	237	206	151	152.3	191	191.7
Jun 2, 2015	Alkalinity	-	-	615.1	627.3	615.1	595.5	576	549.2
	Chloride	-	-	182	226	128	146	136	124
Jun 22, 2015	Alkalinity	-	-	623.8	619.9	619.9	600.4	576	568.7
	Chloride	-	-	270	226	192	156	174	162
Jul 8, 2015	Alkalinity	-	-	616.3	611.4	613.3	600.4	574	562.6
	Chloride	-	-	248	240	194	168	176	170

In comparison with 2014, Cl^- content and alkalinity expressed by bicarbonate concentration remained in the same order of magnitude whatever the PZ, the depth and the sampling date. These results evidence that the injection of nZVI particles did not affect the natural attenuation that was occurring.

Evolution of TCE, cis-1,2-DCE, 1,1-DCE and VC content

Table **6.21** presents the individual evolution of TCE, cis-1,2-DCE, 1,1-DCE and VC concentration in cPZs of line 2. The reduction of the tCOCs in DCC2.1 and DCC2.2 relates to TCE, cis-1,2-DCE and 1,1-DCE, with a relative increase in VC content. This shows the limitation of the treatment due to an insufficiency in nZVI loading on DCC2.2 and DCC2.3 levels.

Table 6.21. TCE, cis-1,2-DCE, 1,1-DCE and VC concentration (µg L^{-1}) in the sampled water at two levels (H and B) of each control piezometer of line 2.

Date	Individual COC	DCI2H	DCI2B	DCC2.1H	DCC2.1B	DCC2.2H	DCC2.2B	DCC2.3H	DCC2.3B
Aug 18, 2014	TCE	6400	6500	5400	5700	5300	3400	160	140
	cis-1,2-DCE	1700	2300	2900	2600	3600	4800	5700	5400
	1,1-DCE	8700	9200	9200	9300	6400	6100	4300	4100
	VC	100	140	180	180	280	320	3700	3600
Jun 2, 2015	TCE	-	-	4800	3900	300	230	140	125
	cis-1,2-DCE	-	-	2400	2800	2900	3300	3100	3000
	1,1-DCE	-	-	9400	9100	2200	2300	2000	1950
	VC	-	-	200	230	3500	4000	4100	4050
Jun 22, 2015	TCE	-	-	4600	3800	3400	3000	160	170
	cis-1,2-DCE	-	-	3400	2800	2800	2500	2200	2700
	1,1-DCE	-	-	7800	7100	5600	4200	940	1000
	VC	-	-	220	260	740	640	2400	2900
Jul 8, 2015	TCE	-	-	3500	3300	2500	3100	220	130
	cis-1,2-DCE	-	-	3200	2900	3300	2500	3300	3400
	1,1-DCE	-	-	11000	1000	8100	8200	2300	2100
	VC	-	-	210	200	1100	800	2800	3000

In DCC2.1, whatever the sample date or the depth, COCs content remained globally in the same order of magnitude from August 2014 to July 2015. However, data presents some characteristics that have to be discussed. From June 2 to July 8, TCE content decreased in the range from 15 to 27%. In the same time, VC content remained in the same order of magnitude, whereas cis-1,2-DCE and 1,1-DCE content increased up to 25% and 14%, respectively. Between June 2 and June 22, the slight decrease in TCE content was accompanied by a slight enhancement of cis-1,2-DCE content. In the same time, a slight decrease in 1,1-DCE content is accompanied by a slight increase in VC. Between June 22 and July 8, the decrease in TCE and cis-1,2-DCE content was accompanied by the increase in 1,1-DCE content, while VC content slightly decreased. These results tend to evidence the occurrence of biological processes in agreement with the natural attenuation (Morrison and Murphy 2006). As already discussed, the slight decrease in VC content between June 22 and July 8 could result from a temporary bio-oxidative process due to the sampling and the measurements campaign. The pursuit of TCE biodechlorination strengthened that anaerobic reactions continued after the consumption of oxygen.

Regarding DCC2.2, only the data acquired in June 2 showed a practical interest. In comparison with 2014, results clearly evidenced treatment effect of nZVI. The drastic decrease observed for TCE, cis-1,2-DCE and 1,1-DCE content, respectively up to 94%, 31% and 66%, resulted in the increase in VC content up to 90%. Although the use of ZVI particles should result in VC circumvention (Arnold and Roberts 2000), the progressive decrease in ZVI reactivity, associated with the growth and transformation of the oxide shell, can lead to a change in the degradation pathways from β-elimination to hydrogenolysis, in agreement with the accumulation of VC.

The treatment effect of nZVI particles was emphasized in DCC2.3 regarding the results acquired between June 2 and June 22. From August 2014 to June 2, 2015, the use of nZVI particles resulted in the drastic decrease in cis-1,2-DCE content (44-46%), 1,1-DCE content (52-53%) and, in a lesser extent, in TCE content (10-13%), which was already rather low. In the same time, VC content only

increased up to 11-13%. In comparison with the data obtained for DCC2.2, these results are in a better agreement with the use of nZVI. They clearly evidenced that ZVI circumvented VC (Arnold and Roberts 2000). In comparison with DCC2.2, these results can be explained by the rather low content of TCE in the cPZ. Data acquired in June 22 clearly highlighted the results obtained on June 2. The decrease in ZVI reactivity was nevertheless clearly evidenced versus time, from June 22 to July 8 with a progressive increase in TCE content and its degradation products.

In comparison with the data acquired at laboratory scale, the use of nZVI resulted in higher reductions (up to 60% versus 10% at laboratory scale). This result can be explained by a symbiosis between the implementation of the reductive process and the natural attenuation occurring on site. This hypothesis is supported by the results acquired for alkalinity, which remained in the same order of magnitude versus time.

5.3.4. Line 3: nZVI and dithionite

New and confidential injection techniques have been used to inject sequentially nZVI at four levels into DCI3:

- Level 1: April 2, 2015: injection of 1 canister of nZVI solution: water flowrate of 400 L h^{-1} and nZVI solution flowrate of 84 mL min^{-1}; i.e., continuously 12.6 mL of nZVI per liter of water;
- Level 2: April 3, 2015: injection of 1 canister of nZVI solution: water flowrate of 375 L h^{-1} and nZVI solution flowrate of 84 mL min^{-1}; i.e., continuously 13.44 mL of nZVI per liter of water;
- Level 3: April 7, 2015: injection of 1 canister of nZVI solution: water flowrate of 321 L h^{-1} and nZVI solution flowrate of 84 mL min^{-1}; i.e., continuously 5.70 mL of nZVI per liter of water;
- Level 4: April 9, 2015: injection of 1 canister nZVI solution.

During the period from May 18 to June 18, 2015, only dithionite was injected simultaneously at the four levels as follows: injection at 20 L h^{-1} of a 150 g L^{-1} dithionite solution diluted on line to reach a flowrate of 200 L h^{-1} (an average of 3 kg of dithionite were injected each hour during 1 month with a constant flowrate of 200 L h^{-1}).

Evolution of the total content of COCs (tCOCs)

Figure **6.21** presents the reduction percentage of tCOCs content obtained at the two levels (H and B) of each cPZ (DCC3.1, DCC3.2, DCC3.3) of line 3 compared to the results obtained during the reference sampling performed in August 2014. Let us recall that these reductions are first regarded as ascribable to nZVI injection, and then supplemented by dithionite solution injections. Globally, the results are in the same order of magnitude as those obtained by using dithionite solution alone, although the tCOCs was two times higher.

COCs abatement percentages ranged between 10 and 85% according to the sampling period, the cPZ (distance of this one from the injector DCI2) and the sampling level (H or B). The impact of the treatment was obviously stronger on DCC3.1, located at 5 m from the injector DCI3, in which the reductions reached 85%. The second and third cPZs presented lower reductions, ranging from 5 to 30% for DCC3.2 and 32% to 51% for DCC3.3.

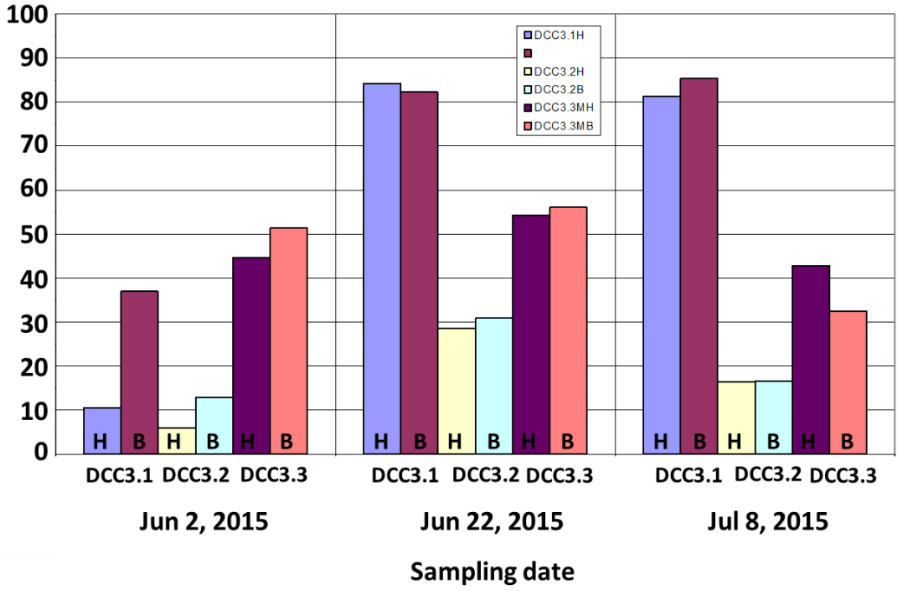

Figure 6.21. Reduction percentage of total COCs compared to the reference of August 18, 2014, at two levels of each control piezometer of the line 3.

Evolution of alkalinity expressed as bicarbonate and of chloride content

Table **6.22** presents alkalinity expressed as bicarbonate concentration and chloride concentration in the sampled water at two levels (H and B) of each control piezometer of line 3.

Table 6.22. Alkalinity expressed as bicarbonate concentration (mg L^{-1}) and chloride concentration (mg L^{-1}) in the sampled water at two levels (H and B) of each control piezometer of line 3.

Date	Element	DCI3H	DCI3B	DCC3.1H	DCC3.1B	DCC3.2H	DCC3.2B	DCC3.3H	DCC3.3B
Aug 18, 2014	Alkalinity	578.4	582.6	587.1	598.6	614.6	625.3	635.2	621.1
	Chloride	99.3	251.3	179.7	188	229	222	216	225.3
Jun 2, 2015	Alkalinity	-	-	541.8	571.1	549.2	500.3	583.3	519.9
	Chloride	-	-	178	308	274	222	128	194
Jun 22, 2015	Alkalinity	-	-	916.5	868.9	566.2	561.4	571.1	547.9
	Chloride	-	-	500	500	338	378	166	260
Jul 8, 2015	Alkalinity	-	-	1198.4	1189.8	547.2	554	571.1	579.7
	Chloride	-	-	500	500	234	244	152	242

Alkalinity content expressed as bicarbonate concentration, already rather high in 2014 (around 600 mg L^{-1}), slightly decreased, except in DCC3.1 H and B, where the increase was ascribable to the degradation products of dithionite. This result is also supported by the increase in Cl^- content in DCC3.1. The data also indicated that dithionite did not reach DCC3.2 and DCC3.3; even if a slight increase in Cl^- content was observed in DCC3.2, it was not related to an increase in alkalinity. As previously mentioned, dithionite can be consumed by organic matter, clays and other trace elements in presence. Here, dithionite can also reduce the passive layer on the surface of aged nZVI particles, resulting in the rejuvenation of the particles (Xie and Cwiertny 2010).

Concerning the data acquired between June 2 and July 8, 2015, alkalinity and Cl^- content remained in the same order of magnitude for DCC3.2 and 3.3. A slight increase in both parameters is nevertheless of interest in DCC3.2, and in a lesser extent in DCC3.3. As dithionite did not reach DCC3.2, dechlorination process downstream from the injection wells can thus be attributed to the previous nZVI solution injections, natural attenuation or both.

In agreement with the presence of iron-reducing bacteria (IRB) and dithionite, the reduction of Fe(III) in Fe(II) species could have depassivate iron particles (Roden and Zachara 1996; Gerlach et al. 2000; Williams et al. 2005), resulting in the reactivation of the particles for reductive dechlorination. This process can be envisaged until the total depletion of nZVI particles.

Evolution of TCE, cis-1,2-DCE, 1,1-DCE and VC content

Table **6.23** presents the individual evolution of TCE, cis-1,2-DCE, 1,1-DCE and VC content in the control piezometers of line 3.

Table 6.23. TCE, cis-1,2-DCE, 1,1-DCE and VC concentration (µg L^{-1}) in the sampled water at two levels (H and B) of each control piezometer of line 3.

Date	Individual COC	DCI3H	DCI3B	DCC3.1H	DCC3.1B	DCC3.2H	DCC3.2B	DCC3.3H	DCC3.3B
Aug 18, 2014	TCE	11000	11000	11000	12000	10500	11000	3600	4500
	cis-1,2-DCE	66	490	450	410	2000	1300	7800	7800
	1,1-DCE	12000	12000	13000	12000	12700	13000	8200	9900
	VC	68	130	110	120	150	150	2700	1900
Jun 2, 2015	TCE	-	-	8500	4000	9600	8800	350	420
	cis-1,2-DCE	-	-	1300	2800	710	960	3900	3800
	1,1-DCE	-	-	12000	8000	13000	12000	4000	2600
	VC	-	-	170	890	200	130	3600	4600
Jun 22, 2015	TCE	-	-	1900	2100	7800	7600	440	740
	cis-1,2-DCE	-	-	180	220	950	1100	3700	3600
	1,1-DCE	-	-	1600	1800	8800	8400	3200	3400
	VC	-	-	18	19	100	120	2500	2500
Jul 8, 2015	TCE	-	-	2600	2200	6900	6900	370	720
	cis-1,2-DCE	-	-	160	190	1200	1200	4400	5900
	1,1-DCE	-	-	1500	950	13000	13000	4900	5800
	VC	-	-	18	16	110	110	2900	3800

In DCC3.1, a decrease in all four compounds was observed between June 2 and July 8. At both levels, TCE reached an abatement in the range from 45 and 70%. It reached 88-93% for cis-1,2-DCE, 88% for 1,1-DCE and 90-100% for VC. Results showed that the use of dithionite in combination with nZVI clearly decreased COCs content up to 100% in the first cPZ DCC1.1 "H" and "B". In comparison, the effective mixture of both reagents resulted in higher reductions at the laboratory scale. The difficulty and problems encountered for the injection of nZVI particles clearly highlight the superiority of using dithionite solution for *in situ* reductive dechlorination.

The observed behavior for DCC3.1 is clearly different for DCC3.2 and DCC3.3, evidencing that dithionite did not reach either DCC3.2 or DCC3.3. In DCC3.2, two different behaviors were observed versus time. Between June 2 and June 22, a slight but remarkable decrease was observed for TCE content; reduction reached 14-19%, whereas it reached 9-12% between June 22 and July 8. In the same time, cis-1,2-DCE increased in the range from 13 to 25% between June 2 and June 22, and from 8 to 20% between June 22 and July 8. Both results tended to evidence the occurrence of biological processes occurring in DCC3.2; they highlight a slight increase of the biostimulation between June 2 and June 22. The same behavior as the one observed for TCE was observed for 1,1-DCE and VC. In the first period, 1,1-DCE content decreased by 30-32% and VC content decreased up to 50%. In the second period, VC remained in the same order of magnitude, whereas 1,1-DCE content increased by 47-54%.

The same behavior was observed in DCC3, but in a lesser extent.

5.3.5. Case study synthesis

Within the pilot zone, the total COCs content was about 30 mg L^{-1}. The weight fractions of COCs were: 0.3-1.0% for PCE, 25-45% for TCE, 0.3-0.4% for trans-1,2-DCE, 0.5-15.0% for cis,1,2-DCE, 40-50% for 1,1-DCE, 0.7-30.0% for VC, 0.8-1.3% for 1,1-DCA, 0.2-0.4% for DCM, 3.5-6.0% for TCM, and 0.3-0.4% for CT.

The existence of mild anaerobic conditions, the production and consumption of Fe(II), the existence of a source of fermentable substrates (organic matter as well as BTEX), and the high concentration of chloride ions are among the qualitative indicators evidencing the natural attenuation of chlorinated solvents through a biologically mediated abiotic dechlorination by Fe(II) species and dehalorespiring bacteria.

Regarding the setting up for the reduction processes, it is to be highlighted that neither the digging of the PZ in 2014 nor the involved reduction process implemented in 2015 disturbed the natural attenuation.

Results show that insufficient dithionite quantity leads to the accumulation of 1,1-DCE and VC. Conversely, efficient use of dithionite clearly decreased COCs content up to 100%. These results agreed with those obtained at laboratory scale. They also highlighted the applicability of dithionite treatment, whose injection is facilitated in groundwater by using a soluble reductant.

The use of nZVI particles resulted in higher abatements (up to 60%) in comparison with the data obtained at laboratory scale (up to 10%). This result can be explained by a symbiosis between the implementation of the reductive process and the natural attenuation, due to the release of hydrogen. This hypothesis was supported by the results acquired for alkalinity, which remained in the same order of magnitude versus time.

The combination of the use of dithionite and nZVI particles was able to decrease COCs content up to 100% but reductions rather reached 90%. This result was essentially attributed to the sequential injection of nZVI and dithionite, which resulted in dithionite consumption for the rejuvenation of aged nZVI particles. Consequently, dithionite did not reach the second cPZ. In comparison, the effective mixture of both reagents resulted in higher reductions at the laboratory scale (almost 100%). The difficulty and problems encountered for the injection of nZVI particles clearly highlight the superiority of using dithionite solution for *in situ* reductive dechlorination.

6. Summary

Chlorinated organic compounds are widely used for their specific properties in many commercial applications, and their physical and chemical properties determine their general behavior and fate as pollutants. Understanding natural attenuation and COCs transport and fate processes is one of the first steps in order to optimize chemical remediation contaminated groundwater.

Chemical reduction is an effective technique for the remediation of COCs in groundwater. Due to its core-shell structure, ZVI particles possess unique properties for soil and groundwater remediation, and the degradation mechanisms include adsorption, encapsulation, precipitation and chemical reduction. Since its introduction in permeable reactive barriers, the use of ZVI is the subject of extensive researches to improve the reactivity, stability and transport of the particles in subsurface environment. First, the development of small particles was then necessary to facilitate the delivery of ZVI particles for the treatment of a source of contamination. As shown by field experiments, the use of mZVI

particles appears as a great option as they are less expensive, exhibit less bactericidal effects and have a longer lifetime and a higher removal efficiency in comparison with nZVI particles. The use of a polymeric coating or a dispersant proves essential to improve both the stability and the transport of the particles. Then, the use of bimetallic particles, especially Pd/Fe particles, can be used to increase degradation rates by taking advantage from hydrodechlorination/hydrogenation reactions due to the generation of atomic hydrogen. However, the significant improvement in degradation rates has not yet been proven in field experiments. More recently, sulfidated particles have been developed and appear as a cost-effective alternative of bimetallic particles, but field experiments are required to fully understand their reactivity. Finally, the impact of iron-based technology on microbial activity needs to be evaluated in real conditions to combine efficiently abiotic and biotic degradation. Indeed, long-term studies on the fate and behavior of iron-based particles on groundwater are still necessary, in order to improve the development of simulation tools for predicting their performance in environmental applications.

It should be noted that COCs chemical reduction by ZVI particles of is strongly impacted by the presence of ions, metals/metalloids or other contaminants and by geological/hydrogeological characteristics of the polluted site. Thus, there is a need to conduct preliminary studies case by case to select the most suitable method for each situation, according to the initial site conditions, the performance goals, and the cost.

Acknowledgments

The authors acknowledge the ADEME AMI SILPHES project and the BRGM project MULTISCALEXPER PSO3 of D3E division for financial support for writing this chapter. The case study was supported by ADEME (French Environment and Energy Management Agency) in the framework of Eco-Industries 2011 program (project DECHLORED, contract no. 1172C0034) and received financial support by BRGM research division. The authors acknowledge Clément Zornig for creating and providing Fig. 6.5.

References

Abazari R, Heshmatpour F, Balalaie S (2013) Pt/Pd/Fe Trimetallic Nanoparticle Produced via Reverse Micelle Technique: Synthesis, Characterization, and Its Use as an Efficient Catalyst for Reductive Hydrodehalogenation of Aryl and Aliphatic Halides under Mild Conditions. ACS Catal 3:139–149. https://doi.org/10.1021/cs300507a

Adeleye AS, Keller AA, Miller RJ, Lenihan HS (2013) Persistence of Commercial Nanoscaled Zero-Valent Iron (nZVI) and By-Products. J Nanoparticle Res 15:1418. https://doi.org/10.1007/s11051-013-1418-7

Ai J, Yin W, B. Hansen HC (2019) Fast Dechlorination of Chlorinated Ethylenes by Green Rust in the Presence of Bone Char. Environ Sci Technol Lett 6:191–196. https://doi.org/10.1021/acs.estlett.9b00053

Al-Shamsi MA, Thomson NR (2013) Treatment of Organic Compounds by Activated Persulfate Using Nanoscale Zerovalent Iron. Ind Eng Chem Res 52:13564–13571. https://doi.org/10.1021/ie400387p

Allen-King RM, Grathwohl P, Ball WP (2002) New Modeling Paradigms for the Sorption of Hydrophobic Organic Chemicals to Heterogeneous Carbonaceous Matter in Soils, Sediments, and Rocks. Adv Water Resour 25:985–1016. https://doi.org/10.1016/S0309-1708(02)00045-3

Alvarez PJJ, Illman WA (2005a) Bioremediation and Natural Attenuation: Process Fundamentals and

Mathematical Models, John Wiley. John Wiley & Sons

Alvarez PJJ, Illman WA (2005b) Fundamentals of Groundwater Flow and Contaminant Transport Processes. In: Bioremediation and Natural Attenuation. John Wiley & Sons, Inc., Hoboken, NJ, USA, pp 115-167.

Amir A, Lee W (2011) Enhanced Reductive Dechlorination of Tetrachloroethene by Nano-Sized Zero Valent Iron with Vitamin B12. Chem Eng J 170:492–497. https://doi.org/10.1016/j.cej.2011.01.048

Amonette JE (2002) Iron Redox Chemistry of Clays and Oxydes: Environmental Applications. In: Fitch A (ed) Electrochemical Properties of Clays, Vol. 10. Aurora, Colorado, pp 90-147.

Amonette JE, Szecsody JE, Schaef HT, et al (1994) Abiotic Reduction of Aquifer Materials by Dithionite: A Promising In-Situ Remediation Technology. In: Gee GW, Wing NR (eds) In-Situ Remediation: Scientific Basis for Current and Future Technologies, Part 2, Battelle P. Richland, Washington, pp 851-881.

Amonette JE, Workman DJ, Kennedy DW, et al (2000) Dechlorination of Carbon Tetrachloride by Fe(II) Associated with Goethite. Environ Sci Technol 34:4606–4613. https://doi.org/10.1021/es9913582

Arnold WA, Ball WP, Roberts AL (1999) Polychlorinated Ethane Reaction with Zero-Valent Zinc: Pathways and Rate Control. J Contam Hydrol 40:183–200. https://doi.org/10.1016/S0169-7722(99)00045-5

Arnold WA, Roberts AL (1998) Pathways of Chlorinated Ethylene and Chlorinated Acetylene Reaction with Zn(0). Environ Sci Technol 32:3017–3025. https://doi.org/10.1021/es980252o

Arnold WA, Roberts AL (2000) Pathways and Kinetics of Chlorinated Ethylene and Chlorinated Acetylene Reaction with Fe(0) Particles. Environ Sci Technol 34:1794–1805. https://doi.org/10.1021/es990884q

Arnold WA, Winget P, Cramer CJ (2002) Reductive Dechlorination of 1,1,2,2-tetrachloroethane. Environ Sci Technol 36:3536–3541. https://doi.org/10.1021/es025655+

Auffan M, Achouak W, Rose J, et al (2008) Relation between the Redox State of Iron-Based Nanoparticles and Their Cytotoxicity toward Escherichia coli. Environ Sci Technol 42:6730–6735. https://doi.org/10.1021/es800086f

Aziz CE, Wymore RA, Steffan RJ (2013) Bioaugmentation Considerations. In: Bioaugmentation for Groundwater Remediation. Springer New York, New York, NY, pp 141–169

Babakhani P, Bridge J, Doong R, Phenrat T (2017) Continuum-Based Models and Concepts for the Transport of Nanoparticles in Saturated Porous Media: A State-of-the-Science Review. Adv Colloid Interface Sci 246:75–104. https://doi.org/10.1016/j.cis.2017.06.002

Bae S, Collins RN, Waite TD, Hanna K (2018) Advances in Surface Passivation of Nanoscale Zerovalent Iron (NZVI): A Critical Review. Environ Sci Technol 52:12010–12025. https://doi.org/10.1021/acs.est.8b01734

Bae S, Gim S, Kim H, Hanna K (2016) Effect of NaBH4 on Properties of Nanoscale Zero-Valent Iron and its Catalytic Activity for Reduction of p-nitrophenol. Appl Catal B Environ 182:541–549. https://doi.org/10.1016/j.apcatb.2015.10.006

Bae S, Hanna K (2015) Reactivity of Nanoscale Zero-Valent Iron in Unbuffered Systems: Effect of pH and Fe(II) Dissolution. Environ Sci Technol 49:10536–10543. https://doi.org/10.1021/acs.est.5b01298

Baer DR, Amonette JE, Engelhard MH, et al (2008) Characterization Challenges for Nanomaterials. Surf Interface Anal 40:529–537. https://doi.org/10.1002/sia.2726

Balda M, Kopinke F-D (2020) The Role of Nickel Traces in Fine Chemicals for Hydrodechlorination Reactions with Zero-Valent Iron. Chem Eng J 124185. https://doi.org/10.1016/j.cej.2020.124185

Ballschmiter K (2003) Pattern and Sources of Naturally Produced Organohalogens in the Marine Environment: Biogenic Formation of Organohalogens. Chemosphere 52:313–324. https://doi.org/10.1016/S0045-6535(03)00211-X

Baltruschat H, Beltowska-Brzezinska M, Dülberg A (1993) Reactions of Halogenated Hydrocarbons at Platinum Group Metals. Part I: A DEMS Study of the Adsorption of CH3CCl3. Electrochim Acta 38:281–284. https://doi.org/10.1016/0013-4686(93)85140-T

Barbash JE, Reinhard M (1989) Abiotic Dehalogenation of 1,2-Dichloroethane and 1,2-Dibromoethane in Aqueous Solution Containing Hydrogen Sulfide. Environ Sci Technol 23:1349–1358. https://doi.org/10.1021/es00069a004

Basnet M, Gershanov A, Wilkinson KJ, et al (2016) Interaction Between Palladium-Doped Zerovalent Iron Nanoparticles and Biofilm in Granular Porous Media: Characterization, Transport and Viability. Environ Sci Nano 3:127–137. https://doi.org/10.1039/C5EN00109A

Basnet M, Ghoshal S, Tufenkji N (2013) Rhamnolipid Biosurfactant and Soy Protein Act as Effective Stabilizers in the Aggregation and Transport of Palladium-Doped Zerovalent Iron Nanoparticles in Saturated Porous Media. Environ Sci Technol 47:13355–13364. https://doi.org/10.1021/es402619v

Basnet M, Tommaso C Di, Ghoshal S, Tufenkji N (2015) Reduced Transport Potential of a Palladium-Doped Zero Valent Iron Nanoparticle in a Water Saturated Loamy Sand. Water Res 68:354–363. https://doi.org/10.1016/j.watres.2014.09.039

Bennett P, He F, Zhao D, et al (2010) In Situ Testing of Metallic Iron Nanoparticle Mobility and Reactivity in a Shallow Granular Aquifer. J Contam Hydrol 116:35–46. https://doi.org/10.1016/j.jconhyd.2010.05.006

Bent BE (1996) Mimicking Aspects of Heterogeneous Catalysis: Generating, Isolating, and Reacting Proposed Surface Intermediates on Single Crystals in Vacuum. Chem Rev 96:1361–1390. https://doi.org/10.1021/cr940201j

Berge ND, Ramsburg CA (2009) Oil-in-Water Emulsions for Encapsulated Delivery of Reactive Iron Particles. Environ Sci Technol 43:5060–5066. https://doi.org/10.1021/es900358p

Betelu S, Ignatiadis I (2013) Electrochemical Investigation of the Reductive Dechlorination of Perchloroethylene (PCE) by Nano-Sized Zero Valent Iron (nZVI) using Screen-Printed Electrodes (SPE). In: Proceedings of the 12th International Conference on Sustainable Use and Management of Soil, Sediment and Water Resources. Barcelona, Spain, pp 115-118.

Betelu S, Rodrigues R, Noel C, et al (2015) Development and In Situ Implementation of a Chemical Process for Reductive Dechlorination of Chlorinated Solvents in Polluted Aquifers. Summer School on Contaminated Soils, June 29-July 3, 2015. Marne la Vallée, France

Beverskog B, Puigdomenech I (1996) Revised Pourbaix Diagrams for Iron at 25–300 °C. Corros Sci 38:2121–2135. https://doi.org/10.1016/S0010-938X(96)00067-4

Bhattacharjee S, Basnet M, Tufenkji N, Ghoshal S (2016) Effects of Rhamnolipid and Carboxymethylcellulose Coatings on Reactivity of Palladium-Doped Nanoscale Zerovalent Iron Particles. Environ Sci Technol 50:1812–1820. https://doi.org/10.1021/acs.est.5b05074

Bhattacharjee S, Ghoshal S (2018a) Optimal Design of Sulfidated Nanoscale Zerovalent Iron for Enhanced Trichloroethene Degradation. Environ Sci Technol 52:11078–11086. https://doi.org/10.1021/acs.est.8b02399

Bhattacharjee S, Ghoshal S (2018b) Sulfidation of Nanoscale Zerovalent Iron in the Presence of Two Organic Macromolecules and its Effects on Trichloroethene Degradation. Environ Sci Nano 5:782–791. https://doi.org/10.1039/C7EN01205E

Bi E, Bowen I, Devlin JF (2009) Effect of Mixed Anions (HCO3- - SO42- - ClO4-) on Granular Iron (Fe 0) Reactivity. Environ Sci Technol 43:5975–5981. https://doi.org/10.1021/es900599x

Bianco C, Tosco T, Sethi R (2016) A 3-Dimensional Micro- and Nanoparticle Transport and Filtration Model (MNM3D) Applied to the Migration of Carbon-Based Nanomaterials in Porous Media. J Contam Hydrol 193:10–20. https://doi.org/10.1016/j.jconhyd.2016.08.006

Boethling RS, Mackay D (2000) Handbook of Property Estimation Methods for Chemicals : Environmental and Health Sciences. CRC Press, Boca Raton, FL, USA.

Borden RC (2007) Effective Distribution of Emulsified Edible Oil for Enhanced Anaerobic Bioremediation. J Contam Hydrol 94:1–12. https://doi.org/10.1016/j.jconhyd.2007.06.001

Bossa N, Carpenter AW, Kumar N, et al (2017) Cellulose Nanocrystal Zero-Valent Iron Nanocomposites for Groundwater Remediation. Environ Sci Nano 4:1294–1303. https://doi.org/10.1039/C6EN00572A

Bouwer H (1991) Simple Derivation of the Retardation Equation and Application to Preferential Flow and Macrodispersion. Ground Water 29:41–46. https://doi.org/10.1111/j.1745-6584.1991.tb00495.x

Bradley PM, Chapelle FH (1996) Anaerobic Mineralization of Vinyl Chloride in Fe(III)-Reducing, Aquifer Sediments. Environ Sci Technol 30:2084–2086. https://doi.org/10.1021/es950926K

Brown RA (2010) Chemical Oxidation and Reduction for Chlorinated Solvent Remediation. In: Stroo HF, Ward CH (eds) In Situ Remediation of Chlorinated Solvent Plumes. Springer, New York, NY, pp 481-535.

Brown RA, Mueller JG, Seech AG, et al (2009) Interactions between Biological and Abiotic Pathways in the Reduction of Chlorinated Solvents. Remediat J 20:9–20. https://doi.org/10.1002/rem.20226

Bruton TA, Pycke BFG, Halden RU (2015) Effect of Nanoscale Zero-Valent Iron Treatment on Biological Reductive Dechlorination: A Review of Current Understanding and Research Needs. Crit Rev Environ Sci Technol 45:1148–1175. https://doi.org/10.1080/10643389.2014.924185

Budavari S (1996) The Merck Index, Print Version, Twelfth Edition. CRC Press, Whitehouse Station, NJ, USA

Burris DR, Allen-King RM, Manoranjan VS, et al (1998) Chlorinated Ethene Reduction by Cast Iron: Sorption and Mass Transfer. J Environ Eng 124:1012–1019. https://doi.org/10.1061/(ASCE)0733-9372(1998)124:10(1012)

Burris DR, Campbell TJ, Manoranjan VS (1995) Sorption of Trichloroethylene and Tetrachloroethylene in a Batch Reactive Metallic Iron-Water System. Environ Sci Technol 29:2850–2855. https://doi.org/10.1021/es00011a022

Burris DR, Delcomyn CA, Smith MH, Roberts AL (1996) Reductive Dechlorination of Tetrachloroethylene and Trichloroethylene Catalyzed by Vitamin B12 in Homogeneous and Heterogeneous Systems. Environ Sci Technol 30:3047–3052. https://doi.org/10.1021/es960116o

Busch J, Meißner T, Potthoff A, et al (2015) A Field Investigation on Transport of Carbon-Supported Nanoscale Zero-Valent Iron (nZVI) in Groundwater. J Contam Hydrol 181:59–68. https://doi.org/10.1016/j.jconhyd.2015.03.009

Butler EC, Hayes KF (1998) Effects of Solution Composition and pH on the Reductive Dechlorination of Hexachloroethane by Iron Sulfide. Environ Sci Technol 32:1276–1284. https://doi.org/10.1021/es9706864

Butler EC, Hayes KF (2000) Kinetics of the Transformation of Halogenated Aliphatic Compounds by Iron Sulfide. Environ Sci Technol 34:422–429. https://doi.org/10.1021/es980946X

Bylaska EJ, Dupuis M, Tratnyek PG (2008) One-Electron-Transfer Reactions of Polychlorinated Ethylenes: Concerted and Stepwise Cleavages. J Phys Chem A 112:3712–3721. https://doi.org/10.1021/jp711021D

Calvet R, Barriuso E, Bedos C, et al (2005) Les pesticides dans le sol : conséquences agronomiques et environnementales., France Agr

Cao Z, Liu X, Xu J, et al (2017) Removal of Antibiotic Florfenicol by Sulfide-Modified Nanoscale Zero-Valent Iron. Environ Sci Technol 51:11269–11277. https://doi.org/10.1021/acs.est.7b02480

Cecchinc I, Reddy KR, Thomé A, et al (2017) Nanobioremediation: Integration of Nanoparticles and Bioremediation for Sustainable Remediation of Chlorinated Organic Contaminants in Soils. Int Biodeterior Biodegradation 119:419–428. https://doi.org/10.1016/j.ibiod.2016.09.027

Chaplin BP, Reinhard M, Schneider WF, et al (2012) Critical Review of Pd-Based Catalytic Treatment of Priority Contaminants in Water. Environ Sci Technol 46:3655–3670. https://doi.org/10.1021/es204087q

Chekli L, Bayatsarmadi B, Sekine R, et al (2016a) Analytical Characterisation of Nanoscale Zero-Valent Iron: A Methodological Review. Anal Chim Acta 903:13–35. https://doi.org/10.1016/j.aca.2015.10.040

Chekli L, Brunetti G, Marzouk ER, et al (2016b) Evaluating the Mobility of Polymer-Stabilised Zero-Walent Iron Nanoparticles and their Potential to Co-transport Contaminants in Intact Soil Cores. Environ Pollut 216:636–645. https://doi.org/10.1016/j.envpol.2016.06.025

Chen F, Freedman DL, Falta RW, Murdoch LC (2012) Henry's Law Constants of Chlorinated Solvents at Elevated Temperatures. Chemosphere 86:156–165. https://doi.org/10.1016/j.chemosphere.2011.10.004

Chen J-L, Al-Abed SR, Ryan JA, Li Z (2001) Effects of pH on Dechlorination of Trichloroethylene by Zero-Valent Iron. J Hazard Mater 83:243–254. https://doi.org/10.1016/S0304-3894(01)00193-5

Chen J, Xiu Z, Lowry G V., Alvarez PJJ (2011) Effect of Natural Organic Matter on Toxicity and Reactivity of Nano-Scale Zero-Valent Iron. Water Res 45:1995–2001. https://doi.org/10.1016/j.watres.2010.11.036

Chen S-S, Hsu H-D, Li C-W (2004) A New Method to Produce Nanoscale Iron for Nitrate Removal. J Nanoparticle Res 6:639–647. https://doi.org/10.1007/s11051-004-6672-2

Chen W-F, Wang W, Zhang J, et al (2016) Effects of Co-Present Cations and Anions on Hexachlorobenzene Removal by Activated Carbon, Nano Zerovalent Iron and Nano Zerovalent/Activated Carbon Composite. Desalin Water Treat 57:1–9. https://doi.org/10.1080/19443994.2015.1108238

Cheng S-F, Wu S-C (2000) The Enhancement Methods for the Degradation of TCE by Zero-Valent Metals. Chemosphere 41:1263–1270. https://doi.org/10.1016/S0045-6535(99)00530-5

Cheng Y, Dong H, Lu Y, et al (2019) Toxicity of Sulfide-Modified Nanoscale Zero-Valent Iron to Escherichia coli in Aqueous Solutions. Chemosphere 220:523–530. https://doi.org/10.1016/j.chemosphere.2018.12.159

Chiou CT, Kile DE (1998) Deviations from Sorption Linearity on Soils of Polar and Nonpolar Organic Compounds at Low Relative Concentrations. Environ Sci Technol 32:338–343. https://doi.org/10.1021/es970608G

Chiou CT, Kile DE, Brinton TI, et al (1987) A Comparison of Water Solubility Enhancements of Organic Solutes by Aquatic Humic Materials and Commercial Humic Acids. Environ Sci Technol 21:1231–1234. https://doi.org/10.1021/es00165a012

Chiu WA, Jinot J, Scott CS, et al (2012) Human Health Effects of Trichloroethylene: Key Findings and Scientific Issues. Environ Health Perspect 121:303–311. https://doi.org/10.1289/ehp.1205879

Cho H-H, Park J-W (2006) Sorption and Reduction of Tetrachloroethylene with Zero Valent Iron and Amphiphilic Molecules. Chemosphere 64:1047–1052. https://doi.org/10.1016/j.chemosphere.2005.12.062

Choi H, Al-Abed SR, Agarwal S, Dionysiou DD (2008) Synthesis of Reactive Nano-Fe/Pd Bimetallic System-Impregnated Activated Carbon for the Simultaneous Adsorption and Dechlorination of PCBs. Chem Mater 20:3649–3655. https://doi.org/10.1021/cm8003613

Chowdhury AIA, Krol MM, Kocur CM, et al (2015) nZVI Injection into Variably Saturated Soils: Field and Modeling Study. J Contam Hydrol 183:16–28. https://doi.org/10.1016/j.jconhyd.2015.10.003

Coleman N V, Mattes TE, Gossett JM, Spain JC (2002) Biodegradation of cis-Dichloroethene as the Sole Carbon Source by a -Proteobacterium. Appl Environ Microbiol 68:2726–2730. https://doi.org/10.1128/AEM.68.6.2726-2730.2002

Colombano S, Saada A, Guerin V, et al (2010) Quelles techniques pour quels traitements - Analyse coûts-bénéfices

Colombo A, Dragonetti C, Magni M, Roberto D (2015) Degradation of Toxic Halogenated Organic Compounds by Iron-Containing Mono-, Bi- and Tri-Metallic Particles in Water. Inorganica Chim Acta 431:48–60. https://doi.org/10.1016/j.ica.2014.12.015

Comba S, Dalmazzo D, Santagata E, Sethi R (2011a) Rheological Characterization of Xanthan Suspensions of Nanoscale Iron for Injection in Porous Media. J Hazard Mater 185:598–605. https://doi.org/10.1016/j.jhazmat.2010.09.060

Comba S, Di Molfetta A, Sethi R (2011b) A Comparison Between Field Applications of Nano-, Micro-, and Millimetric Zero-Valent Iron for the Remediation of Contaminated Aquifers. Water, Air, Soil Pollut 215:595–607. https://doi.org/10.1007/s11270-010-0502-1

Cornell RM, Schwertmann U (2003) The Iron Oxides: Structure, Properties, Reactions, Occurrences, and Uses. Wiley-VCH

Crampon M, Hellal J, Mouvet C, et al (2018) Do Natural Biofilm Impact nZVI Mobility and Interactions with Porous Media? A Column Study. Sci Total Environ 610–611:709–719. https://doi.org/10.1016/j.scitotenv.2017.08.106

Crane RA, Scott TB (2012) Nanoscale Zero-Valent Iron: Future Prospects for an Emerging Water Treatment Technology. J Hazard Mater 211:112–125. https://doi.org/10.1016/j.jhazmat.2011.11.073

Culpepper JD, Scherer MM, Robinson TC, et al (2018) Reduction of PCE and TCE by Magnetite Revisited. Environ Sci Process Impacts 20:1340–1349. https://doi.org/10.1039/C8EM00286J

Cushman CS (2014) Destruction of Chlorinated Hydrocarbons by Zero-Valent Zinc and Bimetallic Zinc Reductants in Bench-Scale Investigations. Wright State University.

Cwiertny DM, Arnold WA, Kohn T, et al (2010) Reactivity of Alkyl Polyhalides toward Granular Iron: Development of QSARs and Reactivity Cross Correlations for Reductive Dehalogenation. Environ Sci Technol 44:7928–7936. https://doi.org/10.1021/es1018866

Cwiertny DM, Bransfield SJ, Livi KJT, et al (2006) Exploring the Influence of Granular Iron Additives on 1,1,1-Trichloroethane Reduction. Environ Sci Technol 40:6837–6843. https://doi.org/10.1021/es060921v

Cwiertny DM, Scherer MM (2010) Abiotic Processes Affecting the Remediation of Chlorinated Solvents. In: Stroo HF, Ward CH (eds) In Situ Remediation of Chlorinated Solvent Plumes. Springer, New York, NY, USA, pp 69-108.

Danko AS, Luo M, Bagwell CE, et al (2004) Involvement of Linear Plasmids in Aerobic Biodegradation of Vinyl Chloride. Appl Environ Microbiol 70:6092–6097. https://doi.org/10.1128/AEM.70.10.6092-6097.2004

de Bruin WP, Kotterman MJ, Posthumus MA, et al (1992) Complete Biological Reductive Transformation of Tetrachloroethene to Ethane. Appl Environ Microbiol 58:1996–2000

Dean JA (2004) Lange's Handbook of Chemistry, Fifteenth Edition. McGraw-Hill.

DiStefano TD, Gossett JM, Zinder SH (1992) Hydrogen as an Electron Donor for Dechlorination of Tetrachloroethene by an Anaerobic Mixed Culture. Appl Environ Microbiol 58:3622–3629

Doherty RE (2000a) A History of the Production and Use of Carbon Tetrachloride, Tetrachloroethylene, Trichloroethylene and 1,1,1-Trichloroethane in the United States: Part 1--Historical Background; Carbon Tetrachloride and Tetrachloroethylene. Environ Forensics 1:69–81. https://doi.org/10.1006/enfo.2000.0010

Doherty RE (2000b) A History of the Production and Use of Carbon Tetrachloride, Tetrachloroethylene, Trichloroethylene and 1,1,1-Trichloroethane in the United States: Part 2--Trichloroethylene and 1,1,1-Trichloroethane. Environ Forensics 1:83–93. https://doi.org/10.1006/enfo.2000.0011

Dolfing J, Van Eekert M, Mueller J (2006) Thermodynamics of Low Eh Reactions. In: Battelle's Fifth International Conference on Remediation of Chlorinated and Recalcitrant Compounds. Monterey, CA, USA.

Domínguez CM, Parchão J, Rodriguez S, et al (2016) Kinetics of Lindane Dechlorination by Zero Valent Iron Microparticles: Effect of Different Salts and Stability Study. Ind Eng Chem Res 55:12776–12785. https://doi.org/10.1021/acs.iecr.6b03434

Dong H, Cheng Y, Lu Y, et al (2018a) Comparison of Toxicity of Fe/Ni and Starch-Stabilized Fe/Ni Nanoparticles toward Escherichia coli. Sep Purif Technol 210:504–510. https://doi.org/10.1016/j.seppur.2018.08.042

Dong H, Jiang Z, Deng J, et al (2018b) Physicochemical Transformation of Fe/Ni Bimetallic Nanoparticles during Aging in Simulated Groundwater and the Consequent Effect on Contaminant Removal. Water Res 129:51–57. https://doi.org/10.1016/j.watres.2017.11.002

Dong H, Li L, Wang Y, et al (2019) Aging of zero- valent iron- based nanoparticles in aqueous environment and the consequent effects on their reactivity and toxicity. Water Environ Res

wer.1265. https://doi.org/10.1002/wer.1265

Dong H, Xie Y, Zeng G, et al (2016a) The Dual Effects of Carboxymethyl Cellulose on the Colloidal Stability and Toxicity of Nanoscale Zero-Valent Iron. Chemosphere 144:1682–1689. https://doi.org/10.1016/j.chemosphere.2015.10.066

Dong H, Zhang C, Deng J, et al (2018c) Factors Influencing Degradation of Trichloroethylene by Sulfide-Modified Nanoscale Zero-Calent Iron in Aqueous Solution. Water Res 135:1–10. https://doi.org/10.1016/j.watres.2018.02.017

Dong H, Zhao F, Zeng G, et al (2016b) Aging Study on Carboxymethyl Cellulose-Coated Zero-Valent Iron Nanoparticles in Water: Chemical Transformation and Structural Evolution. J Hazard Mater 312:234–242. https://doi.org/10.1016/j.jhazmat.2016.03.069

Dong T, Luo H, Wang Y, et al (2011) Stabilization of Fe–Pd Bimetallic Nanoparticles with Sodium Carboxymethyl Cellulose for Catalytic Reduction of para-Nitrochlorobenzene in Water. Desalination 271:11–19. https://doi.org/10.1016/j.desal.2010.12.003

Doong R, Lai Y-J (2005) Dechlorination of Tetrachloroethylene by Palladized Iron in the Presence of Humic Acid. Water Res 39:2309–2318. https://doi.org/10.1016/j.watres.2005.04.036

Doong R, Lai Y (2006) Effect of Metal Ions and Humic Acid on the Dechlorination of Tetrachloroethylene by Zerovalent Iron. Chemosphere 64:371–378. https://doi.org/10.1016/j.chemosphere.2005.12.038

Doong R, Wu S-C (1992) Reductive Dechlorination of Chlorinated Hydrocarbons in Aqueous Solutions Containing Ferrous and Sulfide Ions. Chemosphere 24:1063–1075. https://doi.org/10.1016/0045-6535(92)90197-Y

Dries J, Bastiaens L, Springael D, et al (2002) Kinetics of Trichloroethene (TCE) Reduction by Zero-Valent Iron: Effect of Medium Composition. In: Thornton SF, Oswald SE (eds) Groundwater Quality: Natural and Enhanced Restoration of Groundwater Pollution (Proceedings of the Groundwater Quality 2001 Conference held at Sheffield, UK, June 2001), IAHS Press. pp 397-402.

Dries J, Bastiaens L, Springael D, et al (2004) Competition for Sorption and Degradation of Chlorinated Ethenes in Batch Zero-Valent Iron Systems. Environ Sci Technol 38:2879–2884. https://doi.org/10.1021/es034933h

Dries J, Bastiaens L, Springael D, et al (2005) Combined Removal of Chlorinated Ethenes and Heavy Metals by Zerovalent Iron in Batch and Continuous Flow Column Systems. Environ Sci Technol 39:8460–8465. https://doi.org/10.1021/es050251d

Dror I, Schlautman MA (2004) Cosolvent Effect on the Catalytic Reductive Dechlorination of PCE. Chemosphere 57:1505–1514. https://doi.org/10.1016/j.chemosphere.2004.08.078

Elango VK, Liggenstoffer AS, Fathepure BZ (2006) Biodegradation of Vinyl Chloride and cis-Dichloroethene by a Ralstonia sp. Strain TRW-1. Appl Microbiol Biotechnol 72:1270–1275. https://doi.org/10.1007/s00253-006-0424-4

Elliott DW, Zhang W (2001) Field Assessment of Nanoscale Bimetallic Particles for Groundwater Treatment. Environ Sci Technol 35:4922–4926. https://doi.org/10.1021/es0108584

Elsner M, Schwarzenbach RP, Haderlein SB (2004) Reactivity of Fe(II)-Bearing Minerals toward Reductive Transformation of Organic Contaminants. Environ Sci Technol 38:799–807. https://doi.org/10.1021/es0345569

Erbs M, Hansen HCB, Olsen CE (1998) Reductive Dechlorination of Carbon Tetrachloride Using

Iron(II) Iron(III) Hydroxide Sulfate (Green Rust). Environ Sci Technol 33:307–311. https://doi.org/10.1021/es980221T

European Chlorinated Solvent Association ECSA Product & Application Toolbox - Guidance on Safe & Sustainable Use of Chlorinated Solvents

Ezzatahmadi N, Ayoko GA, Millar GJ, et al (2017) Clay-Supported Nanoscale Zero-Valent Iron Composite Materials for the Remediation of Contaminated Aqueous Solutions: A Review. Chem Eng J 312:336–350. https://doi.org/10.1016/j.cej.2016.11.154

Fajardo C, Ortíz LT, Rodríguez-Membibre ML, et al (2012) Assessing the Impact of Zero-Valent Iron (ZVI) Nanotechnology on Soil Microbial Structure and Functionality: A Molecular Approach. Chemosphere 86:802–808. https://doi.org/10.1016/j.chemosphere.2011.11.041

Fajardo C, Saccà ML, Martinez-Gomariz M, et al (2013) Transcriptional and Proteomic Stress Responses of a Soil Bacterium Bacillus cereus to Nanosized Zero-Valent Iron (nZVI) Particles. Chemosphere 93:1077–1083. https://doi.org/10.1016/j.chemosphere.2013.05.082

Fan D, Anitori RP, Tebo BM, et al (2013) Reductive Sequestration of Pertechnetate (99TcO4–) by Nano Zerovalent Iron (nZVI) Transformed by Abiotic Sulfide. Environ Sci Technol 47:5302–5310. https://doi.org/10.1021/es304829z

Fan D, Bradley MJ, Hinkle AW, et al (2016a) Chemical Reactivity Probes for Assessing Abiotic Natural Attenuation by Reducing Iron Minerals. Environ Sci Technol 50:1868–1876. https://doi.org/10.1021/acs.est.5b05800

Fan D, Chen S, Johnson RL, Tratnyek PG (2015) Field Deployable Chemical Redox Probe for Quantitative Characterization of Carboxymethylcellulose Modified Nano Zerovalent Iron. Environ Sci Technol 49:10589–10597. https://doi.org/10.1021/acs.est.5b02804

Fan D, Lan Y, Tratnyek PG, et al (2017) Sulfidation of Iron-Based Materials: A Review of Processes and Implications for Water Treatment and Remediation. Environ Sci Technol 51:13070–13085. https://doi.org/10.1021/acs.est.7b04177

Fan D, O'Brien Johnson G, Tratnyek PG, Johnson RL (2016b) Sulfidation of Nano Zerovalent Iron (nZVI) for Improved Selectivity During In-Situ Chemical Reduction (ISCR). Environ Sci Technol 50:9558–9565. https://doi.org/10.1021/acs.est.6b02170

Fan D, O'Carroll DM, Elliott DW, et al (2016c) Selectivity of Nano Zerovalent Iron in In Situ Chemical Reduction: Challenges and Improvements. Remediat J 26:27–40. https://doi.org/10.1002/rem.21481

Fan G, Wang Y, Fang G, et al (2016d) Review of Chemical and Electrokinetic Remediation of PCBs Contaminated Soils and Sediments. Environ Sci Process Impacts 18:1140–1156. https://doi.org/10.1039/C6EM00320F

Fang L, Xu C, Zhang W, Huang L-Z (2018a) The Important Role of Polyvinylpyrrolidone and Cu on Enhancing Dechlorination of 2,4-dichlorophenol by Cu/Fe Nanoparticles: Performance and Mechanism Study. Appl Surf Sci 435:55–64. https://doi.org/10.1016/j.apsusc.2017.11.084

Fang Y, Wen J, Zeng G, et al (2018b) From nZVI to SNCs: Development of a Better Material for Pollutant Removal in Water. Environ Sci Pollut Res 25:6175–6195. https://doi.org/10.1007/s11356-017-1143-3

Farrell J, Kason M, Melitas N, Li T (2000) Investigation of the Long-Term Performance of Zero-Valent Iron for Reductive Dechlorination of Trichloroethylene. Environ Sci Technol 34:514–521. https://doi.org/10.1021/es990716y

Fennelly JP, Roberts AL (1998) Reaction of 1,1,1-Trichloroethane with Zero-Valent Metals and Bimetallic Reductants. Environ Sci Technol 32:1980–1988. https://doi.org/10.1021/es970784p

Filip J, Karlický F, Marušák Z, et al (2014) Anaerobic Reaction of Nanoscale Zerovalent Iron with Water: Mechanism and Kinetics. J Phys Chem C 118:13817–13825. https://doi.org/10.1021/jp501846f

Flores Orozco A, Velimirovic M, Tosco T, et al (2015) Monitoring the Injection of Microscale Zerovalent Iron Particles for Groundwater Remediation by Means of Complex Electrical Conductivity Imaging. Environ Sci Technol 49:5593–5600. https://doi.org/10.1021/acs.est.5b00208

Freedman DL, Gossett JM (1989) Biological Reductive Dechlorination of Tetrachloroethylene and Trichloroethylene to Ethylene under Methanogenic Conditions. Appl Environ Microbiol 55:2144–2151

FRTR (2007) Remediation Technologies Screening Matrix and Reference Guide, Version 4.0

Fu F, Dionysiou DD, Liu H (2014a) The Use of Zero-Valent Iron for Groundwater Remediation and Wastewater Treatment: A Review. J Hazard Mater 267:194–205. https://doi.org/10.1016/j.jhazmat.2013.12.062

Fu PP, Xia Q, Hwang H-M, et al (2014b) Mechanisms of Nanotoxicity: Generation of Reactive Oxygen Species. J Food Drug Anal 22:64–75. https://doi.org/10.1016/j.jfda.2014.01.005

Gastone F, Tosco T, Sethi R (2014) Green Stabilization of Microscale Iron Particles Using Guar Gum: Bulk Rheology, Sedimentation Rate and Enzymatic Degradation. J Colloid Interface Sci 421:33–43. https://doi.org/10.1016/j.jcis.2014.01.021

Gerlach R, Cunningham AB, Caccavo FJ (2000) Dissimilatory Iron-Reducing Bacteria Can Influence the Reduction of Carbon Tetrachloride by Iron Metal. Environ Sci Technol 34:2461–2464. https://doi.org/10.1021/es991200H

Ghauch A, Assi HA, Baydoun H, et al (2011) Fe0-Based Trimetallic Systems for the Removal of Aqueous Diclofenac: Mechanism and Kinetics. Chem Eng J 172:1033–1044. https://doi.org/10.1016/j.cej.2011.07.020

Ghosh I, Mukherjee A, Mukherjee A (2017) In planta Genotoxicity of nZVI: Influence of Colloidal Stability on Uptake, DNA Damage, Oxidative Stress and Cell Death. Mutagenesis 32:371–387. https://doi.org/10.1093/mutage/gex006

Gil-Díaz M, Lobo MC (2018) Phytotoxicity of Nanoscale Zerovalent Iron (nZVI) in Remediation Strategies. In: Phytotoxicity of Nanoparticles. Springer International Publishing, Cham, pp 301–333

Gillham RW, O'Hannesin SF (1994) Enhanced Degradation of Halogenated Aliphatics by Zero-Valent Iron. Ground Water 32:958–967. https://doi.org/10.1111/j.1745-6584.1994.tb00935.x

Gillham RW, Vogan J, Gui L, et al (2010) Iron Barrier Walls for Chlorinated Solvent Remediation. In: Stroo HF, Ward CH (eds) In Situ Remediation of Chlorinated Solvent Plumes. Springer, New York, NY, USA, pp 537-571.

Glod G, Brodmann U, Angst W, et al (1997) Cobalamin-Mediated Reduction of cis- and trans-Dichloroethene, 1,1-Dichloroethene, and Vinyl Chloride in Homogeneous Aqueous Solution: Reaction Kinetics and Mechanistic Considerations. Environ Sci Technol 31:3154–3160. https://doi.org/10.1021/es9701220

Gong X, Huang D, Liu Y, et al (2018) Remediation of Contaminated Soils by Biotechnology with

Nanomaterials: Bio-Behavior, Applications, and Perspectives. Crit Rev Biotechnol 38:455–468. https://doi.org/10.1080/07388551.2017.1368446

Gong Y, Tang J, Zhao D (2016) Application of Iron Sulfide Particles for Groundwater and Soil Remediation: A Review. Water Res 89:309–320. https://doi.org/10.1016/j.watres.2015.11.063

Gorski CA, Edwards R, Sander M, et al (2016) Thermodynamic Characterization of Iron Oxide-Aqueous Fe2+ Redox Couples. Environ Sci Technol 50:8538–8547. https://doi.org/10.1021/acs.est.6b02661

Gorski CA, Nurmi JT, Tratnyek PG, et al (2010) Redox Behavior of Magnetite: Implications for Contaminant Reduction. Environ Sci Technol 44:55–60. https://doi.org/10.1021/es9016848

Gorski CA, Scherer MM (2009) Influence of Magnetite Stoichiometry on FeII Uptake and Nitrobenzene Reduction. Environ Sci Technol 43:3675–3680. https://doi.org/10.1021/es803613a

Gossett JM (2010) Sustained Aerobic Oxidation of Vinyl Chloride at Low Oxygen Concentrations. Environ Sci Technol 44:1405–1411. https://doi.org/10.1021/es9033974

Greenlee LF, Torrey JD, Amaro RL, Shaw JM (2012) Kinetics of Zero Valent Iron Nanoparticle Oxidation in Oxygenated Water. Environ Sci Technol 46:12913–12920. https://doi.org/10.1021/es303037k

Greenwood NN, Earnshaw A (1997) Chemistry of the Elements, 2nd Edition. Butterworth-Heinemann.

Gribble GW (2003) The Diversity of Naturally Produced Organohalogens. Chemosphere 52:289–297. https://doi.org/10.1016/S0045-6535(03)00207-8

Grieger KD, Fjordbøge A, Hartmann NB, et al (2010) Environmental Benefits and Risks of Zero-Valent Iron Nanoparticles (nZVI) for In Situ Remediation: Risk Mitigation or Trade-Off? J Contam Hydrol 118:165–183. https://doi.org/10.1016/j.jconhyd.2010.07.011

Gu Y, Gong L, Qi J, et al (2019) Sulfidation Mitigates the Passivation of Zero Valent Iron at Alkaline pHs: Experimental Evidences and Mechanism. Water Res. https://doi.org/10.1016/J.WATRES.2019.04.061

Gu Y, Wang B, He F, et al (2017) Mechanochemically Sulfidated Microscale Zero Valent Iron: Pathways, Kinetics, Mechanism, and Efficiency of Trichloroethylene Dechlorination. Environ Sci Technol acs.est.7b03604. https://doi.org/10.1021/acs.est.7b03604

Guan X, Sun Y, Qin H, et al (2015) The Limitations of Applying Zero-Valent Iron Technology in Contaminants Sequestration and the Corresponding Countermeasures: The Development in Zero-Valent Iron Technology in the Last Two Decades (1994–2014). Water Res 75:224–248. https://doi.org/10.1016/j.watres.2015.02.034

Han J, Xin J, Zheng X, et al (2016a) Remediation of Trichloroethylene-Contaminated Groundwater by Three Modifier-Coated Microscale Zero-Valent Iron. Environ Sci Pollut Res 23:14442–14450. https://doi.org/10.1007/s11356-016-6368-z

Han L, Yang L, Wang H, et al (2016b) Sustaining Reactivity of Fe0 for Nitrate Reduction via Electron Transfer between Dissolved Fe2+ and Surface Iron Oxides. J Hazard Mater 308:208–215. https://doi.org/10.1016/j.jhazmat.2016.01.047

Han Y, Liu C, Horita J, Yan W (2016c) Trichloroethene Hydrodechlorination by Pd-Fe Bimetallic Nanoparticles: Solute-Induced Catalyst Deactivation Analyzed by Carbon Isotope Fractionation. Appl Catal B Environ 188:77–86. https://doi.org/10.1016/j.apcatb.2016.01.047

Han Y, Liu C, Horita J, Yan W (2018) Trichloroethene (TCE) Hydrodechlorination by Ni Fe Nanoparticles: Influence of Aqueous Anions on Catalytic Pathways. Chemosphere 205:404–413. https://doi.org/10.1016/j.chemosphere.2018.04.083

Han Y, Yan W (2016) Reductive Dechlorination of Trichloroethene by Zero-Valent Iron Nanoparticles: Reactivity Enhancement through Sulfidation Treatment. Environ Sci Technol 50:12992–13001. https://doi.org/10.1021/acs.est.6b03997

Han Y, Yan W (2014) Bimetallic Nickel–Iron Nanoparticles for Groundwater Decontamination: Effect of Groundwater Constituents on Surface Deactivation. Water Res 66:149–159. https://doi.org/10.1016/j.watres.2014.08.001

Han Y, Yang MDY, Zhang W, Yan W (2015) Optimizing Synthesis Conditions of Nanoscale Zero-Valent Iron (nZVI) through Aqueous Reactivity Assessment. Front Environ Sci Eng 9:813–822. https://doi.org/10.1007/s11783-015-0784-z

Haneda K, Morrish AH (1977) Magnetite to Maghemite Transformation in Ultrafine Particles. Le J Phys Colloq 38:C1-321-C1-323. https://doi.org/10.1051/jphyscol:1977166

Harendra S, Vipulanandan C (2008) Degradation of High Concentrations of PCE Solubilized in SDS and Biosurfactant with Fe/Ni Bi-Metallic Particles. Colloids Surfaces A Physicochem Eng Asp 322:6–13. https://doi.org/10.1016/j.colsurfa.2008.02.009

Harendra S, Vipulanandan C (2011) Solubilization and Degradation of Perchloroethylene (PCE) in Cationic and Nonionic Surfactant Solutions. J Environ Sci (China) 23:1240–1248

Hartmans S, De Bont JA (1992) Aerobic Vinyl Chloride Metabolism in Mycobacterium aurum L1. Appl Environ Microbiol 58:1220–6

Hawley GG (1981) Hawley's Condensed Chemical Dictionary, 10th ed. Van Nostrand Reinhold., New York, NY, USA

He C-S, He D, Collins RN, et al (2018a) Effects of Good's Buffers and pH on the Structural Transformation of Zero Valent Iron and the Oxidative Degradation of Contaminants. Environ Sci Technol 52:1393–1403. https://doi.org/10.1021/acs.est.7b04030

He D, Ma J, Collins RN, Waite TD (2016) Effect of Structural Transformation of Nanoparticulate Zero-Valent Iron on Generation of Reactive Oxygen Species. Environ Sci Technol 50:3820–3828. https://doi.org/10.1021/acs.est.5b04988

He F, Gong L, Fan D, et al (2020) Quantifying the efficiency and selectivity of organohalide dechlorination by zerovalent iron. Environ Sci Process Impacts. https://doi.org/10.1039/C9EM00592G

He F, Li Z, Shi S, et al (2018b) Dechlorination of Excess Trichloroethene by Bimetallic and Sulfidated Nanoscale Zero-Valent Iron. Environ Sci Technol 52:8627–8637. https://doi.org/10.1021/acs.est.8B01735

He F, Zhao D (2005) Preparation and Characterization of a New Class of Starch-Stabilized Bimetallic Nanoparticles for Degradation of Chlorinated Hydrocarbons in Water. Environ Sci Technol 39:3314–3320. https://doi.org/10.1021/es048743y

He F, Zhao D (2007) Manipulating the Size and Dispersibility of Zerovalent Iron Nanoparticles by Use of Carboxymethyl Cellulose Stabilizers. Environ Sci Technol 41:6216–6221. https://doi.org/10.1021/es0705543

He F, Zhao D (2008) Hydrodechlorination of Trichloroethene Using Stabilized Fe-Pd Nanoparticles: Reaction Mechanism and Effects of Stabilizers, Catalysts and Reaction Conditions. Appl Catal B

Environ 84:533–540. https://doi.org/10.1016/j.apcatb.2008.05.008

He F, Zhao D, Liu J, Roberts CB (2007) Stabilization of Fe−Pd Nanoparticles with Sodium Carboxymethyl Cellulose for Enhanced Transport and Dechlorination of Trichloroethylene in Soil and Groundwater. Ind Eng Chem Res 46:29–34. https://doi.org/10.1021/ie0610896

He F, Zhao D, Paul C (2010) Field Assessment of Carboxymethyl Cellulose Stabilized Iron Nanoparticles for In Situ Destruction of Chlorinated Solvents in Source Zones. Water Res 44:2360–2370. https://doi.org/10.1016/j.watres.2009.12.041

He YT, Wilson JT, Su C, Wilkin RT (2015) Review of Abiotic Degradation of Chlorinated Solvents by Reactive Iron Minerals in Aquifers. Groundw Monit Remediat 35:57–75. https://doi.org/10.1111/GWMR.12111

Heck KN, Janesko BG, Scuseria GE, et al (2008) Observing Metal-Catalyzed Chemical Reactions in Situ Using Surface-Enhanced Raman Spectroscopy on Pd-Au Nanoshells. J Am Chem Soc 130:16592–16600. https://doi.org/10.1021/ja803556k

Henderson AD, Demond AH (2007) Long-Term Performance of Zero-Valent Iron Permeable Reactive Barriers: A Critical Review. Environ Eng Sci 24:401–423. https://doi.org/10.1089/ees.2006.0071

Heron G, Christensen TH, Enfield CG (1998) Henry's Law Constant for Trichloroethylene between 10 and 95 °C. Environ Sci Technol 32:1433–1437. https://doi.org/10.1021/es9707015

Hotze EM, Phenrat T, Lowry G V. (2010) Nanoparticle Aggregation: Challenges to Understanding Transport and Reactivity in the Environment. J Environ Qual 39:1909. https://doi.org/10.2134/jeq2009.0462

Huang B, Isse AA, Durante C, et al (2012) Electrocatalytic Properties of Transition Metals toward Reductive Dechlorination of Polychloroethanes. Electrochim Acta 70:50–61. https://doi.org/10.1016/jelectacta.2012.03.009

Huang B, Long J, Chen W, et al (2016a) Linear Free Energy Relationships of Electrochemical and Thermodynamic Parameters for the Electrochemical Reductive Dechlorination of Chlorinated Volatile Organic Compounds (Cl-VOCs). Electrochim Acta 208:195–201. https://doi.org/10.1016/j.electacta.2016.04.182

Huang B, Qian W, Yu C, et al (2016b) Effective Catalytic Hydrodechlorination of o-, p- and m-Chloronitrobenzene over Ni/Fe Nanoparticles: Effects of Experimental Parameter and Molecule Structure on the Reduction Kinetics and Mechanisms. Chem Eng J 306:607–618. https://doi.org/10.1016/j.cej.2016.07.109

Huang L-Z, Yin Z, Cooper NGA, et al (2018) Copper-Mediated Reductive Dechlorination by Green Rust Intercalated with Dodecanoate. J Hazard Mater 345:18–26. https://doi.org/10.1016/j.jhazmat.2017.11.011

Huang YH, Zhang TC (2005) Effects of Dissolved Oxygen on Formation of Corrosion Products and Concomitant Oxygen and Nitrate Reduction in Zero-Valent Iron Systems with or without Aqueous Fe2+. Water Res 39:1751–1760. https://doi.org/10.1016/j.watres.2005.03.002

Hwang Y-H, Kim D-G, Shin H-S (2011) Effects of Synthesis Conditions on the Characteristics and Reactivity of Nano Scale Zero Valent Iron. Appl Catal B Environ 105:144–150. https://doi.org/10.1016/j.apcatb.2011.04.005

Hwang Y, Kim D, Shin H-S (2015) Inhibition of Nitrate Reduction by NaCl Adsorption on a Nano-Zero-Valent Iron Surface during a Concentrate Treatment for Water Reuse. Environ Technol 36:1178–1187. https://doi.org/10.1080/09593330.2014.982723

Hydutsky BW, Mack EJ, Beckerman BB, et al (2007) Optimization of Nano- and Microiron Transport through Sand Columns Using Polyelectrolyte Mixtures. Environ Sci Technol 41:6418–6424. https://doi.org/10.1021/ES0704075

Hyman M, Dupont RR (2001) Groundwater Remediation Using Carbon Adsorption. In: Groundwater and Soil Remediation: Process Design and Cost Estimating of Proven Technologies. ASCE Press, Reston, VA, pp 109-135.

Hyun SP, Hayes KF (2015) Abiotic Reductive Dechlorination of cis-DCE by Ferrous Monosulfide Mackinawite. Environ Sci Pollut Res 22:16463–16474. https://doi.org/10.1007/s11356-015-5033-2

Ignatiadis I, Betelu S, Colombano S, et al (2016) Déchloration réductive chimique in situ des solvants chlorés présents dans les aquifères : pilote de démonstration sur le site de Néry-Saintines. Rapport final BRGM/RC-65722-FR, 262 p.

Ignatiadis I, Betelu S, Colombano S, et al (2014) DECHLORED: Development and In Situ Implementation of a Chemical Process for the Reductive Dechlorination of Chlorinated Solvents in Polluted Groundwater. Intersol, March 18-20, 2014. Lille, France.

Ignatiadis I, Betelu S, Rodrigues R, et al (2015) Mechanisms of Natural Reductive Biodechlorination (RDC) of Chlorinated Solvents in an Old Polluted Site. 6th European Bioremediation Conference, June 29-July 2, 2015. Chania, Greece.

Iranzo A, Chauvet F, Tzedakis T (2015) Influence of Electrode Material and Roughness on Iron Electrodeposits Dispersion by Ultrasonification. Electrochim Acta 184:436–451. https://doi.org/10.1016/j.electacta.2015.10.052

Jafvert CT (1994) Solubilization of Non-Polar Compounds by Non-Ionic Surfactant Micelles. Water Res 28:1009–1017. https://doi.org/10.1016/0043-1354(94)90185-6

Janda V, Vasek P, Bizova J, Belohlav Z (2004) Kinetic Models for Volatile Chlorinated Hydrocarbons Removal by Zero-Valent Iron. Chemosphere 54:917–925. https://doi.org/10.1016/j.chemosphere.2003.08.033

Jang M-H, Lim M, Hwang YS (2014) Potential Environmental Implications of Nanoscale Zero-Valent Iron Particles for Environmental Remediation. Environ Health Toxicol 29:e2014022. https://doi.org/10.5620/eht.e2014022

Jeffers PM, Ward LM, Woytowitch LM, Wolfe NL (1989) Homogeneous Hydrolysis Rate Constants for Selected Chlorinated Methanes, Ethanes, Ethenes, and Propanes. Environ Sci Technol 23:965–969. https://doi.org/10.1021/es00066a006

Jeong HY, Anantharaman K, Han Y-S, Hayes KF (2011) Abiotic Reductive Dechlorination of cis-Dichloroethylene by Fe Species Formed during Iron- or Sulfate-Reduction. Environ Sci Technol 45:5186–5194. https://doi.org/10.1021/es104387w

Jeong HY, Anantharaman K, Hyun SP, et al (2013) pH Impact on Reductive Dechlorination of cis-Dichloroethylene by Fe Precipitates: An X-ray Absorption Spectroscopy Study. Water Res 47:6639–6649. https://doi.org/10.1016/j.watres.2013.08.035

Jeong HY, Kim H, Hayes KF (2007) Reductive Dechlorination Pathways of Tetrachloroethylene and Trichloroethylene and Subsequent Transformation of Their Dechlorination Products by Mackinawite (FeS) in the Presence of Metals. Environ Sci Technol 41:7736–7743. https://doi.org/10.1021/es0708518

Jiang D, Zeng G, Huang D, et al (2018) Remediation of Contaminated Soils by Enhanced Nanoscale Zero Valent Iron. Environ Res 163:217–227. https://doi.org/10.1016/j.envres.2018.01.030

Jiang G, Lan M, Zhang Z, et al (2017) Identification of Active Hydrogen Species on Palladium Nanoparticles for an Enhanced Electrocatalytic Hydrodechlorination of 2,4-Dichlorophenol in Water. Environ Sci Technol 51:7599–7605. https://doi.org/10.1021/acs.est.7b01128

Jiao Y, Qiu C, Huang L, et al (2009) Reductive Dechlorination of Carbon Tetrachloride by Zero-Valent Iron and Related Iron Corrosion. Appl Catal B Environ 91:434–440. https://doi.org/10.1016/j.apcatb.2009.06.012

Johnson RL, Johnson PC (2012) In Situ Sparging for Delivery of Gases in the Subsurface. In: Delivery and Mixing in the Subsurface. Springer, New York, NY, USA, pp 193-216.

Johnson RL, Nurmi JT, O'Brien Johnson GS, et al (2013) Field-Scale Transport and Transformation of Carboxymethylcellulose-Stabilized Nano Zero-Valent Iron. Environ Sci Technol 47:1573–1580. https://doi.org/10.1021/es304564q

Johnson RL, Pankow JF (1992) Dissolution of Dense Chlorinated Solvents into Groundwater. 2. Source Functions for Pools of Solvent. Environ Sci Technol 26:896–901. https://doi.org/10.1021/es00029a004

Johnson TL, Fish W, Gorby YA, Tratnyek PG (1998) Degradation of Carbon Tetrachloride by Iron Metal: Complexation Effects on the Oxide Surface. J Contam Hydrol 29:379–398. https://doi.org/10.1016/S0169-7722(97)00063-6

Johnson TL, Scherer MM, Tratnyek PG (1996) Kinetics of Halogenated Organic Compound Degradation by Iron Metal. Environ Sci Technol 30:2634–2640. https://doi.org/10.1021/es9600901

Kaifas D (2014) Déchloration réductive par les nanoparticules de fer zéro-valent : une solution innovante pour la réhabilitation des aquifères souterrains contaminés par le trichloroéthylène. Aix-Marseille Université

Kaifas D, Malleret L, Kumar N, et al (2014) Assessment of Potential Positive Effects of nZVI Surface Modification and Concentration Levels on TCE Dechlorination in the Presence of Competing Strong Oxidants, using an Experimental Design. Sci Total Environ 481:335–342. https://doi.org/10.1016/j.scitotenv.2014.02.043

Karn B, Kuiken T, Otto M (2009) Nanotechnology and In Situ Remediation: A Review of the Benefits and Potential Risks. Environ Health Perspect 117:1813–31. https://doi.org/10.1289/ehp.0900793

Kašlík J, Kolařík J, Filip J, et al (2018) Nanoarchitecture of Advanced Core-Shell Zero-Valent Iron Particles with Controlled Reactivity for Contaminant Removal. Chem Eng J 354:335–345. https://doi.org/10.1016/j.cej.2018.08.015

Keenan CR, Goth-Goldstein R, Lucas D, Sedlak DL (2009) Oxidative Stress Induced by Zero-Valent Iron Nanoparticles and Fe(II) in Human Bronchial Epithelial Cells. Environ Sci Technol 43:4555–4560. https://doi.org/10.1021/es9006383

Keenan CR, Sedlak DL (2008) Factors Affecting the Yield of Oxidants from the Reaction of Nanoparticulate Zero-Valent Iron and Oxygen. Environ Sci Technol 42:1262–1267. https://doi.org/10.1021/es7025664

Keith PD, Lai CK, Kjeldsen P, Lo IMC (2005) Effect of Groundwater Inorganics on the Reductive Dechlorination of TCE by Zero-Valent Iron. Water, Air, Soil Pollut 162:401–420. https://doi.org/10.1007/s11270-005-7420-7

Kharissova O V., Dias HVR, Kharisov BI, et al (2013) The Greener Synthesis of Nanoparticles. Trends Biotechnol 31:240–248. https://doi.org/10.1016/j.tibtech.2013.01.003

Kim E-J, Kim J-H, Azad A-M, Chang Y-S (2011) Facile Synthesis and Characterization of Fe/FeS Nanoparticles for Environmental Applications. ACS Appl Mater Interfaces 3:1457–1462. https://doi.org/10.1021/am200016v

Kim H-H, Kim MS, Kim H-E, et al (2017a) Nanoparticulate Zero-Valent Iron coupled with Polyphosphate: The Sequential Redox Treatment of Organic Compounds and its Stability and Bacterial Toxicity. Environ Sci Nano 4:396–405. https://doi.org/10.1039/C6EN00502K

Kim H-J, Leitch M, Naknakorn B, et al (2017b) Effect of Emplaced nZVI Mass and Groundwater Velocity on PCE Dechlorination and Hydrogen Evolution in Water-Saturated Sand. J Hazard Mater 322:136–144. https://doi.org/10.1016/j.jhazmat.2016.04.037

Kim H-S, Ahn J-Y, Hwang K-Y, et al (2010a) Atmospherically Stable Nanoscale Zero-Valent Iron Particles Formed under Controlled Air Contact: Characteristics and Reactivity. Environ Sci Technol 44:1760–1766. https://doi.org/10.1021/es902772r

Kim H-S, Kim T, Ahn J-Y, et al (2012) Aging Characteristics and Reactivity of Two Types of Nanoscale Zero-Valent Iron Particles (FeBH and FeH2) in Nitrate Reduction. Chem Eng J 197:16–23. https://doi.org/10.1016/j.cej.2012.05.018

Kim JY, Park H-J, Lee C, et al (2010b) Inactivation of Escherichia coli by Nanoparticulate Zerovalent Iron and Ferrous Ion. Appl Environ Microbiol 76:7668–70. https://doi.org/10.1128/AEM.01009-10

Kim YH, Carraway ER (2003) Reductive Dechlorination of TCE by Zero Valent Bimetals. Environ Technol 24:69–75. https://doi.org/10.1080/09593330309385537

Kingston JLT, Johnson PC, Kueper BH, Mumford KG (2014) In Situ Thermal Treatment of Chlorinated Solvent Source Zones. In: Kueper BH, Stroo HF, Vogel CM, Ward CH (eds) Chlorinated Solvent Source Zone Remediation. Springer, New York, NY, pp 509–557

Kirschling TL, Golas PL, Unrine JM, et al (2011) Microbial Bioavailability of Covalently Bound Polymer Coatings on Model Engineered Nanomaterials. Environ Sci Technol 45:5253–5259. https://doi.org/10.1021/es200770z

Kirschling TL, Gregory KB, Minkley, Jr. EG, et al (2010) Impact of Nanoscale Zero Valent Iron on Geochemistry and Microbial Populations in Trichloroethylene Contaminated Aquifer Materials. Environ Sci Technol 44:3474–3480. https://doi.org/10.1021/es903744f

Klečka GM, Gonsior SJ (1984) Reductive Dechlorination of Chlorinated Methanes and Ethanes by Reduced Iron (II) Porphyrins. Chemosphere 13:391–402. https://doi.org/10.1016/0045-6535(84)90097-3

Knauss KG, Dibley MJ, Leif RN, et al (2000) The Aqueous Solubility of Trichloroethene (TCE) and Tetrachloroethene (PCE) as a Function of Temperature. Appl Geochemistry 15:501–512. https://doi.org/10.1016/S0883-2927(99)00058-X

Kocur CM, Chowdhury AI, Sakulchaicharoen N, et al (2014) Characterization of nZVI Mobility in a Field Scale Test. Environ Sci Technol 48:2862–2869. https://doi.org/10.1021/es4044209

Kocur CMD, Lomheim L, Boparai HK, et al (2015) Contributions of Abiotic and Biotic Dechlorination Following Carboxymethyl Cellulose Stabilized Nanoscale Zero Valent Iron Injection. Environ Sci Technol 49:8648–56. https://doi.org/10.1021/acs.est.5b00719

Kocur CMD, Lomheim L, Molenda O, et al (2016) Long-Term Field Study of Microbial Community and Dechlorinating Activity Following Carboxymethyl Cellulose-Stabilized Nanoscale Zero-Valent Iron Injection. Environ Sci Technol 50:7658–7670. https://doi.org/10.1021/acs.est.6b01745

Koenig JC, Boparai HK, Lee MJ, et al (2016) Particles and Enzymes: Combining Nanoscale Zero Valent Iron and Organochlorine Respiring Bacteria for the Detoxification of Chloroethane Mixtures. J Hazard Mater 308:106–112. https://doi.org/10.1016/j.jhazmat.2015.12.036

Koproch N, Dahmke A, Köber R (2018) The Aqueous Solubility of Common Organic Groundwater Contaminants as a Function of Temperature between 5 and 70 °C. Chemosphere 217:166–175. https://doi.org/10.1016/J.CHEMOSPHERE.2018.10.153

Kozma G, Rónavári A, Kónya Z, Kukovecz Á (2016) Environmentally Benign Synthesis Methods of Zero-Valent Iron Nanoparticles. ACS Sustain Chem Eng 4:291–297. https://doi.org/10.1021/acssuschemeng.5b01185

Krol MM, Oleniuk AJ, Kocur CM, et al (2013) A Field-Validated Model for In Situ Transport of Polymer-Stabilized nZVI and Implications for Subsurface Injection. Environ Sci Technol 47:7332–7340. https://doi.org/10.1021/es3041412

Kueper BH, Stroo HF, Vogel CM, Ward CH (2014) Source Zone Remediation: The State of the Practice. In: Kueper BH, Stroo HF, Vogel CM, Ward CH (eds) Chlorinated Solvent Source Zone Remediation. Springer New York, New York, NY, pp 1-27.

Kueper BH, Wealthall GP, Smith JWN, et al (2003) An Illustrated Handbook of DNAPL Transport and Fate in the Subsurface. Environment Agency, Bristol, UK.

Kumar N, Auffan M, Gattacceca J, et al (2014a) Molecular Insights of Oxidation Process of Iron Nanoparticles: Spectroscopic, Magnetic, and Microscopic Evidence. Environ Sci Technol 48:13888–13894. https://doi.org/10.1021/es503154q

Kumar N, Labille J, Bossa N, et al (2017) Enhanced Transportability of Zero Valent Iron Nanoparticles in Aquifer Sediments: Surface Modifications, Reactivity, and Particle Traveling Distances. Environ Sci Pollut Res 24:9269–9277. https://doi.org/10.1007/s11356-017-8597-1

Kumar N, Lezama Pacheco J, Noël V, et al (2018) Sulfidation Mechanisms of Fe(III)-(Oxyhydr)Oxide Nanoparticles: A Spectroscopic Study. Environ Sci Nano 5:1012–1026. https://doi.org/10.1039/C7EN01109A

Kumar N, Omoregie EO, Rose J, et al (2014b) Inhibition of Sulfate Reducing Bacteria in Aquifer Sediment by Iron Nanoparticles. Water Res 51:64–72. https://doi.org/10.1016/j.watres.2013.09.042

Kutílek M, Nielsen DR (1994) Soil Hydrology. Catena Verlag, Cremlingen Destedt.

Lasaga AC (1981) Transition State Theory. Rev Mineral Geochemistry 8:135–168

Laumann S, Mici V, Lowry G V, Hofmann T (2013) Carbonate Minerals in Porous Media Decrease Mobility of Polyacrylic Acid Modified Zero-Valent Iron Nanoparticles used for Groundwater Remediation. Environ Pollut 179:53–60. https://doi.org/10.1016/j.envpol.2013.04.004

Lee C (2015) Oxidation of Organic Contaminants in Water by Iron-Induced Oxygen Activation: A Short Review. Environ Eng Res 20:205–211. https://doi.org/10.4491/eer.2015.051

Lee C, Kim JY, Lee W Il, et al (2008) Bactericidal Effect of Zero-Valent Iron Nanoparticles on Escherichia coli. Environ Sci Technol 42:4927–4933. https://doi.org/10.1021/es800408u

Lee C, Sedlak DL (2008) Enhanced Formation of Oxidants from Bimetallic Nickel−Iron Nanoparticles in the Presence of Oxygen. Environ Sci Technol 42:8528–8533. https://doi.org/10.1021/es801947h

Lee HH, Lee HH, Kim H-E, et al (2014) Oxidant Production from Corrosion of Nano- and

Microparticulate Zero-Valent Iron in the Presence of Oxygen: A Comparative Study. J Hazard Mater 265:201–207. https://doi.org/10.1016/j.jhazmat.2013.11.066

Lee W (2004) Removal of Trichloroethylene in Reduced Soil Columns. J Hazard Mater 113:175–180. https://doi.org/10.1016/j.jhazmat.2004.06.027

Lee W, Batchelor B (2002a) Abiotic Reductive Dechlorination of Chlorinated Ethylenes by Iron-Bearing Soil Minerals. 2. Green Rust. Environ Sci Technol 36:5348–5354. https://doi.org/10.1021/es0258374

Lee W, Batchelor B (2002b) Abiotic Reductive Dechlorination of Chlorinated Ethylenes by Iron-Bearing Soil Minerals. 1. Pyrite and Magnetite. Environ Sci Technol 36:5147–5154. https://doi.org/10.1021/es025836b

Leeson A, Johnson P, Bruce C, et al (2002) Design Paradigm: Air Sparging Technology Transfer and Multi-Site Evaluation. Alexandria, VA, USA.

Lefevre E, Bossa N, Wiesner MR, Gunsch CK (2016) A Review of the Environmental Implications of In Situ Remediation by Nanoscale Zero Valent Iron (nZVI): Behavior, Transport and Impacts on Microbial Communities. Sci Total Environ 565:889–901. https://doi.org/10.1016/j.scitotenv.2016.02.003

Lei C, Sun Y, Tsang DCW, Lin D (2018) Environmental Transformations and Ecological Effects of Iron-Based Nanoparticles. Environ Pollut 232:10–30. https://doi.org/10.1016/j.envpol.2017.09.052

Lemaire J, Buès M, Kabeche T, et al (2013a) Oxidant Selection to Treat an Aged PAH Contaminated Soil by In Situ Chemical Oxidation. J Environ Chem Eng 1:1261–1268. https://doi.org/10.1016/j.jece.2013.09.018

Lemaire J, Laurent F, Leyval C, et al (2013b) PAH Oxidation in Aged and Spiked Soils Investigated by Column Experiments. Chemosphere 91:406–414. https://doi.org/10.1016/j.chemosphere.2012.12.003

Lemming G, Chambon JC, Binning PJ, Bjerg PL (2012) Is There an Environmental Benefit from Remediation of a Contaminated Site? Combined Assessments of the Risk Reduction and Life Cycle Impact of Remediation. J Environ Manage 112:392–403. https://doi.org/10.1016/j.jenvman.2012.08.002

Levin DB, Pitt L, Love M (2004) Biohydrogen Production: Prospects and Limitations to Practical Application. Int J Hydrogen Energy 29:173–185. https://doi.org/10.1016/S0360-3199(03)00094-6

Li D, Mao Z, Zhong Y, et al (2016a) Reductive Transformation of Tetrabromobisphenol A by Sulfidated Nano Zerovalent Iron. Water Res 103:1–9. https://doi.org/10.1016/j.watres.2016.07.003

Li H, Qiu Y, Wang X, et al (2017a) Biochar Supported Ni/Fe Bimetallic Nanoparticles to Remove 1,1,1-trichloroethane under Various Reaction Conditions. Chemosphere 169:534–541. https://doi.org/10.1016/j.chemosphere.2016.11.117

Li J, Rajajayavel SRC, Ghoshal S (2016b) Transport of Carboxymethyl Cellulose-Coated Zerovalent Iron Nanoparticles in a Sand Tank: Effects of Sand Grain Size, Nanoparticle Concentration and Injection Velocity. Chemosphere 150:8–16. https://doi.org/10.1016/j.chemosphere.2015.12.075

Li J, Zhang X, Liu M, et al (2018) Enhanced Reactivity and Electron Selectivity of Sulfidated Zerovalent Iron toward Chromate under Aerobic Conditions. Environ Sci Technol 52:2988–2997. https://doi.org/10.1021/acs.est.7b06502

Li J, Zhang X, Sun Y, et al (2017b) Advances in Sulfidation of Zerovalent Iron for Water Decontamination. Environ Sci Technol 51:13533–13544. https://doi.org/10.1021/acs.est.7b02695

Li L, Fan M, Brown RC, et al (2006a) Synthesis, Properties, and Environmental Applications of Nanoscale Iron-Based Materials: A Review. Crit Rev Environ Sci Technol 36:405–431. https://doi.org/10.1080/10643380600620387

Li S, Ding Y, Wang W, Lei H (2016c) A Facile Method for Determining the Fe(0) Content and Reactivity of Zero Valent Iron. Anal Methods 8:1239–1248. https://doi.org/10.1039/C5AY02182K

Li S, Wang W, Liang F, Zhang W (2017c) Heavy Metal Removal using Nanoscale Zero-Valent Iron (nZVI): Theory and Application. J Hazard Mater 322:163–171. https://doi.org/10.1016/j.jhazmat.2016.01.032

Li S, Yan W, Zhang W (2009) Solvent-Free Production of Nanoscale Zero-Valent Iron (nZVI) with Precision Milling. Green Chem 11:1618. https://doi.org/10.1039/b913056j

Li X, Elliott DW, Zhang W (2006b) Zero-Valent Iron Nanoparticles for Abatement of Environmental Pollutants: Materials and Engineering Aspects. Crit Rev Solid State Mater Sci 31:111–122. https://doi.org/10.1080/10408430601057611

Li X, Zhang W (2007) Sequestration of Metal Cations with Zerovalent Iron Nanoparticles: A Study with High Resolution X-ray Photoelectron Spectroscopy (HR-XPS). J Phys Chem C 111:6939–6946. https://doi.org/10.1021/jp0702189

Li Y, Li X, Han D, et al (2017d) New Insights into the Role of Ni Loading on the Surface Structure and the Reactivity of nZVI toward Tetrabromo- and Tetrachlorobisphenol A. Chem Eng J 311:173–182. https://doi.org/10.1016/j.cej.2016.11.084

Li Z, Greden K, Alvarez PJJ, et al (2010) Adsorbed Polymer and NOM Limits Adhesion and Toxicity of Nano Scale Zerovalent Iron to *E. coli*. Environ Sci Technol 44:3462–3467. https://doi.org/10.1021/es9031198

Lien H-L, Jhuo Y-S, Chen L-H (2007) Effect of Heavy Metals on Dechlorination of Carbon Tetrachloride by Iron Nanoparticles. Environ Eng Sci 24:21–30. https://doi.org/10.1089/ees.2007.24.21

Lien H-L, Zhang W (2001) Nanoscale Iron Particles for Complete Reduction of Chlorinated Ethenes. Colloids Surfaces A Physicochem Eng Asp 191:97–105. https://doi.org/10.1016/S0927-7757(01)00767-1

Lien H-L, Zhang W (2007) Nanoscale Pd/Fe Bimetallic Particles: Catalytic Effects of Palladium on Hydrodechlorination. Appl Catal B Environ 77:110–116. https://doi.org/10.1016/j.apcatb.2007.07.014

Lien H-L, Zhang W (1999) Transformation of Chlorinated Methanes by Nanoscale Iron Particles. J Environ Eng 125:1042–1047. https://doi.org/10.1061/(ASCE)0733-9372(1999)125:11(1042)

Lien H-L, Zhang W (2005) Hydrodechlorination of Chlorinated Ethanes by Nanoscale Pd/Fe Bimetallic Particles. J Environ Eng 131:4–10. https://doi.org/10.1061/(ASCE)0733-9372(2005)131:1(4)

Lima AT, Hofmann A, Reynolds D, et al (2017) Environmental Electrokinetics for a Sustainable Subsurface. Chemosphere 181:122–133. https://doi.org/10.1016/j.chemosphere.2017.03.143

Lin CJ, Lo S-L (2005) Effects of Iron Surface Pretreatment on Sorption and Reduction Kinetics of Trichloroethylene in a Closed Batch System. Water Res 39:1037–1046.

https://doi.org/10.1016/j.watres.2004.06.035

Lin CJ, Lo SL, Liou YH (2004) Dechlorination of Trichloroethylene in Aqueous Solution by Noble Metal-Modified Iron. J Hazard Mater 116:219–228. https://doi.org/10.1016/j.jhazmat.2004.09.005

Lin K-S, Mdlovu NV, Chen C-Y, et al (2018) Degradation of TCE, PCE, and 1,2–DCE DNAPLs in Contaminated Groundwater using Polyethylenimine-Modified Zero-Valent Iron Nanoparticles. J Clean Prod 175:456–466. https://doi.org/10.1016/j.jclepro.2017.12.074

Ling L, Huang X, Li M, Zhang W (2017) Mapping the Reactions in a Single Zero-Valent Iron Nanoparticle. Environ Sci Technol 51:14293–14300. https://doi.org/10.1021/acs.est.7b02233

Ling L, Zhang W (2014a) Reactions of Nanoscale Zero-Valent Iron with Ni(II): Three-Dimensional Tomography of the "Hollow Out" Effect in a Single Nanoparticle. Environ Sci Technol Lett 1:209–213. https://doi.org/10.1021/ez4002054

Ling L, Zhang W (2014b) Sequestration of Arsenate in Zero-Valent Iron Nanoparticles: Visualization of Intraparticle Reactions at Angstrom Resolution. Environ Sci Technol Lett 1:305–309. https://doi.org/10.1021/ez5001512

Ling L, Zhang W (2017) Visualizing Arsenate Reactions and Encapsulation in a Single Zero-Valent Iron Nanoparticle. Environ Sci Technol 51:2288–2294. https://doi.org/10.1021/acs.est.6b04315

Ling L, Zhang W (2014c) Structures of Pd–Fe(0) Bimetallic Nanoparticles near 0.1 nm Resolution. RSC Adv 4:33861. https://doi.org/10.1039/C4RA04311A

Lipczynska-Kochany E, Harms S, Milburn R, et al (1994) Degradation of Carbon Tetrachloride in the Presence of Iron and Sulphur Containing Compounds. Chemosphere 29:1477–1489. https://doi.org/10.1016/0045-6535(94)90279-8

Liu A, Liu J, Pan B, Zhang W (2014a) Formation of Lepidocrocite (γ-FeOOH) from Oxidation of Nanoscale Zero-Valent Iron (nZVI) in Oxygenated Water. RSC Adv 4:57377–57382. https://doi.org/10.1039/C4RA08988J

Liu F, Rotaru A-E, Shrestha PM, et al (2012) Promoting Direct Interspecies Electron Transfer with Activated Carbon. Energy Environ Sci 5:8982. https://doi.org/10.1039/c2ee22459c

Liu R, Zhao H, Zhao X, et al (2018) Defect Sites in Ultrathin Pd Nanowires Facilitate the Highly Efficient Electrochemical Hydrodechlorination of Pollutants by H*ads. Environ Sci Technol 52:9992–10002. https://doi.org/10.1021/acs.est.8b02740

Liu W-J, Qian T-T, Jiang H (2014b) Bimetallic Fe Nanoparticles: Recent Advances in Synthesis and Application in Catalytic Elimination of Environmental Pollutants. Chem Eng J 236:448–463. https://doi.org/10.1016/j.cej.2013.10.062

Liu Y, Choi H, Dionysiou D, Lowry G V. (2005a) Trichloroethene Hydrodechlorination in Water by Highly Disordered Monometallic Nanoiron. Chem Mater 17:5315–5322. https://doi.org/10.1021/cm0511217

Liu Y, Lowry G V. (2006) Effect of Particle Age (Fe0 Content) and Solution pH on NZVI Reactivity: H2 Evolution and TCE Dechlorination. Environ Sci Technol 40:6085–6090. https://doi.org/10.1021/es060685o

Liu Y, Majetich SA, Tilton RD, et al (2005b) TCE Dechlorination Rates, Pathways, and Efficiency of Nanoscale Iron Particles with Different Properties. Environ Sci Technol 39:1338–1345. https://doi.org/10.1021/es049195R

Liu Y, Phenrat T, Lowry G V (2007) Effect of TCE Concentration and Dissolved Groundwater Solutes on NZVI-Promoted TCE Dechlorination and H2 Evolution. Environ Sci Technol 41:7881–7887. https://doi.org/10.1021/es0711967

Loraine GA (2001) Effects of Alcohols, Anionic and Nonionic Surfactants on the Reduction of PCE and TCE by Zero-Valent Iron. Water Res 35:1453–1460. https://doi.org/10.1016/S0043-1354(00)00422-X

Louie SM, Tilton RD, Lowry G V (2016) Critical Review: Impacts of Macromolecular Coatings on Critical Physicochemical Processes Controlling Environmental Fate of Nanomaterials. Environ Sci Nano 3:283–310. https://doi.org/10.1039/C5EN00104H

Lowry G V., Casman EA (2009) Nanomaterial Transport, Transformation, and Fate in the Environment. In: Nanomaterials: Risks and Benefits. Springer Netherlands, Dordrecht, pp 125–137

Lowry G V., Gregory KB, Apte SC, Lead JR (2012) Transformations of Nanomaterials in the Environment. Environ Sci Technol 46:6893–6899. https://doi.org/10.1021/es300839e

Lowry G V, Reinhard M (1999) Hydrodehalogenation of 1- to 3-Carbon Halogenated Organic Compounds in Water Using a Palladium Catalyst and Hydrogen Gas. Environ Sci Technol 33:1905–1910. https://doi.org/10.1021/es980963m

Lu M-C, Anotai J, Chyan J-M, Ting W-P (2006) Effect of Chloride Ions on the Dechlorination of Hexachlorobenzene in the Presence of Zero-Valent Iron. Pract Period Hazardous, Toxic, Radioact Waste Manag 10:226–230. https://doi.org/10.1061/(ASCE)1090-025X(2006)10:4(226)

Lu X, Li M, Tang C, et al (2012) Electrochemical Depassivation for Recovering Fe0 Reactivity by Cr(VI) Removal with a Permeable Reactive Barrier System. J Hazard Mater 213–214:355–360. https://doi.org/10.1016/j.jhazmat.2012.02.007

Luna M, Gastone F, Tosco T, et al (2015) Pressure-Controlled Injection of Guar Gum Stabilized Microscale Zerovalent Iron for Groundwater Remediation. J Contam Hydrol 181:46–58. https://doi.org/10.1016/j.jconhyd.2015.04.007

Luo F, Yang D, Chen Z, et al (2016) One-Step Green Synthesis of Bimetallic Fe/Pd Nanoparticles Used to Degrade Orange II. J Hazard Mater 303:145–153. https://doi.org/10.1016/j.jhazmat.2015.10.034

Luo J, Farrell J (2013) Understanding pH Effects on Trichloroethylene and Perchloroethylene Adsorption to Iron in Permeable Reactive Barriers for Groundwater Remediation. Int J Environ Sci Technol 10:77–84. https://doi.org/10.1007/s13762-012-0082-2

Ma C, Wu Y (2008) Dechlorination of Perchloroethylene using Zero-Valent Metal and Microbial Community. Environ Geol 55:47–54. https://doi.org/10.1007/s00254-007-0963-8

Ma J, He D, Collins RN, et al (2016) The Tortoise versus the Hare - Possible Advantages of Microparticulate Zerovalent Iron (mZVI) over Nanoparticulate Zerovalent Iron (nZVI) in Aerobic Degradation of Contaminants. Water Res 105:331–340. https://doi.org/10.1016/j.watres.2016.09.012

Machado S, Pacheco JG, Nouws HPA, et al (2015) Characterization of Green Zero-Valent Iron Nanoparticles Produced with Tree Leaf Extracts. Sci Total Environ 533:76–81. https://doi.org/10.1016/j.scitotenv.2015.06.091

Mackay D, Shiu W-Y, Ma K-C, Lee SC (2006) Handbook of Physical-Chemical Properties and Environmental Fate for Organic Chemicals, Second Edition. CRC Press, Boca Raton, FL, USA

Mackay DM, Freyberg DL, Roberts P V., Cherry JA (1986) A Natural Gradient Experiment on Solute Transport in a Sand Aquifer: 1. Approach and Overview of Plume Movement. Water Resour Res 22:2017–2029. https://doi.org/10.1029/WR022i013p02017

Mackenzie K, Bleyl S, Georgi A, Kopinke F-D (2012) Carbo-Iron - An Fe/AC Composite - As Alternative to Nano-Iron for Groundwater Treatment. Water Res 46:3817–3826. https://doi.org/10.1016/j.watres.2012.04.013

Maire J, Joubert A, Kaifas D, et al (2018) Assessment of Flushing Methods for the Removal of Heavy Chlorinated Compounds DNAPL in an Alluvial Aquifer. Sci Total Environ 612:1149–1158. https://doi.org/10.1016/j.scitotenv.2017.08.309

Makota S, Nde-Tchoupe AI, Mwakabona HT, et al (2017) Metallic Iron for Water Treatment: Leaving the Valley of Confusion. Appl Water Sci 1–20. https://doi.org/10.1007/s13201-017-0601-x

Mangayayam MC, Dideriksen K, Tobler DJ (2018) Can or Cannot Green Rust Reduce Chlorinated Ethenes? Energy Procedia 146:173–178. https://doi.org/10.1016/j.egypro.2018.07.022

Mao X, Jiang R, Xiao W, Yu J (2015) Use of Surfactants for the Remediation of Contaminated Soils: A Review. J Hazard Mater 285:419–435. https://doi.org/10.1016/j.jhazmat.2014.12.009

Marques CA, Selva M, Tundo P (1993) Facile Hydrodehalogenation with Hydrogen and Palladium/Carbon Catalyst under Multiphase Conditions. J Org Chem 58:5256–5260. https://doi.org/10.1021/jo00071a041

Martin JE, Herzing AA, Yan W, et al (2008) Determination of the Oxide Layer Thickness in Core−Shell Zerovalent Iron Nanoparticles. Langmuir 24:4329–4334. https://doi.org/10.1021/la703689K

Matheson LJ, Tratnyek PG (1994) Reductive Dehalogenation of Chlorinated Methanes by Iron Metal. Environ Sci Technol 28:2045–2053. https://doi.org/10.1021/es00061a012

Mattes TE, Alexander AK, Coleman N V. (2010) Aerobic Biodegradation of the Chloroethenes: Pathways, Enzymes, Ecology, and Evolution. FEMS Microbiol Rev 34:445–475. https://doi.org/10.1111/j.1574-6976.2010.00210.x

Mayhew SG (1978) The Redox Potential of Dithionite and SO-2 from Equilibrium Reactions with Flavodoxins, Methyl Viologen and Hydrogen plus Hydrogenase. Eur J Biochem 85:535–547. https://doi.org/10.1111/j.1432-1033.1978.tb12269.x

Mayhew SG, Massey V (1973) Studies on the kinetics and mechanism of reduction of flavodoxin from Peptostreptococcus elsdenii by sodium dithionite. Biochim Biophys Acta - Enzymol 315:181–190. https://doi.org/10.1016/0005-2744(73)90141-1

Maymó-Gatell X, Anguish T, Zinder SH (1999) Reductive Dechlorination of Chlorinated Ethenes and 1, 2-dichloroethane by Dehalococcoides ethenogenes 195. Appl Environ Microbiol 65:3108–13

Maymó-Gatell X, Tandoi V, Gossett JM, Zinder SH (1995) Characterization of an H2-Utilizing Enrichment Culture that Reductively Dechlorinates Tetrachloroethene to Vinyl Chloride and Ethene in the Absence of Methanogenesis and Acetogenesis. Appl Environ Microbiol 61:3928–3933

McCarty PL (2010) Groundwater Contamination by Chlorinated Solvents: History, Remediation Technologies and Strategies. In: Stroo HF, Ward CH (eds) In Situ Remediation of Chlorinated Solvent Plumes. Springer, New York, NY, USA, pp 1-28.

McCarty PL, Semprini L (1994) Ground-water Treatment for Chlorinated Solvents. In: Handbook of Bioremediation, Robert Nor. Lewis Publishers, Boca Raton, FL, USA.

McCauley KM, Wilson SR, van der Donk WA (2002) Synthesis and Characterization of Chlorinated Alkenylcobaloximes To Probe the Mechanism of Vitamin B12-Catalyzed Dechlorination of Priority Pollutants. Inorg Chem 41:393–404. https://doi.org/10.1021/ic011023X

McCormick ML, Adriaens P (2004) Carbon Tetrachloride Transformation on the Surface of Nanoscale Biogenic Magnetite Particles. Environ Sci Technol 38:1045–1053. https://doi.org/10.1021/es030487M

McDaniel T V, Martin PA, Ross N, et al (2004) Effects of Chlorinated Solvents on Four Species of North American Amphibians. Arch Environ Contam Toxicol 47:101–9

Middeldorp PJM, Luijten MLGC, Pas BA van de, et al (1999) Anaerobic Microbial Reductive Dehalogenation of Chlorinated Ethenes. Bioremediat J 3:151–169. https://doi.org/10.1080/10889869991219280

Miehr R, Tratnyek PG, Bandstra JZ, et al (2004) Diversity of Contaminant Reduction Reactions by Zerovalent Iron: Role of the Reductate. Environ Sci Technol 38:139–147. https://doi.org/10.1021/es034237h

Millington RJ, Quirk JP (1961) Permeability of Porous Solides. Trans Faraday Soc 57:1200–1207

Montgomery JH (2007) Groundwater Chemicals Desk Reference, Fourth Edition. CRC Press, Boca Raton, FL, USA.

Montgomery JM (1985) Water Treatment Principles and Design. MWH

Morrison RD (2000) Environmental Forensics: Principles & Applications. CRC Press, Boca Raton, FL, USA.

Morrison RD, Murphy B (2006) Environmental Forensics: Contaminant Specific Guide. Elsevier Academic Press

Mu Y, Jia F, Ai Z, Zhang L (2017) Iron Oxide Shell Mediated Environmental Remediation Properties of Nano Zero-Valent Iron. Environ Sci Nano 4:27–45. https://doi.org/10.1039/C6EN00398B

Mueller NC, Braun J, Bruns J, et al (2012) Application of Nanoscale Zero Valent Iron (NZVI) for Groundwater Remediation in Europe. Environ Sci Pollut Res 19:550–558. https://doi.org/10.1007/s11356-011-0576-3

Muftikian R, Fernando Q, Korte N (1995) A Method for the Rapid Dechlorination of Low Molecular Weight Chlorinated Hydrocarbons in Water. Water Res 29:2434–2439. https://doi.org/10.1016/0043-1354(95)00102-Q

Muftikian R, Nebesny K, Fernando Q, Korte N (1996) X-ray Photoelectron Spectra of the Palladium−Iron Bimetallic Surface Used for the Rapid Dechlorination of Chlorinated Organic Environmental Contaminants. Environ Sci Technol 30:3593–3596. https://doi.org/10.1021/es960289D

Müller U, Dülberg A, Stoyanova A, Baltruschat H (1997) Reactions of Halogenated Hydrocarbons at Pt-group Metals—II. on the Adsorption Rate at Pt and Pd Electrodes. Electrochim Acta 42:2499–2509. https://doi.org/10.1016/S0013-4686(96)00439-2

Munakata N, Reinhard M (2007) Palladium-Catalyzed Aqueous Hydrodehalogenation in Column Reactors: Modeling of Deactivation Kinetics with Sulfide and Comparison of Regenerants. Appl Catal B Environ 75:1–10. https://doi.org/10.1016/j.apcatb.2007.03.005

Němeček J, Pokorný P, Lhotský O, et al (2016) Combined Nano-Biotechnology for In-Situ Remediation of Mixed Contamination of Groundwater by Hexavalent Chromium and

Chlorinated Solvents. Sci Total Environ 563–564:822–834. https://doi.org/10.1016/J.SCITOTENV.2016.01.019

Ni S-Q, Yang N (2014) Cation Exchange Resin Immobilized Bimetallic Nickel–Iron Nanoparticles to Facilitate their Application in Pollutants Degradation. J Colloid Interface Sci 420:158–165. https://doi.org/10.1016/j.jcis.2014.01.010

Nidheesh PV, Khatri J, Singh TSA, et al (2018) Review of Zero-Valent Aluminium Based Water and Wastewater Treatment Methods. Chemosphere 200:621–631. https://doi.org/10.1016/j.chemosphere.2018.02.155

Nie X, Liu J, Zeng X (2012) Effect of Surfactant on HCB Dechlorination by Ag/Fe Bimetal in Polluted Soil Eluent. Procedia Environ Sci 16:320–326. https://doi.org/10.1016/j.proenv.2012.10.045

Nie X, Liu J, Zeng X, Yue D (2013) Rapid Degradation of Hexachlorobenzene by Micron Ag/Fe Bimetal Particles. J Environ Sci 25:473–478. https://doi.org/10.1016/S1001-0742(12)60088-6

Noel C, Gourry J-C, Betelu S, Ignatiadis I (2013) Improved Monitoring of the Reductive Dechlorination of PCE in Polluted Soils by Using Geophysical and Electrochemical Measurements Carried Out in Columns. In: Proceedings of the 12th International Conference on Sustainable Use and Management of Soil, Sediment and Water Resources. pp 111-121.

Notini L, Latta DE, Neumann A, et al (2018) The Role of Defects in Fe(II)–Goethite Electron Transfer. Environ Sci Technol 52:2751–2759. https://doi.org/10.1021/acs.est.7b05772

Noubactep C (2008) A Critical Review on the Process of Contaminant Removal in Fe0-H2O Systems. Environ Technol 29:909–920. https://doi.org/10.1080/09593330802131602

Noubactep C (2009) On the Validity of Specific Rate Constants (kSA) in Fe0/H2O Systems. J Hazard Mater 164:835–837. https://doi.org/10.1016/j.jhazmat.2008.08.074

Noubactep C (2010a) The Fundamental Mechanism of Aqueous Contaminant Removal by Metallic Iron. Water SA 36:. https://doi.org/10.4314/wsa.v36i5.62000

Noubactep C (2012) Investigating the Processes of Contaminant Removal in Fe0/H2O Systems. Korean J Chem Eng 29:1050–1056. https://doi.org/10.1007/s11814-011-0298-8

Noubactep C (2010b) The Suitability of Metallic Iron for Environmental Remediation. Environ Prog Sustain Energy 29:286–291. https://doi.org/10.1002/ep.10406

Noubactep C (2016) Research on Metallic Iron for Environmental Remediation: Stopping Growing Sloppy Science. Chemosphere 153:528–530. https://doi.org/10.1016/j.chemosphere.2016.03.088

Noubactep C (2011) On the Mechanism of Microbe Inactivation by Metallic Iron. J Hazard Mater 198:383–386. https://doi.org/10.1016/j.jhazmat.2011.08.063

Noubactep C, Caré S (2010) On Nanoscale Metallic Iron for Groundwater Remediation. J Hazard Mater 182:923–927. https://doi.org/10.1016/j.jhazmat.2010.06.009

Noubactep C, Caré S, Crane R (2012) Nanoscale Metallic Iron for Environmental Remediation: Prospects and Limitations. Water, Air, Soil Pollut 223:1363–1382. https://doi.org/10.1007/s11270-011-0951-1

Nowack B, Bucheli TD (2007) Occurrence, Behavior and Effects of Nanoparticles in the Environment. Environ Pollut 150:5–22. https://doi.org/10.1016/j.envpol.2007.06.006

Nunez Garcia A, Boparai HK, Chowdhury AIA, et al (2020a) Sulfidated nano zerovalent iron (S-

nZVI) for in situ treatment of chlorinated solvents: A field study. Water Res 115594. https://doi.org/10.1016/j.watres.2020.115594

Nunez Garcia A, Boparai HK, de Boer C V., et al (2020b) Fate and transport of sulfidated nano zerovalent iron (S-nZVI): A field study. Water Res 170:115319. https://doi.org/10.1016/j.watres.2019.115319

Nunez Garcia A, Boparai HK, O'Carroll DM (2016) Enhanced Dechlorination of 1,2-Dichloroethane by Coupled Nano Iron-Dithionite Treatment. Environ Sci Technol 50:5243–5251. https://doi.org/10.1021/acs.est.6b00734

Nurmi JT, Tratnyek PG, Sarathy V, et al (2005) Characterization and Properties of Metallic Iron Nanoparticles: Spectroscopy, Electrochemistry, and Kinetics. Environ Sci Technol 39:1221–1230. https://doi.org/10.1021/es049190U

O'Hannesin SF, Gillham RW (1998) Long-Term Performance of an In Situ "Iron Wall" for Remediation of VOCs. Ground Water 36:164–170. https://doi.org/10.1111/j.1745-6584.1998.tb01077.x

O'Loughlin EJ, Burris DR (2004) Reduction of Halogenated Ethanes by Green Rust. Environ Toxicol Chem 23:41. https://doi.org/10.1897/03-45

O 'Carroll D, Sleep B, Krol M, et al (2013) Nanoscale Zero Valent Iron and Bimetallic Particles for Contaminated Site Remediation. Adv Water Resour 51:104–122. https://doi.org/10.1016/j.advwatres.2012.02.005

Obiri-Nyarko F, Grajales-Mesa SJ, Malina G (2014) An Overview of Permeable Reactive Barriers for In Situ Sustainable Groundwater Remediation. Chemosphere 111:243–259. https://doi.org/10.1016/j.chemosphere.2014.03.112

Odziemkowski MS, Schuhmacher TT, Gillham RW, Reardon EJ (1998) Mechanism of Oxide Film Formation on Iron in Simulating Groundwater Solutions: Raman Spectroscopic Studies. Corros Sci 40:371–389. https://doi.org/10.1016/S0010-938X(97)00141-8

Odziemkowski MS, Simpraga RP (2004) Distribution of Oxides on Iron Materials used for Remediation of Organic Groundwater Contaminants — Implications for Hydrogen Evolution Reactions. Can J Chem 82:1495–1506. https://doi.org/10.1139/v04-120

Ogata A (1970) Theory of Dispersion in Granular Medium: USGS Professional Paper 411-I

Oleszek-Kudlak S, Shibata E, Nakamura T (2004) The Effects of Temperature and Inorganic Salts on the Aqueous Solubility of Selected Chlorobenzenes. J Chem Eng Data 49:570–575. https://doi.org/10.1021/je034170d

Olson MR, Sale TC, Shackelford CD, et al (2012) Chlorinated Solvent Source-Zone Remediation via ZVI-Clay Soil Mixing: 1-Year Results. Ground Water Monit Remediat 32:63–74. https://doi.org/10.1111/j.1745-6592.2011.01391.x

Omar S, Palomar J, Gómez-Sainero LM, et al (2011) Density Functional Theory Analysis of Dichloromethane and Hydrogen Interaction with Pd Clusters: First Step to Simulate Catalytic Hydrodechlorination. J Phys Chem C 115:14180–14192. https://doi.org/10.1021/jp200329j

Onanong S, Comfort SD, Burrow PD, Shea PJ (2007) Using Gas-Phase Molecular Descriptors to Predict Dechlorination Rates of Chloroalkanes by Zerovalent Iron. Environ Sci Technol 41:1200–1205. https://doi.org/10.1021/es061746l

Orsetti S, Laskov C, Haderlein SB (2013) Electron Transfer between Iron Minerals and Quinones: Estimating the Reduction Potential of the Fe(II)-Goethite Surface from AQDS Speciation.

Environ Sci Technol 47:14161–14168. https://doi.org/10.1021/es403658g

Orth WS, Gillham RW (1996) Dechlorination of Trichloroethene in Aqueous Solution Using Fe0. Environ Sci Technol 30:66–71. https://doi.org/10.1021/es950053u

Otto WH, Britten DJ, Larive CK (2003) NMR Diffusion Analysis of Surfactant–Humic Substance Interactions. J Colloid Interface Sci 261:508–513. https://doi.org/10.1016/S0021-9797(03)00062-6

Pankow JF, Cherry JA (1996) Dense Chlorinated Solvents and Other DNAPLs in Groundwater: History, Behavior, and Remediation. Waterloo Press.

Park KT, Klier K, Wang CB, Zhang WX (1997) Interaction of Tetrachloroethylene with Pd(100) Studied by High-Resolution X-ray Photoemission Spectroscopy. J Phys Chem B 101:5420–5428. https://doi.org/10.1021/jp9711398

Park S-W, Kim S-K, Kim J-B, et al (2006) Particle Surface Hydrophobicity and the Dechlorination of Chloro-Compounds by Iron Sulfides. Water, Air, Soil Pollut Focus 6:97–110. https://doi.org/10.1007/s11267-005-9016-z

Patterson E V., Cramer CJ, Truhlar DG (2001) Reductive Dechlorination of Hexachloroethane in the Environment: Mechanistic Studies via Computational Electrochemistry. J Am Chem Soc 123:2025–2031. https://doi.org/10.1021/ja0035349

Pennell KD, Cápiro NL, Walker DI (2014) Surfactant and Cosolvent Flushing. In: Kueper BH, Stroo HF, Vogel CM, Ward CH (eds) Chlorinated Solvent Source Zone Remediation. Springer, New York, NY, USA, pp 353-394.

Perlinger JA, Venkatapathy R, Harrison JF (2000) Linear Free Energy Relationships for Polyhalogenated Alkane Transformation by Electron-Transfer Mediators in Model Aqueous Systems. J Phys Chem A 104:2752–2763. https://doi.org/10.1021/jp993273t

Phenrat T, Cihan A, Kim H-J, et al (2010) Transport and Deposition of Polymer-Modified Fe0 Nanoparticles in 2-D Heterogeneous Porous Media: Effects of Particle Concentration, Fe0 Content, and Coatings. Environ Sci Technol 44:9086–9093. https://doi.org/10.1021/es102398e

Phenrat T, Liu Y, Tilton RD, Lowry G V (2009a) Adsorbed Polyelectrolyte Coatings Decrease Fe(0) Nanoparticle Reactivity with TCE in Water: Conceptual Model and Mechanisms. Environ Sci Technol 43:1507–14. https://doi.org/10.1021/es802187d

Phenrat T, Long TC, Lowry G V., Veronesi B (2009b) Partial Oxidation ("Aging") and Surface Modification Decrease the Toxicity of Nanosized Zerovalent Iron. Environ Sci Technol 43:195–200. https://doi.org/10.1021/es801955n

Phenrat T, Saleh N, Sirk K, et al (2007) Aggregation and Sedimentation of Aqueous Nanoscale Zerovalent Iron Dispersions. Environ Sci Technol 41:284–290. https://doi.org/10.1021/es061349a

Phenrat T, Saleh N, Sirk K, et al (2008) Stabilization of Aqueous Nanoscale Zerovalent Iron Dispersions by Anionic Polyelectrolytes: Adsorbed Anionic Polyelectrolyte Layer Properties and Their Effect on Aggregation and Sedimentation. J Nanoparticle Res 10:795–814. https://doi.org/10.1007/s11051-007-9315-6

Pilling MJ, Seakins PW (1995) Reaction Kinetics. Oxford University Press, New York, NY, USA.

Pizarro S, Araya M, Delgadillo A (2018) Hexachloroethane Reduction Catalyzed by Cobaloximes. Effect of the Substituents on the Equatorial Ligands. Polyhedron 141:94–99. https://doi.org/10.1016/j.poly.2017.11.005

Portois C, Essouayed E, Annable MD, et al (2018) Field Demonstration of Foam Injection to Confine a Chlorinated Solvent Source Zone. J Contam Hydrol 214:16–23

Pourbaix M (1974) Atlas of Electrochemical Equilibria in Aqueous Solutions, 2nd Edn. National Association of Corrosion Engineers, Houston, Texas, USA

Pullin H, Crane RA, Morgan DJ, Scott TB (2017a) The Effect of Common Groundwater Anions on the Aqueous Corrosion of Zero-Valent Iron Nanoparticles and Associated Removal of Aqueous Copper and Zinc. J Environ Chem Eng 5:1166–1173. https://doi.org/10.1016/j.jece.2017.01.038

Pullin H, Springell R, Parry S, Scott T (2017b) The Effect of Aqueous Corrosion on the Structure and Reactivity of Zero-Valent Iron Nanoparticles. Chem Eng J 308:568–577. https://doi.org/10.1016/j.cej.2016.09.088

Qin H, Guan X, Bandstra JZ, et al (2018a) Modeling the Kinetics of Hydrogen Formation by Zerovalent Iron: Effects of Sulfidation on Micro- and Nano-Scale Particles. Environ Sci Technol 52:13887–13896. https://doi.org/10.1021/acs.est.8b04436

Qin H, Sun Y, Yang H, et al (2018b) Unexpected Effect of Buffer Solution on Removal of Selenite and Selenate by Zerovalent Iron. Chem Eng J 334:296–304. https://doi.org/10.1016/j.cej.2017.10.025

Quinn J, Geiger C, Clausen C, et al (2005) Field Demonstration of DNAPL Dehalogenation Using Emulsified Zero-Valent Iron. Environ Sci Technol 39:1309–1318. https://doi.org/10.1021/es0490018

Rajajayavel SRC, Ghoshal S (2015) Enhanced Reductive Dechlorination of Trichloroethylene by Sulfidated Nanoscale Zerovalent Iron. Water Res 78:144–153. https://doi.org/10.1016/j.watres.2015.04.009

Rajan CSR (2011) Nanotechnology in Groundwater Remediation. Int J Environ Sci Dev 182–187. https://doi.org/10.7763/IJESD.2011.V2.121

Ranc B, Faure P, Croze V, Simonnot MO (2016) Selection of Oxidant Doses for In Situ Chemical Oxidation of Soils Contaminated by Polycyclic Aromatic Hydrocarbons (PAHs): A Review. J Hazard Mater 312:280–297. https://doi.org/10.1016/j.jhazmat.2016.03.068

Rayaroth MP, Lee C-S, Aravind UK, et al (2017) Oxidative Degradation of Benzoic Acid using Fe0- and Sulfidized Fe0-Activated Persulfate: A Comparative Study. Chem Eng J 315:426–436. https://doi.org/10.1016/j.cej.2017.01.031

Rebodos RL, Vikesland PJ (2010) Effects of Oxidation on the Magnetization of Nanoparticulate Magnetite. Langmuir 26:16745–16753. https://doi.org/10.1021/la102461z

Reijnders L (2006) Cleaner Nanotechnology and Hazard Reduction of Manufactured Nanoparticles. J Clean Prod 14:124–133. https://doi.org/10.1016/j.jclepro.2005.03.018

Reinsch BC, Forsberg B, Penn RL, et al (2010) Chemical Transformations during Aging of Zerovalent Iron Nanoparticles in the Presence of Common Groundwater Dissolved Constituents. Environ Sci Technol 44:3455–3461. https://doi.org/10.1021/es902924h

Rémazeilles C, Refait P (2007) On the formation of β-FeOOH (Akaganéite) in chloride-containing environments. Corros Sci 49:844–857. https://doi.org/10.1016/j.corsci.2006.06.003

Ribas D, Černík M, Benito JA, et al (2017) Activation Process of Air Stable Nanoscale Zero-Valent Iron Particles. Chem Eng J 320:290–299. https://doi.org/10.1016/j.cej.2017.03.056

Roberts AL, Gschwend PM (1991) Mechanism of Pentachloroethane Dehydrochlorination to

Tetrachloroethylene. Environ Sci Technol 25:76–86. https://doi.org/10.1021/es00013a006

Roberts AL, Sanborn PN, Gschwend PM (1992) Nucleophilic Substitution Reactions of Dihalomethanes with Hydrogen Sulfide Species. Environ Sci Technol 26:2263–2274. https://doi.org/10.1021/es00035a027

Roberts AL, Totten LA, Arnold WA, et al (1996) Reductive Elimination of Chlorinated Ethylenes by Zero-Valent Metals. Environ Sci Technol 30:2654–2659. https://doi.org/10.1021/es9509644

Roberts P V., Goltz MN, Mackay DM (1986) A Natural Gradient Experiment on Solute Transport in a Sand Aquifer: 3. Retardation Estimates and Mass Balances for Organic Solutes. Water Resour Res 22:2047–2058. https://doi.org/10.1029/WR022i013p02047

Roden EE, Zachara JM (1996) Microbial Reduction of Crystalline Iron(III) Oxides: Influence of Oxide Surface Area and Potential for Cell Growth. Environ Sci Technol 30:1618–1628. https://doi.org/10.1021/es9506216

Rodrigues R, Betelu S, Colombano S, et al (2017a) Reductive Dechlorination of Hexachlorobutadiene by a Pd/Fe Microparticle Suspension in Dissolved Lactic Acid Polymers: Degradation Mechanism and Kinetics. Ind Eng Chem Res 56:12092–12100. https://doi.org/10.1021/acs.iecr.7b03012

Rodrigues R, Betelu S, Colombano S, et al (2019) Elucidating the Dechlorination Mechanism of Hexachloroethane by Pd-Doped Zerovalent Iron Microparticles in Dissolved Lactic Acid Polymers Using Chromatography and Indirect Monitoring of Iron Corrosion. Environ Sci Pollut Res 26:7177–7194. https://doi.org/10.1007/s11356-019-04128-y

Rodrigues R, Betelu S, Colombano S, et al (2017b) Influence of Temperature and Surfactants on the Solubilization of Hexachlorobutadiene and Hexachloroethane. J Chem Eng Data 62:3252–3260. https://doi.org/10.1021/acs.jced.7b00320

Rosen MJ, Kunjappu JT (2012) Surfactants and Interfacial Phenomena, Fourth Edition. Wiley-Blackwell, Hoboken, NJ, USA

Ruder AM (2006) Potential Health Effects of Occupational Chlorinated Solvent Exposure. Ann N Y Acad Sci 1076:207–27. https://doi.org/10.1196/annals.1371.050

Rushing JC, McNeill LS, Edwards M (2003) Some Effects of Aqueous Silica on the Corrosion of Iron. Water Res 37:1080–1090. https://doi.org/10.1016/S0043-1354(02)00136-7

Rybnikova V, Usman M, Hanna K (2016) Removal of PCBs in Contaminated Soils by Means of Chemical Reduction and Advanced Oxidation Processes. Environ Sci Pollut Res 23:17035–17048. https://doi.org/10.1007/s11356-016-6881-0

Saif S, Tahir A, Chen Y (2016) Green Synthesis of Iron Nanoparticles and Their Environmental Applications and Implications. Nanomaterials 6:209. https://doi.org/10.3390/nano6110209

Saleh N, Kim H-J, Phenrat T, et al (2008) Ionic Strength and Composition Affect the Mobility of Surface-Modified Fe0 Nanoparticles in Water-Saturated Sand Columns. Environ Sci Technol 42:3349–3355. https://doi.org/10.1021/es071936b

Saleh N, Sirk K, Liu Y, et al (2007) Surface Modifications Enhance Nanoiron Transport and NAPL Targeting in Saturated Porous Media. Environ Eng Sci 24:45–57. https://doi.org/10.1089/ees.2007.24.45

San Román I, Galdames A, Alonso ML, et al (2016) Effect of Coating on the Environmental Applications of Zero Valent Iron Nanoparticles: The Lindane Case. Sci Total Environ 565:795–803. https://doi.org/10.1016/j.scitotenv.2016.04.034

Sarathy V, Salter AJ, Nurmi JT, et al (2010) Degradation of 1,2,3-Trichloropropane (TCP): Hydrolysis, Elimination, and Reduction by Iron and Zinc. Environ Sci Technol 44:787–793. https://doi.org/10.1021/es902595j

Sarathy V, Tratnyek PG, Nurmi JT, et al (2008) Aging of Iron Nanoparticles in Aqueous Solution: Effects on Structure and Reactivity. J Phys Chem C 112:2286–2293. https://doi.org/10.1021/jp0777418

Scherer M, Cwiertny D, Deeb R, et al (2014) Biologically Mediated Abiotic Degradation of Chlorinated Ethenes: A New Conceptual Framework. Strategic Environmental Research and Development Program ER01-026

Scherer MM, Balko BA, Gallagher DA, Tratnyek PG (1998) Correlation Analysis of Rate Constants for Dechlorination by Zero-Valent Iron. Environ Sci Technol 32:3026–3033. https://doi.org/10.1021/es9802551

Scherer MM, Balko BA, Tratnyek PG (1999) The Role of Oxides in Reduction Reactions at the Metal-Water Interface. In: Mineral-Water Interfacial Reactions: Kinetics and Mechanisms, American C. Washington D.C., pp 301-322.

Schlicker O, Ebert M, Fruth M, et al (2000) Degradation of TCE with Iron: The Role of Competing Chromate and Nitrate Reduction. Ground Water 38:403–409. https://doi.org/10.1111/j.1745-6584.2000.tb00226.x

Schöftner P, Waldner G, Lottermoser W, et al (2015) Electron Efficiency of nZVI does not Change with Variation of Environmental Parameters. Sci Total Environ 535:69–78. https://doi.org/10.1016/j.scitotenv.2015.05.033

Schreier CG, Reinhard M (1995) Catalytic Hydrodehalogenation of Chlorinated Ethylenes using Palladium and Hydrogen for the Treatment of Contaminated Water. Chemosphere 31:3475–3487. https://doi.org/10.1016/0045-6535(95)00200-R

Schrick B, Blough JL, Jones AD, Mallouk TE (2002) Hydrodechlorination of Trichloroethylene to Hydrocarbons Using Bimetallic Nickel-Iron Nanoparticles. Chem Mater 14:5140–5147. https://doi.org/10.1021/cm020737i

Schrick B, Hydutsky BW, Blough JL, Mallouk TE (2004) Delivery Vehicles for Zerovalent Metal Nanoparticles in Soil and Groundwater. Chem Mater 16:2187–2193. https://doi.org/10.1021/cm0218108

Schwartz FW, Zhang H (2003) Fundamentals of Ground Water. John Wiley & Sons, Hoboken, NJ, USA.

Schwarzenbach RP, Gschwend PM, Imboden DM (2003) Environmental Organic Chemistry. John Wiley & Sons, Inc., Hoboken, NJ, USA

Schwarzenbach RP, Westall J (1981) Transport of Nonpolar Organic Compounds from Surface Water to Groundwater. Laboratory Sorption Studies. Environ Sci Technol 15:1360–1367. https://doi.org/10.1021/es00093a009

Scott TB, Dickinson M, Crane RA, et al (2010) The Effects of Vacuum Annealing on the Structure and Surface Chemistry of Iron Nanoparticles. J Nanoparticle Res 12:1765–1775. https://doi.org/10.1007/s11051-009-9732-9

Semerád J, Cajthaml T (2016) Ecotoxicity and Environmental Safety Related to Nano-Scale Zerovalent Iron Remediation Applications. Appl Microbiol Biotechnol 100:9809–9819. https://doi.org/10.1007/s00253-016-7901-1

Shao H, Butler EC (2007) The Influence of Iron and Sulfur Mineral Fractions on Carbon Tetrachloride Transformation in Model Anaerobic Soils and Sediments. Chemosphere 68:1807–1813. https://doi.org/10.1016/j.chemosphere.2007.04.048

Shao Q, Xu C, Wang Y, et al (2018) Dynamic Interactions Between Sulfidated Zerovalent Iron and Dissolved Oxygen: Mechanistic Insights for Enhanced Chromate Removal. Water Res 135:322–330. https://doi.org/10.1016/j.watres.2018.02.030

Sharma G, Kumar D, Kumar A, et al (2016) Revolution from Monometallic to Trimetallic Nanoparticle Composites, Various Synthesis Methods and their Applications: A Review. Mater Sci Eng C. https://doi.org/10.1016/j.msec.2016.11.002

Shen X, Zhao L, Ding Y, et al (2011) Foam, a Promising Vehicle to Deliver Nanoparticles for Vadose Zone Remediation. J Hazard Mater 186:1773–80. https://doi.org/10.1016/j.jhazmat.2010.12.071

Sherry D (2015) CTC Production and Consumption. SPARC Workshop on "Solving the Mystery of Carbon Tetrachloride". 4-6 October 2015 Zurich, Switzerland

Shi Z, Fan D, Johnson RL, et al (2015) Methods for Characterizing the Fate and Effects of Nano Zerovalent Iron During Groundwater Remediation. J Contam Hydrol 181:17–35. https://doi.org/10.1016/j.jconhyd.2015.03.004

Shi Z, Nurmi JT, Tratnyek PG (2011) Effects of Nano Zero-Valent Iron on Oxidation−Reduction Potential. Environ Sci Technol 45:1586–1592. https://doi.org/10.1021/es103185t

Shih Y, Chen M-Y, Su Y-F (2011a) Pentachlorophenol Reduction by Pd/Fe Bimetallic Nanoparticles: Effects of Copper, Nickel, and Ferric Cations. Appl Catal B Environ 105:24–29. https://doi.org/10.1016/j.apcatb.2011.03.024

Shih Y, Chen M, Su Y, Tso C (2016) Concurrent Oxidation and Reduction of Pentachlorophenol by Bimetallic Zerovalent Pd/Fe Nanoparticles in an Oxic Water. J Hazard Mater 301:416–423. https://doi.org/10.1016/j.jhazmat.2015.08.059

Shih Y, Chen Y-C, Chen M, et al (2009) Dechlorination of Hexachlorobenzene by using Nanoscale Fe and Nanoscale Pd/Fe Bimetallic Particles. Colloids Surfaces A Physicochem Eng Asp 332:84–89. https://doi.org/10.1016/j.colsurfa.2008.09.031

Shih Y, Hsu C, Su Y (2011b) Reduction of Hexachlorobenzene by Nanoscale Zero-Valent Iron: Kinetics, pH Effect, and Degradation Mechanism. Sep Purif Technol 76:268–274. https://doi.org/10.1016/j.seppur.2010.10.015

Shin M-C, Choi H-D, Kim D-H, Baek K (2008) Effect of Surfactant on Reductive Dechlorination of Trichloroethylene by Zero-Valent Iron. Desalination 223:299–307. https://doi.org/10.1016/j.desal.2007.01.223

Silvester E, Charlet L, Tournassat C, et al (2005) Redox Potential Measurements and Mössbauer Spectrometry of FeII Adsorbed onto FeIII (Oxyhydr)oxides. Geochim Cosmochim Acta 69:4801–4815. https://doi.org/10.1016/j.gca.2005.06.013

Sirk KM, Saleh NB, Phenrat T, et al (2009) Effect of Adsorbed Polyelectrolytes on Nanoscale Zero Valent Iron Particle Attachment to Soil Surface Models. Environ Sci Technol 43:3803–3808. https://doi.org/10.1021/es803589t

Sleep BE, Ma Y (1997) Thermal Variation of Organic Fluid Properties and Impact on Thermal Remediation Feasibility. Soil Sediment Contam 6:281–306. https://doi.org/10.1080/15320389709383566

Smuleac V, Varma R, Sikdar S, Bhattacharyya D (2011) Green Synthesis of Fe and Fe/Pd Bimetallic

Nanoparticles in Membranes for Reductive Degradation of Chlorinated Organics. J Memb Sci 379:131–137. https://doi.org/10.1016/j.memsci.2011.05.054

Song H, Carraway ER (2005) Reduction of Chlorinated Ethanes by Nanosized Zero-Valent Iron: Kinetics, Pathways, and Effects of Reaction Conditions. Environ Sci Technol 39:6237–6245. https://doi.org/10.1021/es048262e

Song H, Carraway ER (2006) Reduction of Chlorinated Methanes by Nano-Sized Zero-Valent Iron. Kinetics, Pathways, and Effect of Reaction Conditions. Environ Eng Sci 23:272–284. https://doi.org/10.1089/ees.2006.23.272

Song S, Su Y, Adeleye AS, Zhang Y (2017) Optimal Design and Characterization of Sulfide-Modified Nanoscale Zerovalent Iron for Diclofenac Removal. Appl Catal B Environ 201:211–220. https://doi.org/10.1016/j.apcatb.2016.07.055

Soukupova J, Zboril R, Medrik I, et al (2015) Highly Concentrated, Reactive and Stable Dispersion of Zero-Valent Iron Nanoparticles: Direct Surface Modification and Site Application. Chem Eng J 262:813–822. https://doi.org/10.1016/J.CEJ.2014.10.024

Srirattana S, Piaowan K, Lowry G V., Phenrat T (2017) Electromagnetic Induction of Foam-Based Nanoscale Zerovalent Iron (NZVI) Particles to Thermally Enhance Non-Aqueous Phase Liquid (NAPL) volatilization in Unsaturated Porous Media: Proof of Concept. Chemosphere 183:323–331. https://doi.org/10.1016/j.chemosphere.2017.05.114

Sriwatanapongse W, Reinhard M, Klug CA (2006) Reductive Hydrodechlorination of Trichloroethylene by Palladium-on-Alumina Catalyst: 13C Solid-State NMR Study of Surface Reaction Precursors. Langmuir 22:4158–4164. https://doi.org/10.1021/la053087g

Stefaniuk M, Oleszczuk P, Ok YS (2016) Review on Nano Zerovalent Iron (nZVI): From Synthesis to Environmental Applications. Chem Eng J 287:618–632. https://doi.org/10.1016/j.cej.2015.11.046

Stephenson RM (1992) Mutual Solubilities: Water-Ketones, Water-Ethers, and Water-Gasoline-Alcohols. J Chem Eng Data 37:80–95. https://doi.org/10.1021/je00005a024

Stewart SM, Hofstetter TB, Joshi P, Gorski CA (2018) Linking Thermodynamics to Pollutant Reduction Kinetics by Fe2+ Bound to Iron Oxides. Environ Sci Technol 52:5600–5609. https://doi.org/10.1021/acs.est.8b00481

Stroo HF, West MR, Kueper BH, et al (2014) In Situ Bioremediation of Chlorinated Ethene Source Zones. In: Chlorinated Solvent Source Zone Remediation. Springer New York, New York, NY, pp 395–457

Stumm W, Sigg L, Sulzberger B (1992) Chemistry of the Solid-Water Interface: Processes at the Mineral-Water and Particle-Water Interface in Natural Systems. Wiley

Su C, Puls RW (1999) Kinetics of Trichloroethene Reduction by Zerovalent Iron and Tin: Pretreatment Effect, Apparent Activation Energy, and Intermediate Products. Environ Sci Technol 33:163–168. https://doi.org/10.1021/es980481a

Su J, Lin S, Chen Z, et al (2011) Dechlorination of p-chlorophenol from Aqueous Solution using Bentonite Supported Fe/Pd Nanoparticles: Synthesis, Characterization and Kinetics. Desalination 280:167–173. https://doi.org/10.1016/j.desal.2011.06.067

Su Y, Adeleye AS, Keller AA, et al (2015) Magnetic Sulfide-Modified Nanoscale Zerovalent Iron (S-nZVI) for Dissolved Metal Ion Removal. Water Res 74:47–57. https://doi.org/10.1016/j.watres.2015.02.004

Su Y, Hsu C-Y, Shih Y (2012) Effects of Various Ions on the Dechlorination Kinetics of Hexachlorobenzene by Nanoscale Zero-Valent Iron. Chemosphere 88:1346–1352. https://doi.org/10.1016/j.chemosphere.2012.05.036

Su Y, Jassby D, Song S, et al (2018) Enhanced Oxidative and Adsorptive Removal of Diclofenac in Heterogeneous Fenton-like Reaction with Sulfide Modified Nanoscale Zerovalent Iron. Environ Sci Technol 52:6466–6475. https://doi.org/10.1021/acs.est.8b00231

Su Y, Zhang Y, Ke H, et al (2017) Environmental Remediation of Chlorinated Hydrocarbons Using Biopolymer Stabilized Iron Loaded Halloysite Nanotubes. ACS Sustain Chem Eng 5:10976–10985. https://doi.org/10.1021/acssuschemeng.7b02872

Suchomel EJ, Kavanaugh MC, Mercer JW, Johnson PC (2014) The Source Zone Remediation Challenge. In: Chlorinated Solvent Source Zone Remediation. Springer New York, New York, NY, pp 29–62

Sun X, Yan Y, Wang M, Han Z (2017) Effect of Nanoscale Zero-Valent Iron Confined in Mesostructure on Escherichia coli. Environ Sci Pollut Res 24:24038–24045. https://doi.org/10.1007/s11356-017-0101-4

Sun Y-P, Li X, Cao J, et al (2006) Characterization of Zero-Valent Iron Nanoparticles. Adv Colloid Interface Sci 120:47–56. https://doi.org/10.1016/j.cis.2006.03.001

Sun Y, Li J, Huang T, Guan X (2016) The Influences of Iron Characteristics, Operating Conditions and Solution Chemistry on Contaminants Removal by Zero-Valent Iron: A Review. Water Res 100:277–295. https://doi.org/10.1016/j.watres.2016.05.031

Suthersan SS (2002) Natural and Enhanced Remediation Systems. CRC Press, Boca Raton, Florida

Sweeny KH (1980) Treatment of Reducible Halohydrocarbon Containing Aqueous Stream

Szecsody J, Williams M, Fruchter J, et al (2000) Influence of Sediment Reduction on TCE degradation, Remediation of Chlorinated and Recalcitrant Compounds. In: Chemical Oxidation and Reactive Barriers: Remediation of Chlorinated and Recalcitrant Compounds. Battelle P, pp 369-376.

Tang F, Xin J, Zheng T, et al (2017a) Individual and Combined Effects of Humic Acid, Bicarbonate and Calcium on TCE Removal Kinetics, Aging Behavior and Electron Efficiency of mZVI Particles. Chem Eng J 324:324–335. https://doi.org/10.1016/j.cej.2017.04.144

Tang F, Xin J, Zheng X, et al (2017b) Effect of Solution pH on Aging Dynamics and Surface Structural Evolution of mZVI Particles: H2 Production and Spectroscopic/Microscopic Evidence. Environ Sci Pollut Res 1–11. https://doi.org/10.1007/s11356-017-9976-3

Taylor SR (1964) Abundance of chemical elements in the continental crust: A new table. Geochim Cosmochim Acta 28:1273–1285. https://doi.org/10.1016/0016-7037(64)90129-2

Tee Y-H, Grulke E, Bhattacharyya D (2005) Role of Ni/Fe Nanoparticle Composition on the Degradation of Trichloroethylene from Water. Ind Eng Chem Res 44:7062–7070. https://doi.org/10.1021/ie050086a

Tiraferri A, Chen KL, Sethi R, Elimelech M (2008) Reduced Aggregation and Sedimentation of Zero-Valent Iron Nanoparticles in the Presence of Guar Gum. J Colloid Interface Sci 324:71–79. https://doi.org/10.1016/j.jcis.2008.04.064

Tosco T, Gastone F, Sethi R (2014a) Guar Gum Solutions for Improved Delivery of Iron Particles in Porous Media (Part 2): Iron Transport Tests and Modeling in Radial Geometry. J Contam Hydrol 166:34–51. https://doi.org/10.1016/j.jconhyd.2014.06.014

Tosco T, Papini MP, Cruz Viggi C, Sethi R (2014b) Nanoscale Zerovalent Iron Particles for Groundwater Remediation: A Review. J Clean Prod 77:10–21. https://doi.org/10.1016/j.jclepro.2013.12.026

Tosco T, Sethi R (2010) Transport of Non-Newtonian Suspensions of Highly Concentrated Micro- and Nanoscale Iron Particles in Porous Media: A Modeling Approach. Environ Sci Technol 44:9062–9068. https://doi.org/10.1021/es100868n

Touomo-Wouafo M, Dazie JD, Btatkeu-K BD, et al (2018) Role of Pre-Corrosion of Fe0 on its Efficiency in Remediation Systems: An Electrochemical Study. Chemosphere 209:617–622. https://doi.org/10.1016/j.chemosphere.2018.06.080

Tratnyek PG, Johnson RL (2006) Nanotechnologies for Environmental Cleanup. Nano Today 1:44–48. https://doi.org/10.1016/S1748-0132(06)70048-2

Tratnyek PG, Johnson RL, Lowry G V., Brown RA (2014) In Situ Chemical Reduction for Source Remediation. In: Kueper BH, Stroo HF, Vogel CM, Ward CH (eds) Chlorinated Solvent Source Zone Remediation. Springer New York, New York, NY, pp 307-351.

Tratnyek PG, Macalady DL (2000) Oxidation-Reduction Reactions in the Aquatic Environment. In: Boethling RS., Mackay D (eds) Handbook of Property Estimation Methods for Chemicals: Environmental Health Sciences. CRC Press, Boca Raton, FL, pp 383-415.

Tratnyek PG, Salter AJ, Nurmi JT, Sarathy V (2010) Environmental Applications of Zerovalent Metals: Iron vs. Zinc. In: Nanoscale Materials in Chemistry: Environmental Applications. pp 165–178

Tratnyek PG, Scherer MM, Deng B, Hu S (2001) Effects of Natural Organic Matter, Anthropogenic Surfactants, and Model Quinones on the Reduction of Contaminants by Zero-Valent Iron. Water Res 35:4435–4443. https://doi.org/10.1016/S0043-1354(01)00165-8

Tratnyek PG, Weber EJ, Schwarzenbach RP (2003) Quantitative Structure - Activity Relationships for Chemical Reductions of Organic Contaminants. Environ Toxicol Chem 22:1733. https://doi.org/10.1897/01-236

Travis C, Doty C (1990) ES&T Views: Can Contaminated Aquifers at Superfund Sites be Remediated? Environ Sci Technol 24:1464–1466. https://doi.org/10.1021/es00080a600

Tsakiroglou CD, Sikinioti-Lock A, Terzi K, Theodoropoulou M (2018) A Numerical Model to Simulate the NAPL Source Zone Remediation by Injecting Zero-Valent Iron Nanoparticles. Chem Eng Sci 192:391–413. https://doi.org/10.1016/j.ces.2018.07.037

Uegami M, Kawano J, Okita T, et al (2002) Iron Particles for Purifying Contaminated Soil or Ground Water, Process for Producing the Iron Particles, Purifying Agent Comprising the Iron Particles, Process for Producing the Purifying Agent and Method of Purifying Contaminated Soil or Ground Water

Usman M, Byrne JM, Chaudhary A, et al (2018) Magnetite and Green Rust: Synthesis, Properties, and Environmental Applications of Mixed-Valent Iron Minerals. Chem Rev 118:3251–3304. https://doi.org/10.1021/acs.chemrev.7b00224

Velimirovic M, Auffan M, Carniato L, et al (2018) Effect of Field Site Hydrogeochemical Conditions on the Corrosion of Milled Zerovalent Iron Particles and their Dechlorination Efficiency. Sci Total Environ 618:1619–1627. https://doi.org/10.1016/j.scitotenv.2017.10.002

Velimirovic M, Carniato L, Simons Q, et al (2014) Corrosion Rate Estimations of Microscale Zerovalent Iron Particles via Direct Hydrogen Production Measurements. J Hazard Mater 270:18–26. https://doi.org/10.1016/j.jhazmat.2014.01.034

Velimirovic M, Chen H, Simons Q, Bastiaens L (2012) Reactivity Recovery of Guar Gum Coupled mZVI by Means of Enzymatic Breakdown and Rinsing. J Contam Hydrol 142–143:1–10. https://doi.org/10.1016/j.jconhyd.2012.09.003

Velimirovic M, Larsson P-O, Simons Q, Bastiaens L (2013a) Impact of Carbon, Oxygen and Sulfur Content of Microscale Zerovalent Iron Particles on its Reactivity towards Chlorinated Aliphatic Hydrocarbons. Chemosphere 93:2040–2045. https://doi.org/10.1016/j.chemosphere.2013.07.034

Velimirovic M, Larsson P-O, Simons Q, Bastiaens L (2017) Effect of Boron on Reactivity and Apparent Corrosion Rate of Microscale Zerovalent Irons. J Environ Chem Eng 5:1892–1898. https://doi.org/10.1016/j.jece.2017.03.029

Velimirovic M, Larsson P-O, Simons Q, Bastiaens L (2013b) Reactivity Screening of Microscale Zerovalent Irons and Iron Sulfides towards Different CAHs under Standardized Experimental Conditions. J Hazard Mater 252–253:204–212. https://doi.org/10.1016/j.jhazmat.2013.02.047

Velimirovic M, Schmid D, Wagner S, et al (2016) Agar Agar-Stabilized Milled Zerovalent Iron Particles for In Situ Groundwater Remediation. Sci Total Environ 563–564:713–723. https://doi.org/10.1016/j.scitotenv.2015.11.007

Velimirovic M, Simons Q, Bastiaens L (2015) Use of CAH-Degrading Bacteria as Test-Organisms for Evaluating the Impact of Fine Zerovalent Iron Particles on the Anaerobic Subsurface Environment. Chemosphere 134:338–345. https://doi.org/10.1016/j.chemosphere.2015.04.068

Verce MF, Ulrich RL, Freedman DL (2000) Characterization of an Isolate that uses Vinyl Chloride as a Growth Substrate under Aerobic Conditions. Appl Environ Microbiol 66:3535–42

Verce MF, Ulrich RL, Freedman DL (2001) Transition from Cometabolic to Growth-Linked Biodegradation of Vinyl Chloride by a Pseudomonas sp. Isolated on Ethene. Environ Sci Technol 35:4242–4251. https://doi.org/10.1021/es002064F

Vermeul VR, Szecsody JE, Williams MD, et al (2000) In Situ Redox Manipulation Proof-of-Principle Test at the Fort Lewis Logistics Center: Final Report. PNNL-13357 Final Report, Pacific Northwest National Laboratory. Richland, WA, USA

Verschueren K (1983) Handbook of Environmental Data on Organic Chemicals, 2nd ed. Van Nostrand Reinhold, New York, NY, USA

Vogel M, Nijenhuis I, Lloyd J, et al (2018) Combined Chemical and Microbiological Degradation of Tetrachloroethene during the Application of Carbo-Iron at a Contaminated Field Site. Sci Total Environ 628–629:1027–1036. https://doi.org/10.1016/j.scitotenv.2018.01.310

Vogel TM, Criddle CS, McCarty PL (1987) Transformations of Halogenated Aliphatic Compounds. Environ Sci Technol 21:722–736. https://doi.org/10.1021/es00162a001

Vogel TM, McCarty PL (1985) Biotransformation of Tetrachloroethylene to Trichloroethylene, Dichloroethylene, Vinyl Chloride, and Carbon Dioxide under Methanogenic Conditions. Appl Environ Microbiol 49:1080–1083

Wagner S, Gondikas A, Neubauer E, et al (2014) Spot the Difference: Engineered and Natural Nanoparticles in the Environment-Release, Behavior, and Fate. Angew Chemie Int Ed 53:n/a-n/a. https://doi.org/10.1002/anie.201405050

Wang C-B, Zhang W (1997) Synthesizing Nanoscale Iron Particles for Rapid and Complete Dechlorination of TCE and PCBs. Environ Sci Technol 31:2154–2156. https://doi.org/10.1021/es970039c

Wang C, Baer DR, Amonette JE, et al (2009a) Morphology and Electronic Structure of the Oxide

Shell on the Surface of Iron Nanoparticles. J Am Chem Soc 131:8824–8832. https://doi.org/10.1021/ja900353f

Wang J, Farrell J (2003) Investigating the Role of Atomic Hydrogen on Chloroethene Reactions with Iron Using Tafel Analysis and Electrochemical Impedance Spectroscopy. Environ Sci Technol 37:3891–3896. https://doi.org/10.1021/es0264605

Wang S, Chen S, Wang Y, et al (2016) Integration of Organohalide-Respiring Bacteria and Nanoscale Zero-Valent Iron (Bio-nZVI-RD): A Perfect Marriage for the Remediation of Organohalide Pollutants? Biotechnol Adv 34:1384–1395. https://doi.org/10.1016/j.biotechadv.2016.10.004

Wang S, Mulligan CN (2004) An Evaluation of Surfactant Foam Technology in Remediation of Contaminated Soil. Chemosphere 57:1079–1089. https://doi.org/10.1016/j.chemosphere.2004.08.019

Wang X, Chen C, Chang Y, Liu H (2009b) Dechlorination of Chlorinated Methanes by Pd/Fe Bimetallic Nanoparticles. J Hazard Mater 161:815–823. https://doi.org/10.1016/j.jhazmat.2008.04.027

Wang X, Cong S, Wang P, et al (2017) Novel Green Micelles Pluronic F-127 Coating Performance on Nano Zero-Valent Iron: Enhanced Reactivity and Innovative Kinetics. Sep Purif Technol 174:174–182. https://doi.org/10.1016/j.seppur.2016.09.009

Wang X, Le L, Alvarez PJJ, et al (2015) Synthesis and Characterization of Green Agents Coated Pd/Fe Bimetallic Nanoparticles. J Taiwan Inst Chem Eng 50:297–305. https://doi.org/10.1016/j.jtice.2014.12.030

Wang X, Zhu M, Liu H, et al (2013) Modification of Pd–Fe Nanoparticles for Catalytic Dechlorination of 2,4-dichlorophenol. Sci Total Environ 449:157–167. https://doi.org/10.1016/j.scitotenv.2013.01.008

Wang Z, Peng P, Huang W (2009c) Dechlorination of γ-Hexachlorocyclohexane by Zero-Valent Metallic Iron. J Hazard Mater 166:992–997. https://doi.org/10.1016/j.jhazmat.2008.11.106

Warren KD, Arnold RG, Bishop TL, et al (1995) Kinetics and Mechanism of Reductive Dehalogenation of Carbon Tetrachloride using Zero-Valence Metals. J Hazard Mater 41:217–227. https://doi.org/10.1016/0304-3894(94)00117-Y

Watanabe K, Manefield M, Lee M, Kouzuma A (2009) Electron Shuttles in Biotechnology. Curr Opin Biotechnol 20:633–641. https://doi.org/10.1016/j.copbio.2009.09.006

Weber EJ (1996) Iron-Mediated Reductive Transformations: Investigation of Reaction Mechanism. Environ Sci Technol 30:716–719. https://doi.org/10.1021/es9505210

Weerasooriya R, Dharmasena B (2001) Pyrite-Assisted Degradation of Trichloroethene (TCE). Chemosphere 42:389–396. https://doi.org/10.1016/S0045-6535(00)00160-0

Wei Y-T, Wu S-C, Chou C-M, et al (2010) Influence of Nanoscale Zero-Valent Iron on Geochemical Properties of Groundwater and Vinyl Chloride Degradation: A Field Case Study. Water Res 44:131–140. https://doi.org/10.1016/j.watres.2009.09.012

Weng X, Guo M, Luo F, Chen Z (2017) One-Step Green Synthesis of Bimetallic Fe/Ni Nanoparticles by Eucalyptus Leaf Extract: Biomolecules Identification, Characterization and Catalytic Activity. Chem Eng J 308:904–911. https://doi.org/10.1016/j.cej.2016.09.134

Wiedemeier TH, Rifai HS, Newell CJ, Wilson JT (1999) Natural Attenuation of Fuels and Chlorinated Solvents in the Subsurface. John Wiley & Sons

Wiedemeier TH, Swanson MA, Moutoux DE, et al (1998) Technical Protocol for Evaluating Natural Attenuation of Chlorinated Solvents in Ground Water. United States Environmental Protection Agency, Office of Research and Development. Washington D.C.

Wiesner MR, Bottero J-Y (2007) Environmental Nanotechnology: Applications and Impacts of Nanomaterials. McGraw-Hill., New York, NY, USA

Wiesner MR, Lowry G V., Alvarez P, et al (2006) Assessing the Risks of Manufactured Nanomaterials. Environ Sci Technol 40:4336–4345. https://doi.org/10.1021/es062726m

Wilhelm S (1988) Galvanic Corrosion Caused by Corrosion Products. In: H. P. Hack (ed) Galvanic Corrosion. American Society for Testing and Materials, Philadelphia, PA, USA, pp 23–34

Wilkin RT, Puls RW, Sewell GW (2003) Long-Term Performance of Permeable Reactive Barriers Using Zero-Valent Iron: Geochemical and Microbiological Effects. Ground Water 41:493–503. https://doi.org/10.1111/j.1745-6584.2003.tb02383.x

Williams AGB, Gregory KB, Parkin GF, Scherer MM (2005) Hexahydro-1,3,5-trinitro-1,3,5-triazine Transformation by Biologically Reduced Ferrihydrite: Evolution of Fe Mineralogy, Surface Area, and Reaction Rates. Environ Sci Technol 39:5183–5189. https://doi.org/10.1021/es0490525

Wu Y, Wang Y, Huang X, et al (2018) Surfactant-Facilitated Dechlorination of 2,2′,5,5′-Tetrachlorinated Biphenyl using Zero-Valent Iron in Soil/Sediment Solution: Integrated Effects of Plausible Factors. Chemosphere 212:845–852. https://doi.org/10.1016/j.chemosphere.2018.08.113

Wu Y, Wang Y, Huang X, et al (2017) Zerovalent Iron in Conjunction with Surfactants to Remediate Sediments Contaminated by Polychlorinated Biphenyls and Nickel. Chemosphere 189:479–488. https://doi.org/10.1016/j.chemosphere.2017.09.038

Wu Y, Wu Z, Huang X, et al (2015) Synergistical Enhancement by Ni2+ and Tween-80 of Nanoscale Zerovalent Iron Dechlorination of 2,2',5,5'-Tetrachlorinated Biphenyl in Aqueous Solution. Environ Sci Pollut Res 22:555–564. https://doi.org/10.1007/s11356-014-3278-9

Xie P, Guo Y, Chen Y, et al (2017a) Application of a Novel Advanced Oxidation Process using Sulfite and Zero-Valent Iron in Treatment of Organic Pollutants. Chem Eng J 314:240–248. https://doi.org/10.1016/j.cej.2016.12.094

Xie Y, Cwiertny DM (2013) Chlorinated Solvent Transformation by Palladized Zerovalent Iron: Mechanistic Insights from Reductant Loading Studies and Solvent Kinetic Isotope Effects. Environ Sci Technol 47:7940–7948. https://doi.org/10.1021/es401481a

Xie Y, Cwiertny DM (2010) Use of Dithionite to Extend the Reactive Lifetime of Nanoscale Zero-Valent Iron Treatment Systems. Environ Sci Technol 44:8649–8655. https://doi.org/10.1021/es102451t

Xie Y, Dong H, Zeng G, et al (2017b) The Interactions Between Nanoscale Zero-Valent Iron and Microbes in the Subsurface Environment: A Review. J Hazard Mater 321:390–407. https://doi.org/10.1016/j.jhazmat.2016.09.028

Xiong Z, Lai B, Yang P (2018) Enhancing the Efficiency of Zero Valent Iron by Electrolysis: Performance and Reaction Mechanism. Chemosphere 194:189–199. https://doi.org/10.1016/j.chemosphere.2017.11.167

Xu J, Avellan A, Li H, et al (2020) Sulfur Loading and Speciation Control the Hydrophobicity, Electron Transfer, Reactivity, and Selectivity of Sulfidized Nanoscale Zerovalent Iron. Adv Mater 1906910. https://doi.org/10.1002/adma.201906910

Xu J, Bhattacharyya D (2006) Fe/Pd Nanoparticle Immobilization in Microfiltration Membrane Pores: Synthesis, Characterization, and Application in the Dechlorination of Polychlorinated Biphenyls. Ind Eng Chem Res 46:2348–2359. https://doi.org/10.1021/ie0611498

Xu J, Cao Z, Zhou H, et al (2019a) Sulfur Dose and Sulfidation Time Affect Reactivity and Selectivity of Post-Sulfidized Nanoscale Zerovalent Iron. Environ Sci Technol acs.est.9b04210. https://doi.org/10.1021/acs.est.9b04210

Xu J, Sheng T, Hu Y, et al (2013) Adsorption–Dechlorination of 2,4-Dichlorophenol using Two Specified MWCNTs-Stabilized Pd/Fe Nanocomposites. Chem Eng J 219:162–173. https://doi.org/10.1016/j.cej.2013.01.010

Xu J, Wang Y, Weng C, et al (2019b) Reactivity, Selectivity, and Long-term Performance of Sulfidized Nanoscale Zerovalent Iron with Different Properties. Environ Sci Technol acs.est.9b00511. https://doi.org/10.1021/acs.est.9b00511

Xu Y, Wang C, Hou J, et al (2017) Application of Zero Valent Iron Coupling with Biological Process for Wastewater Treatment: A Review. Rev Environ Sci Bio/Technology 1–27. https://doi.org/10.1007/s11157-017-9445-y

Xu Y, Zhang W (2000) Subcolloidal Fe/Ag Particles for Reductive Dehalogenation of Chlorinated Benzenes. Ind Eng Chem Res 39:2238–2244. https://doi.org/10.1021/ie9903588

Xue D, Sethi R (2012) Viscoelastic Gels of Guar and Xanthan Gum Mixtures Provide Long-Term Stabilization of Iron Micro- and Nanoparticles. J Nanoparticle Res 14:1239. https://doi.org/10.1007/s11051-012-1239-0

Yan W, Herzing AA, Kiely CJ, Zhang W (2010a) Nanoscale Zero-Valent Iron (nZVI): Aspects of the Core-Shell Structure and Reactions with Inorganic Species in Water. J Contam Hydrol 118:96–104. https://doi.org/10.1016/j.jconhyd.2010.09.003

Yan W, Herzing AA, Li X, et al (2010b) Structural Evolution of Pd-Doped Nanoscale Zero-Valent Iron (nZVI) in Aqueous Media and Implications for Particle Aging and Reactivity. Environ Sci Technol 44:4288–4294. https://doi.org/10.1021/es100051q

Yan W, Lien H-L, Koel BE, Zhang W (2013) Iron Nanoparticles for Environmental Clean-up: Recent Developments and Future Outlook. Environ Sci Process Impacts 15:63–77. https://doi.org/10.1039/C2EM30691C

Yang K, Zhu L, Zhao B (2005) Minimizing Losses of Nonionic and Anionic Surfactants to a Montmorillonite Saturated with Calcium Using their Mixtures. J Colloid Interface Sci 291:59–66. https://doi.org/10.1016/j.jcis.2005.04.088

Yang Y, Chen T, Sumona M, et al (2017) Utilization of Iron Sulfides for Wastewater Treatment: A Critical Review. Rev Environ Sci Bio/Technology 16:289–308. https://doi.org/10.1007/s11157-017-9432-3

Yirsaw BD, Megharaj M, Chen Z, Naidu R (2016) Environmental Application and Ecological Significance of Nano-Zero Valent Iron. J Environ Sci 44:88–98. https://doi.org/10.1016/j.jes.2015.07.016

You G, Wang P, Hou J, et al (2017) The Use of Zero-Valent Iron (ZVI)–Microbe Technology for Wastewater Treatment with Special Attention to the Factors Influencing Performance: A Critical Review. Crit Rev Environ Sci Technol 47:877–907. https://doi.org/10.1080/10643389.2017.1334457

Yu R-F, Chi F-H, Cheng W-P, Chang J-C (2014) Application of pH, ORP, and DO Monitoring to Evaluate Chromium(VI) Removal from Wastewater by the Nanoscale Zero-Valent Iron (nZVI)

Process. Chem Eng J 255:568–576. https://doi.org/10.1016/j.cej.2014.06.002

Yuan S, Wen H, Wu X, et al (2010a) Effect of Nonionic and Cationic Surfactants on the Dechlorination Kinetics and Products Distribution of Various Polychlorinated Benzenes by Cu/Fe Particles. Sep Purif Technol 74:130–137. https://doi.org/10.1016/j.seppur.2010.05.015

Yuan S, Zheng Z, Meng X-Z, et al (2010b) Surfactant Mediated HCB Dechlorination in Contaminated Soils and Sediments by Micro and Nanoscale Cu/Fe Particles. Geoderma 159:165–173. https://doi.org/10.1016/j.geoderma.2010.07.008

Zabetakis KM, Niño de Guzmán GT, Torrents A, Yarwood S (2015) Toxicity of Zero-Valent Iron Nanoparticles to a Trichloroethylene-Degrading Groundwater Microbial Community. J Environ Sci Heal Part A 50:794–805. https://doi.org/10.1080/10934529.2015.1019796

Zepp RG, Wolfe N. (1987) Abiotic Transformation of Organic Chemicals at the Particle/Water Interface. In: Aquatic Surface Chemistry: Chemical Processes at the Particle–Water Interface, Wiley. New York, NY, pp 423-455.

Zhang M, Bacik DB, Roberts CB, Zhao D (2013) Catalytic Hydrodechlorination of Trichloroethylene in Water with Supported CMC-Stabilized Palladium Nanoparticles. Water Res 47:3706–3715. https://doi.org/10.1016/j.watres.2013.04.024

Zhang M, He F, Zhao D, Hao X (2011) Degradation of Soil-Sorbed Trichloroethylene by Stabilized Zero Valent Iron Nanoparticles: Effects of Sorption, Surfactants, and Natural Organic Matter. Water Res 45:2401–2414. https://doi.org/10.1016/j.watres.2011.01.028

Zhang M, He F, Zhao D, Hao X (2017) Transport of Stabilized Iron Nanoparticles in Porous Media: Effects of Surface and Solution Chemistry and Role of Adsorption. J Hazard Mater 322:284–291. https://doi.org/10.1016/j.jhazmat.2015.12.071

Zhang W (2003) Nanoscale Iron Particles for Environmental Remediation: An Overview. J Nanoparticle Res 5:323–332. https://doi.org/10.1023/A:1025520116015

Zhang W, Elliott DW (2006) Applications of Iron Nanoparticles for Groundwater Remediation. Remediat J 16:7–21. https://doi.org/10.1002/rem.20078

Zhang W, Wang C-B, Lien H-L (1998) Treatment of Chlorinated Organic Contaminants with Nanoscale Bimetallic Particles. Catal Today 40:387–395. https://doi.org/10.1016/S0920-5861(98)00067-4

Zhang XG (2011) Galvanic Corrosion. In: Revie RW (ed) Uhlig's Corrosion Handbook, Third Edition. John Wiley & Sons, Inc., Hoboken, NJ, USA, pp 123–143

Zhao B, Zhu L, Yang K (2006) Solubilization of DNAPLs by Mixed Surfactant: Reduction in Partitioning Losses of Nonionic Surfactant. Chemosphere 62:772–779. https://doi.org/10.1016/j.chemosphere.2005.04.080

Zhao D, Li M, Zhang D, et al (2013) Reductive Dechlorination of 2,4-Dichlorophenol by Pd/Fe Nanoparticles Prepared in the Presence of Ultrasonic Irradiation. Ultrason Sonochem 20:864–871. https://doi.org/10.1016/j.ultsonch.2012.11.015

Zhao D, Zheng Y, Li M, et al (2014) Catalytic Dechlorination of 2,4-Dichlorophenol by Ni/Fe Nanoparticles Prepared in the Presence of Ultrasonic Irradiation. Ultrason Sonochem 21:1714–1721. https://doi.org/10.1016/j.ultsonch.2014.03.002

Zhao X, Liu W, Cai Z, et al (2016) An Overview of Preparation and Applications of Stabilized Zero-Valent Iron Nanoparticles for Soil and Groundwater Remediation. Water Res 100:245–266. https://doi.org/10.1016/j.watres.2016.05.019

Zheng Z, Yuan S, Liu Y, et al (2009) Reductive Dechlorination of Hexachlorobenzene by Cu/Fe Bimetal in the Presence of Nonionic Surfactant. J Hazard Mater 170:895–901. https://doi.org/10.1016/j.jhazmat.2009.05.052

Zhou Z, Ruan W, Huang H, et al (2016) Fabrication and Characterization of Fe/Ni Nanoparticles Supported by Polystyrene Resin for Trichloroethylene Degradation. Chem Eng J 283:730–739. https://doi.org/10.1016/j.cej.2015.07.076

Zhu B-W, Lim T-T (2007) Catalytic Reduction of Chlorobenzenes with Pd/Fe Nanoparticles: Reactive Sites, Catalyst Stability, Particle Aging, and Regeneration. Environ Sci Technol 41:7523–7529. https://doi.org/10.1021/es0712625

Zhu N, Luan H, Yuan S, et al (2010) Effective Dechlorination of HCB by Nanoscale Cu/Fe Particles. J Hazard Mater 176:1101–1105. https://doi.org/10.1016/j.jhazmat.2009.11.092

Zou H, Hu E, Yang S, et al (2019) Chromium(VI) Removal by Mechanochemically Sulfidated Zero Valent Iron and its Effect on Dechlorination of Trichloroethene as a Co-Contaminant. Sci Total Environ 650:419–426. https://doi.org/10.1016/j.scitotenv.2018.09.003

Zou Y, Wang X, Khan A, et al (2016) Environmental Remediation and Application of Nanoscale Zero-Valent Iron and Its Composites for the Removal of Heavy Metal Ions: A Review. Environ Sci Technol 50:7290–7304. https://doi.org/10.1021/acs.est.6b01897